F61708-96-W0227

VERIFICATION OF MODEL FOR HEAT-MECHANICAL PROCESSES IN ABLATING COMPOSITES

FINAL REPORT

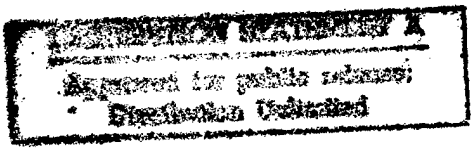

1996

REPORT DOCUMENTATION PAGE

Form Approved OMB No. 0704-0188

1. AGENCY USE ONLY (Leave blank)	2. REPORT DATE	3. REPORT TYPE AND DATES COVERED
	~~28 August 1998~~	Final Report

4. TITLE AND SUBTITLE

Verification Of Model For Heat-Mechanical Processes In Ablating Composites

5. FUNDING NUMBERS

F6170896W0227

6. AUTHOR(S)

Prof. Iourii Dimitrienko

7. PERFORMING ORGANIZATION NAME(S) AND ADDRESS(ES)

Moscow State University
A-1217 Main Building
Moscow 119899
Russia

8. PERFORMING ORGANIZATION REPORT NUMBER

N/A

9. SPONSORING/MONITORING AGENCY NAME(S) AND ADDRESS(ES)

EOARD
PSC 802 BOX 14
FPO 09499-0200

10. SPONSORING/MONITORING AGENCY REPORT NUMBER

SPC 96-4025

11. SUPPLEMENTARY NOTES

12a. DISTRIBUTION/AVAILABILITY STATEMENT

Approved for public release; distribution is unlimited.

12b. DISTRIBUTION CODE

A

13. ABSTRACT (Maximum 200 words)

This report results from a contract tasking Moscow State University as follows: The contractor will conduct testing of the accuracy of the Moscow State mathematical modeling of varying heat-mechanical characteristics of ablating matrix, fiber and the composite itself under heating. He will test the accuracy of the modeling of temperature field in the specimen of composite thermal-protective material under one-sided heating.

14. SUBJECT TERMS

Coatings, Fluids & Lubrication

15. NUMBER OF PAGES

120

16. PRICE CODE

N/A

17. SECURITY CLASSIFICATION OF REPORT	18. SECURITY CLASSIFICATION OF THIS PAGE	19. SECURITY CLASSIFICATION OF ABSTRACT	20. LIMITATION OF ABSTRACT
UNCLASSIFIED	UNCLASSIFIED	UNCLASSIFIED	UL

CONTENTS

INTRODUCTION

In previous reports [1, 2, 3] the model of a coupled thermo-mechanical behaviour of ablative composite materials under intensive heat actions was developed. Different aspects of this model in detail were also presented in our works [5 - 10]. The aim of the previous Report was to verify the model for the example of Generic Carbon-Phenolic Textile Fabric 2-D Composite. Experimental results on thermal and mechanical properties of Carbon-Phenolic Composite were given by Wright Lab. [11]. As the result of the comparison conducted of the theoretical and experimental results, it was established that the model describes a behaviour of ablative composites with an accuracy being sufficiently acceptable for such computations. The best agreement of the results (error $\approx$ 7 - 10 %) has been obtained for heat-physical properties:

- heat-conductivity,
- heat-capacity,
- gas-permeability, and also for mechanical properties (error $\approx$ 10 - 20 %) at room (294 K), high (600 - 1400 K) and superhigh (1400 - 3000 K) temperatures. The worse accuracy was obtained for elevated temperatures (294 - 600 K). The main cause of this fact is the absence of reliable experimental data on mechanical properties of phenolic matrix under high temperatures, as in calculations we used data from scientific literature and also we did not take account of gradientness (nonuniformity) of heating under these temperatures although the heating rate was sufficiently high.

The aim of the present Report is to conduct the next stage of verification of the model: prediction of a behaviour of Generic Carbon/Phenolic Composite as a part of a cylindrical element of a structure under non-uniform heating. A geometric scheme of the structure element, which was calculated, was proposed by Wright Lab. Its peculiarity consists in that principal axes of orthotropy of Textile Composite Material contained in a cylindrical shell are not coincident with axes of the cylindrical coordinate system and are rotated with angle $\pi/6$ from the cylinder axis.

It is evident, that thermo-mechanical characteristics of such turned composite

(further it is called Carbon-Phenolic Bias-Reinforced Fabric Composite (BRFC)) in the cylindrical coordinate system differ from the corresponding characteristics in the principal axes of orthotropy. Therefore, the purpose of Chapters VII and VIII of the present Report (Chapters I - VI were in the previous report [1]) is to determine heat-physical and mechanical properties of BRFC in the cylindrical coordinate system.

Chapter IX is devoted to a description of methods for calculation of an ablation rate of BRFC under intensive non-uniform heating. A main attention in these calculations is paid to establishing a relationship between thermo-mechanical and thermo-chemical partials within a whole mechanism of ablation of BRFC.

Calculation of the ablation rate of Carbon-Phenolic Composite according to thermo-mechanical mechanism, mainly for sublimation and combustion, was investigated sufficiently in detail up to now (see, for example [13]); although many important questions remain still uncleared up. For example, the ablation rate of composite materials under combined diffusive-sublimational regime is usually determined only in a phenomenological way: on the base of working of previous investigations.

Efforts in prediction of thermo-mechanical ablation (mainly mechanical erosion of material within a flow) were started long ago [18]. However, imperfection of the models suggeted before (which considered, in the main, only thermo-stresses and thermocracking at the composite surface) did not allow to obtain effective mathematical methods having a sufficient accuracy for engineering calculations.

In our works [3, 5] the model has been suggested for calculation of thermo-mechanical ablation on the base of a combined analysis of thermo-mechanical stresses and physico-chemical processes occuring in composites at interaction with high-temperature chemically-reacting gas flows.

In § 9.1 of Chapter IX there are results of calculations of the ablation rate of BRFC with taking account of both the mechanisms: thermo-chemical and thermo-mechanical. Comparison of a relation between these two partials has been conducted, and analysis of the effect of Bias angle on ablation rate of BRFC was also performed.

Chapter X is devoted to calculation of heat stresses and a temperature field within a cylindrical shell made of BRFC.

Chapter VII

HEAT-PHYSICAL PROPERTIES OF BIAS-REINFORCED FABRIC COMPOSITE

§7.1. MODEL OF BIAS-REINFORCED FABRIC COMPOSITE (BRFC)

Before, in previous work [1] we gave thermo-mechanical relations of the model of ablative fabric composite in principal axes of orthotropy. Fabric composite, in accordance with the experimental data presented by Wright Lab., is assumed to be transversally isotropic, as properties of the composite are the same along both the warp and weft.

In cylindrical elements of structures, according to data of Wright Lab., the fabric composite is located so that the principal axes of orthotropy of the material Ox_i' $i = 1, 2, 3$ are not coincident with axes of the cylindrical coordinate system of the structure: namely, the axis Ox_3' laying in the direction of the warp is inclined by angle ψ from the axis Ox_3 of the cylinder (Fig. 1).

Since calculation of thermo-mechanical processes within a cylindrical structure under the action of high-speed hot gas flows is conducted in the Ox_i axes of the cylindrical coordinate system, it is necessary to obtain design characteristics of the fabric composite in this coordinate system Ox_i.

Further, such fabric composite with a inclined direction of fabric laying is called Bias-Reinforced Fabric Composite (BRFC).

§7.2. THEORETICAL RELATIONS FOR HEAT-PHYSICAL CONSTANTS OF BRFC

Heat-Conductivity.

Let $k_{ij\psi}$ be components of a heat-conductivity tensor of BRFC in the cylindrical coordinate system Ox_i $i = 1, 2, 3$. These components $k_{ij\psi}$ are connected to

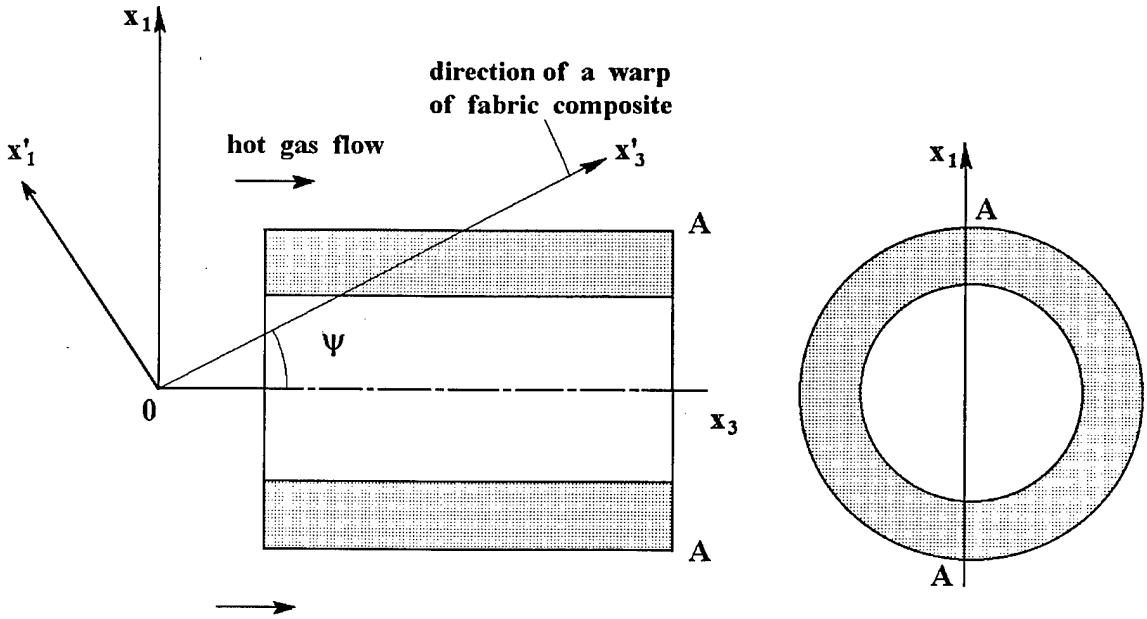

Fig. 1.

A scheme of orientation of principal axes of orthotropy of fabric composite in a cylindrical structure.

components of the heat-conductivity tensor k_{ij} in the principal axes of orthotropy Ox_i' with the help of matrix $Q_{ii'}$ of rotation about the Ox_2' axis by angle ψ:

$$k_{ij\psi} = k_{i'j'} Q_{ii'} Q_{j'j}, \tag{1}$$

where tensors $k_{i'j'}$, $k_{ij\psi}$ and $Q_{ii'}$ have the following structure:

$$k_{i'j'} = \begin{pmatrix} k_1 & 0 & 0 \\ 0 & k_2 & 0 \\ 0 & 0 & k_3 \end{pmatrix} \tag{2}$$

$$k_{ij\psi} = \begin{pmatrix} k_{11\psi} & 0 & k_{13\psi} \\ 0 & k_{22\psi} & 0 \\ k_{13\psi} & 0 & k_{33\psi} \end{pmatrix} \tag{3}$$

$$Q_{i'j} = \begin{pmatrix} \cos\psi & 0 & -\sin\psi \\ 0 & 1 & 0 \\ \sin\psi & 0 & \cos\psi \end{pmatrix} \tag{4}$$

Principal values of the heat-conductivity tensor k_1, k_2 and k_3 are expressed in terms of characteristics of matrix and fibres of the composite by formulae (35) - (38) of the previous Report [1], where $k_2 = k_3$ and non-zero values of the heat-conductivity tensor of BRFC $k_{11\psi}$, $k_{22\psi}$, $k_{33\psi}$ and $k_{13\psi}$ are connected to k_α by the relations:

$$\begin{aligned} k_{11\psi} &= k_1 \cos^2\psi + k_2 \sin^2\psi; \\ k_{33\psi} &= k_1 \sin^2\psi + k_2 \cos^2\psi; \\ k_{13\psi} &= \left(\frac{k_1 - k_2}{2}\right) \sin 2\psi; \\ k_{22\psi} &= k_2; \qquad k_2 = k_3. \end{aligned} \tag{1'}$$

Heat Capacity, Density and Gas Permeability.

Heat capacity c and density ρ of composite BRFC are scalar characteristics and independent of rotation of coordinate axes, and, hence, are expressed by formulae (40) and (42) from [1].

Gas-permeability tensor K_{ij} of fabric composite in Ox_i' axes depend, generally speaking, on orientation of coordinate axes. However, in our previous work [1] it

was established that, in fact, gas permeability of fabric carbon-phenolic composite is the same in the Across Ply direction K_1 and directions of the warp and weft $K_2 = K_3$, i.e. tensor K_{ij} is isotropic: $K_{ij} = K_1\delta_{ij}$ ($K_1 = K_2 = K_3$).

This conclusion is also verified by experimental data of Wright Lab. [11]. Therefore, in rotation of the coordinate system Ox_i tensor K_{ij} does not change and, hence, gas-permeability tensor of composite BRFC $K_{ij\psi}$ is coincident with K_{ij}:

$$K_{ij\psi} = K_{ij} = K_1\delta_{ij}. \tag{5}$$

Expression for K_1 was given in [1] (see formula (43)).

Thermal Expansion.

Components of heat-expansion tensor of composite BRFC $\overset{\circ}{\varepsilon}_{ij\psi}$ in Ox_i axes are connected to components $\overset{\circ}{\varepsilon}_{ij}$ of heat-expansion tensor of the fabric composite in principal axes of orthotropy Ox_i' by formulae being similar to (1) and (1'):

$$\overset{\circ}{\varepsilon}_{ij\psi} = \overset{\circ}{\varepsilon}_{i'j'}Q_{ii'}Q_{j'j}, \tag{6}$$

or:

$$\begin{aligned}
\overset{\circ}{\varepsilon}_{11\psi} &= \overset{\circ}{\varepsilon}_1\cos^2\psi + \overset{\circ}{\varepsilon}_3\sin^2\psi;\\
\overset{\circ}{\varepsilon}_{33\psi} &= \overset{\circ}{\varepsilon}_1\sin^2\psi + \overset{\circ}{\varepsilon}_3\cos^2\psi;\\
\overset{\circ}{\varepsilon}_{13\psi} &= \left(\frac{\overset{\circ}{\varepsilon}_1 - \overset{\circ}{\varepsilon}_3}{2}\right)\sin 2\psi;\\
\overset{\circ}{\varepsilon}_{22\psi} &= \overset{\circ}{\varepsilon}_3; \qquad (\overset{\circ}{\varepsilon}_2 = \overset{\circ}{\varepsilon}_3);
\end{aligned} \tag{7}$$

where tensors $\overset{\circ}{\varepsilon}_{ij\psi}$ and $\overset{\circ}{\varepsilon}_{ij}$ have the following form:

$$\overset{\circ}{\varepsilon}_{ij\psi} = \begin{pmatrix} \overset{\circ}{\varepsilon}_{11\psi} & 0 & \overset{\circ}{\varepsilon}_{13\psi} \\ 0 & \overset{\circ}{\varepsilon}_{22\psi} & 0 \\ \overset{\circ}{\varepsilon}_{13\psi} & 0 & \overset{\circ}{\varepsilon}_{22\psi} \end{pmatrix} \tag{8}$$

$$\overset{\circ}{\varepsilon}_{ij} = \begin{pmatrix} \overset{\circ}{\varepsilon}_1 & 0 & 0 \\ 0 & \overset{\circ}{\varepsilon}_2 & 0 \\ 0 & 0 & \overset{\circ}{\varepsilon}_2 \end{pmatrix}$$

Expressions for $\overset{\circ}{\varepsilon}_1$ and $\overset{\circ}{\varepsilon}_2$ were given in [1] (see formulae (28), (29).

§7.3. CALCULATED RESULTS

In order to analyze the influence of inclination angle ψ on a temperature dependence of heat conductivities of the composite BRFC $k_{11\psi}(\theta)$ and $k_{33\psi}(\theta)$, we conducted numerical calculations by formulae (1') for different values of angle $\psi = 0°, 15°, 30°, 15°, 60°$. Figure 2 shows dependences of heat conductivity $k_{11\psi}$ of BRFC in the transverse direction Ox_1 and Figure 3 – dependences of heat conductivity $k_{33\psi}$ in the longitudinal direction Ox_3 on temperature θ of heating for different values of the angle ψ. Here and further the heating rate is assumed to be a constant: $\dot{\theta}_0 = 5$ K/s. Tables 1 and 2 present corresponding numerical values of $k_{11\psi}$ and $k_{33\psi}$.

With increasing angle ψ, the heat conductivity $k_{11\psi}$ grows but $k_{33\psi}$ decreases. For the main design value $\psi = 30°$ a ratio of heat conductivities $k_{11\psi}$ and k_1 at $\psi = 0°$ is equal to $k_{11\psi}/k_1 \approx 2$ within the temperature θ interval from 300 K to 3000 K.

Changing angle ψ has a less effect on the longitudinal coefficient of heat conductivity $k_{33\psi}$; for example for $\psi = 30°$, the ratio $k_{33\psi}/k_3$ is equal to 0.85 - 0.9 within all the temperature interval.

Analogous investigations on the effect of angle ψ were conducted also for heat expansion. Figures 4 and 5 show results of numerical computations for longitudinal $\overset{\circ}{\varepsilon}_{33\psi}$ and transverse $\overset{\circ}{\varepsilon}_{11\psi}$ heat deformations of BRFC depending on temperature θ of heating for different values of angle $\psi = 15°,\ 30°,\ 45°$.

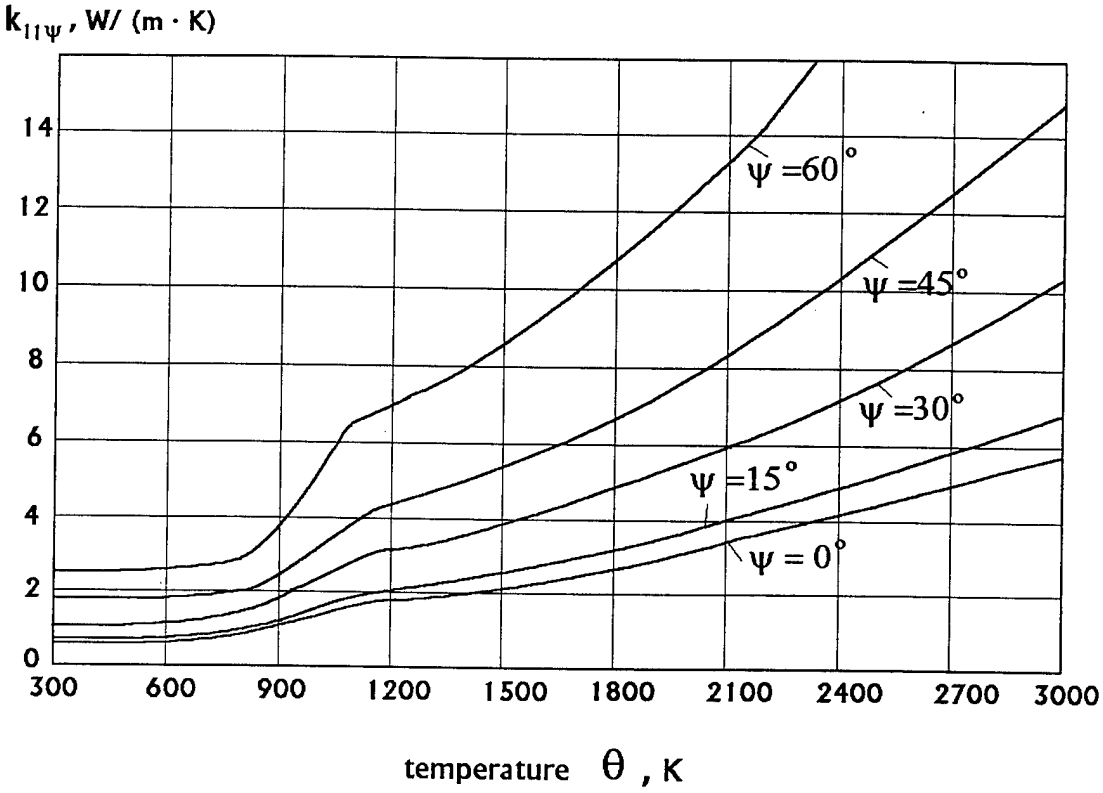

Fig. 2.

Varying Across Ply Thermal Conductivity $k_{11\psi}$
of Carbon/Phenolic BRFC with different bias angles ψ
versus temperature θ of heating at 5 K/s rate.

Tabl.1
Across Ply Thermal Conductivity $k_{11\psi}$
of Carbon/Phenolic BRCM with
different Bias angles ψ

Temperature, K θ	Conductivity W/(m K)		
	angle ψ = 15°	ψ = 30°	ψ = 45°
340	.775	1.104	1.553
400	.779	1.109	1.560
450	.786	1.117	1.568
500	.805	1.136	1.588
560	.841	1.171	1.621
615	.867	1.197	1.647
670	.891	1.223	1.676
800	1.031	1.385	1.867
1000	1.675	2.285	3.119
1200	2.079	3.029	4.326
1400	2.401	3.503	5.008
1600	2.794	4.077	5.829
1800	3.260	4.752	6.791
2000	3.769	5.504	7.874
2200	4.318	6.328	9.073
2400	4.916	7.232	10.395
2600	5.560	8.214	11.839
2800	6.246	9.271	13.402
3000	6.973	10.399	15.080

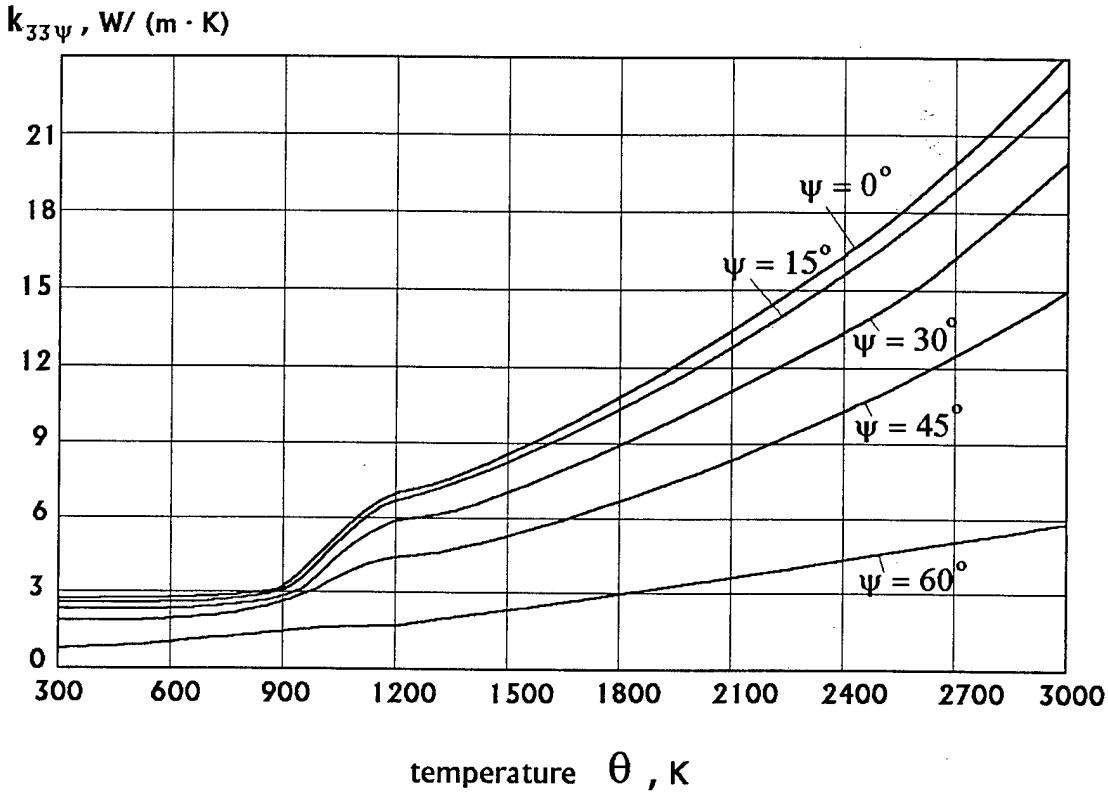

Fig. 3.

Varying Longitudinal Thermal Conductivity $k_{33\psi}$
of Carbon/Phenolic BRFC with different bias angles ψ
versus temperature θ of heating at 5 K/s rate.

Tabl.2

Longtitudional Thermal Conductivity $k_{33\psi}$ of Carbon/Phenolic BRCM with different Bias angle ψ

Temperature, K θ	Conductivity W/(m K)		
	Angle ψ =15°	ψ = 30°	ψ = 45°
340	2.331	2.002	1.553
395	2.342	2.012	1.561
450	2.351	2.020	1.568
505	2.372	2.040	1.588
560	2.400	2.071	1.621
615	2.427	2.097	1.647
670	2.460	2.129	1.676
800	2.703	2.349	1.867
1000	4.563	3.953	3.119
1200	6.573	5.624	4.326
1400	7.615	6.513	5.008
1600	8.864	7.581	5.829
1800	10.323	8.831	6.792
2000	11.979	10.244	7.874
2200	13.828	11.819	9.073
2400	15.876	13.560	10.396
2600	18.119	15.465	11.840
2800	20.557	17.533	13.402
3000	23.188	19.761	15.081

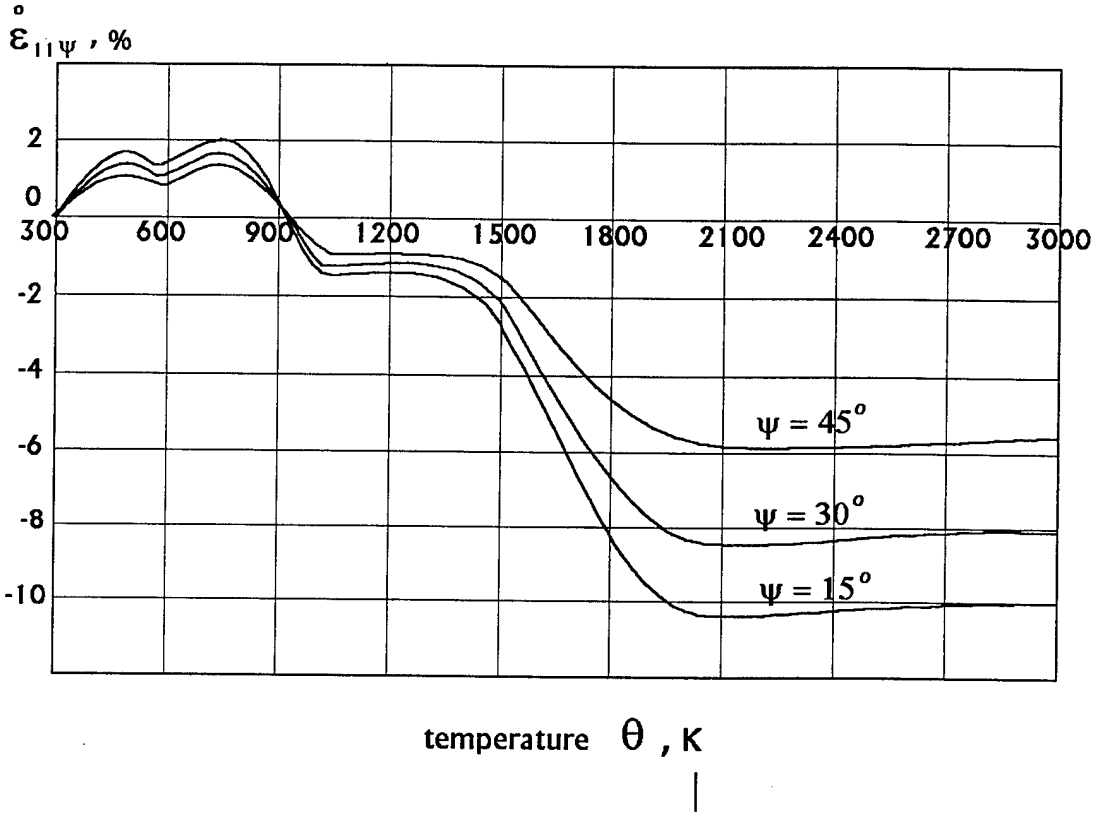

Fig. 4.

Varying Across Ply Thermal Expansion $\mathring{\varepsilon}_{11\psi}$
of Carbon/Phenolic BRFC with different bias angles ψ
versus temperature θ of heating at 5 K/s rate.

Tabl. 3

Across Ply Thermal Expansion $\mathring{\varepsilon}_{11\psi}$ of Carbon/Phenolic BRCM with different Bias angle ψ

Temperature, K θ	Expansion, %		
	angle $\psi = 15^\circ$	$\psi = 30^\circ$	$\psi = 45^\circ$
295.	.045	.037	.025
320.	.270	.219	.151
360.	.628	.511	.350
400.	.983	.798	.546
440.	1.312	1.064	.726
480.	1.533	1.241	.844
490.	1.551	1.256	.853
500.	1.547	1.252	.849
510.	1.521	1.230	.833
520.	1.472	1.190	.805
540.	1.325	1.069	.721
560.	1.184	.954	.640
580.	1.140	.918	.614
600.	1.213	.976	.653
620.	1.347	1.085	.726
640.	.000	.000	.000
660.	1.627	1.311	.879
680.	1.749	1.409	.944
700.	1.850	1.490	.999
720.	1.926	1.551	1.040
730.	1.952	1.572	1.053
740.	1.969	1.586	1.062
750.	1.976	1.592	1.066
760.	1.973	1.588	1.063
780.	1.928	1.552	1.037
800.	1.829	1.471	.982
820.	1.450	1.163	.771
840.	.840	.668	.434
880.	.000	.000	.000
920.	.088	.058	.017
960.	-.638	-.532	-.388
1000.	-1.170	-.966	-.687
1100.	-1.479	-1.219	-.864
1200.	-1.346	-1.112	-.791
1400.	-1.842	-1.510	-1.056
1600.	-4.427	-3.593	-2.454
1800.	-8.481	-6.862	-4.650
2000.	-10.280	-8.309	-5.617
2500.	-10.212	-8.253	-5.576
3000.	-9.958	-8.048	-5.440

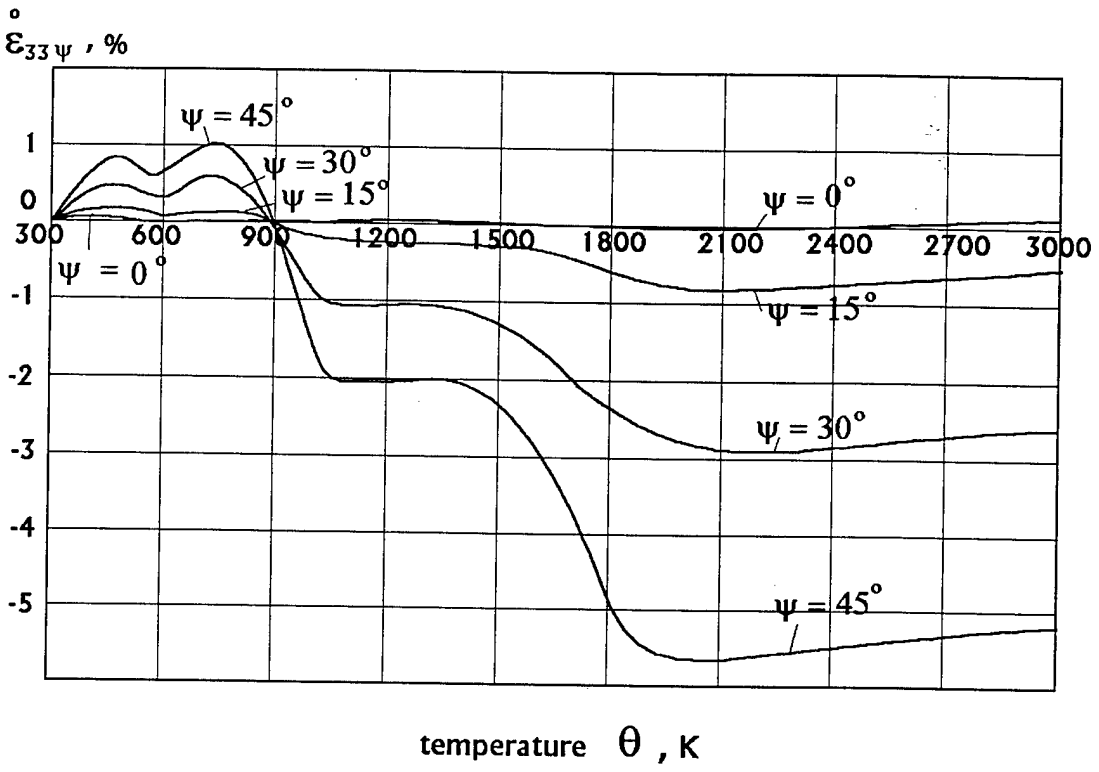

Fig. 5.

Varying Longitudinal Thermal Expansion $\overset{\circ}{\varepsilon}_{33\psi}$
of Carbon/Phenolic BRFC with different bias angles ψ
versus temperature θ of heating at 5 K/s rate.

Tabl. 4

Longitudional Thermal Expansion $\mathring{\varepsilon}_{33\psi}$ of Carbon/Phenolic BRCM with different Bias angles ψ

Temperature, K θ	Expansion, %		
angle	ψ=15°	ψ = 30°	ψ = 45°
295.	.005	.014	.025
320.	.031	.081	.150
360.	.069	.187	.348
400.	.103	.289	.543
440.	.132	.381	.722
480.	.145	.438	.839
490.	.144	.441	.847
500.	.141	.438	.844
510.	.135	.427	.827
520.	.126	.410	.798
540.	.104	.362	.714
560.	.084	.316	.633
580.	.075	.299	.606
600.	.079	.318	.643
620.	.090	.354	.715
640.	.000	.000	.000
660.	.113	.429	.860
680.	.122	.459	.920
700.	.129	.483	.967
720.	.133	.498	.996
730.	.135	.502	1.003
740.	.135	.502	1.003
750.	.134	.499	.997
760.	.132	.492	.983
780.	.125	.465	.930
800.	.113	.420	.839
820.	.071	.265	.529
840.	.006	.026	.052
880.	.000	.000	.000
920.	-.075	-.269	-.535
960.	-.156	-.563	-1.119
1000.	-.217	-.791	-1.575
1100.	-.252	-.978	-1.971
1200.	-.233	-.966	-1.968
1400.	-.234	-1.039	-2.137
1600.	-.392	-1.547	-3.123
1800.	-.697	-2.457	-4.861
2000.	-.809	-2.830	-5.592
2500.	-.706	-2.711	-5.450
3000.	-.594	-2.568	-5.264

Chapter VIII

MECHANICAL PROPERTIES OF BIAS-REINFORCED FABRIC COMPOSITES

§8.1. ELASTIC MODULI

Let us denote now J_{ijkl} components of a tensor of elastic pliabilities of a fabric composite in principal axes of orthotropy Ox_i' and $J_{ijkl\psi}$ in turned axes of orthotropy Ox_i. These components are connected by the relation of rotation:

$$J_{ijkl\psi} = J_{i'j'k'l'} Q_{ii'} Q_{jj'} Q_{ll'} Q_{kk'}. \tag{9}$$

From the relations (9) we can obtain the relations connecting elastic moduli of fabric composite E_i, ν_{ij}, G_{ij} to elastic moduli of Bias-Reinforced Fabric Composites $E_{i\psi}$, $\nu_{ij\psi}$, $G_{ij\psi}$:

$$E_{1\psi} = \left(\frac{\cos^4\psi}{E_1} + \frac{\sin^4\psi}{E_3} + \frac{\sin^2 2\psi}{2}\left(-\frac{\nu_{13}}{E_1} + \frac{1}{G_{13}} \right) \right)^{-1};$$

$$E_{3\psi} = \frac{\sin^4\psi}{E_1} + \frac{\cos^4\psi}{E_3} + \frac{\sin^2 2\psi}{2}\left(-\frac{\nu_{13}}{E_1} + \frac{1}{G_{13}} \right)^{-1}; \tag{10}$$

$$E_{2\psi} = E_2;$$

$$G_{13\psi} = \left(\sin 2\psi \left(\frac{1 + 2\nu_{13}}{E_1} + \frac{1}{E_3} \right) + \frac{\cos 2\psi}{G_{13}} \right)^{-1}.$$

Expression for elastic moduli E_i, ν_{ij}, G_{ij} depending on heating temperature θ were given in [1] (relations (24)).

Figure 6 shows calculated data of a dependence of elastic modulus $E_{3\psi}(\theta)$ on heating temperature θ for different values of angle ψ = 15, 30 and 45°. Table 5 gives corresponding numerical values of modulus $E_{3\psi}$. As seen from the Table 5, with increasing angle ψ, longitudinal elasticity modulus $E_{3\psi}$ of RRFC sharply decreases: for angle $\psi = 30°$ modulus $E_{3\psi}$ is equal only to 7 % of the value E_3 at θ = 295 K and 0.6 % at 2200 K. It can be explained by that for angles $\psi \geq 5°$ elastic properties of a composite are defined, in the main, by properties of its matrix.

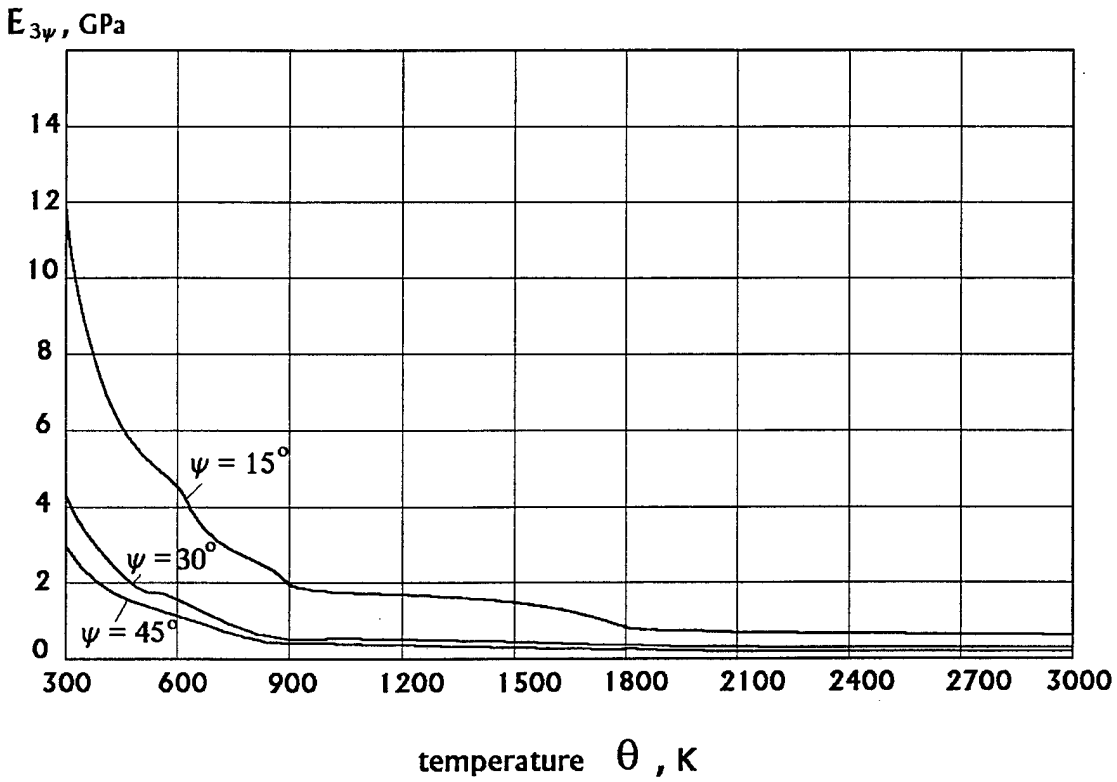

Fig. 6.

Varying Longitudinal Elastic Modulus $E_{3\psi}$
of Carbon/Phenolic BRFC with different bias angles ψ
versus temperature θ of heating at 5 K/s rate.

Tabl. 5

Longitudional Elastic Modulus $E_{3\psi}$ of Carbon/Phenolic BRCM with different Bias angles ψ

Temperature, K θ	Modulus, GPa			
	angle ψ=0°	ψ= 15°	ψ= 30°	ψ= 45°
295.0	60.228	11.897	4.437	3.157
670.0	43.444	3.464	1.181	.825
920.0	37.615	1.987	.664	.461
1365.0	40.691	1.692	.560	.387
2200.0	35.653	.708	.229	.156

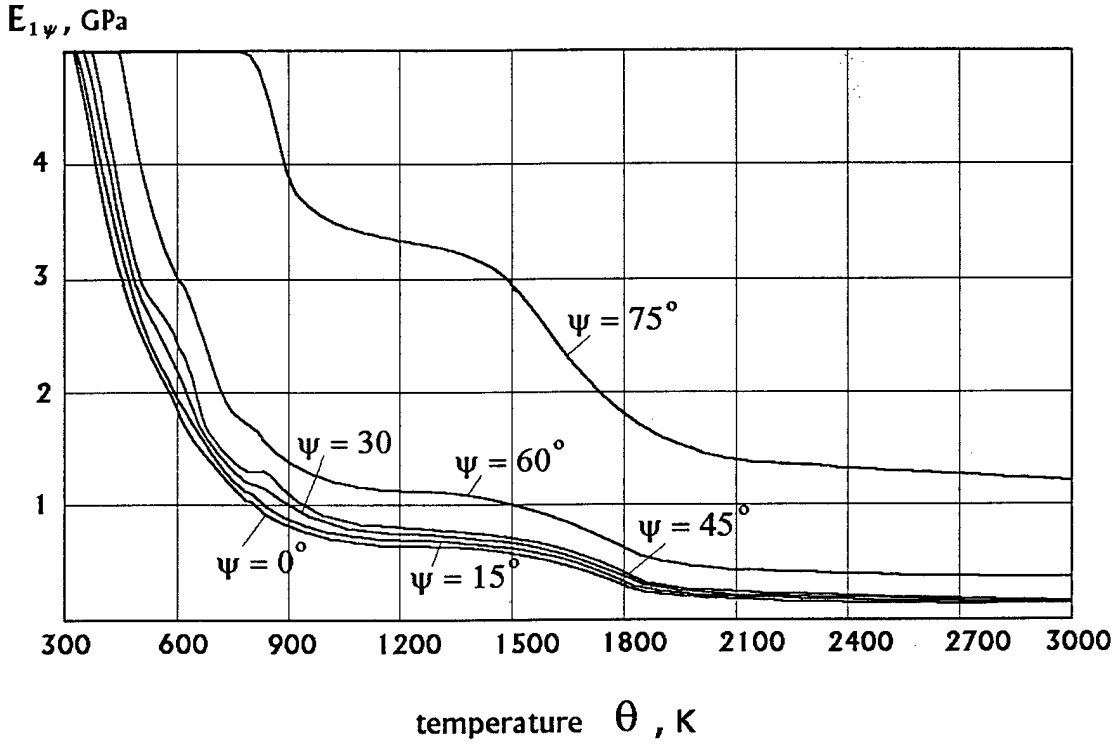

Fig. 7.

Varying Across Ply Elastic Modulus $E_{1\psi}$
of Carbon/Phenolic BRFC with different bias angles ψ
versus temperature θ of heating at 5 K/s rate.

Tabl. 6

Across Ply Elastic Modulus $E_{1\psi}$ of Carbon/Phenolic BRCM with different Bias angles ψ

Temperature, K θ	Modulus, GPa					
	angles: 0	ψ=15°	ψ=30°	ψ=45°	ψ=60°	ψ=75°/
294.0	6.79	6.14	5.34	5.59	8.20	20.16
673.0	1.75	1.59	1.39	1.47	2.23	6.42
922.0	.96	.87	.77	.82	1.26	3.77
1366.0	.78	.72	.64	.69	1.06	3.24
2200.0	.27	.26	.24	.27	.43	1.38

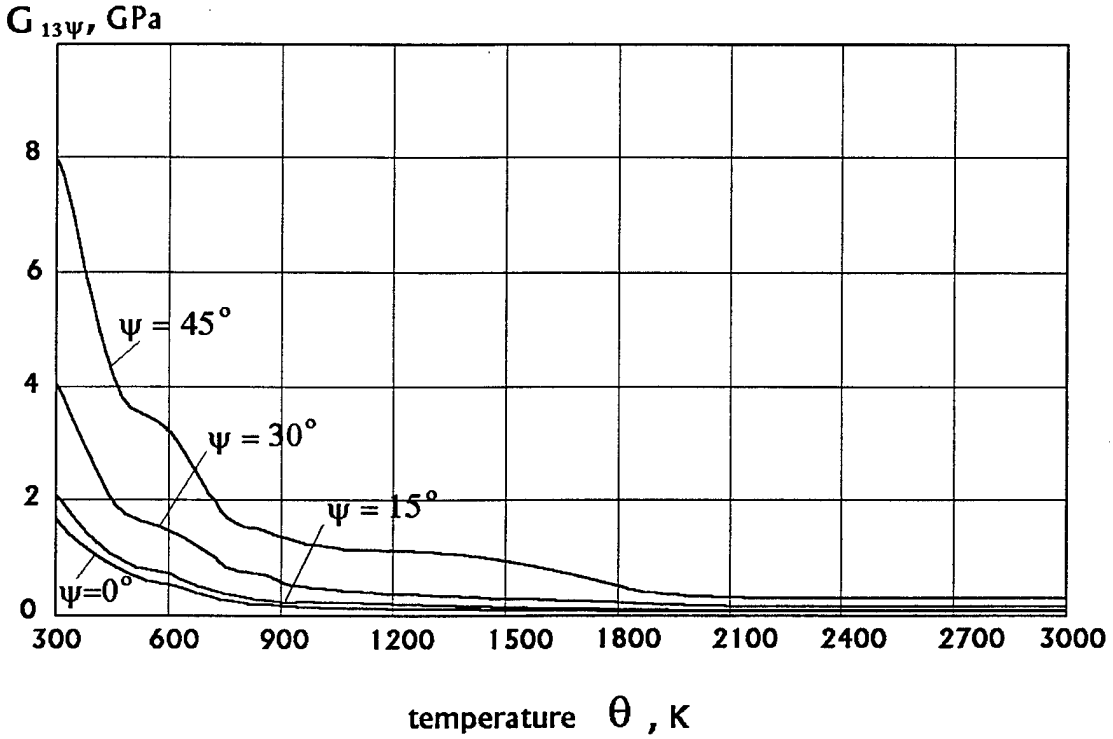

Fig. 8.

Varying Shear Modulus $G_{13\psi}$
of Carbon/Phenolic BRFC with different bias angles ψ
versus temperature θ of heating at 5 K/s rate.

Tabl. 7

Shear Elastic Modulus, GPa of Carbon/Phenolic BRCM with different Bias angles

Temperature, K θ	$G_{13\psi}$ Modulus, GPa				
	angle ψ = 0°	ψ = 15°	ψ = 30°	ψ = 45°	ψ = 60°
295.0	1.679	2.098	4.189	8.353	4.189
675.0	.435	.546	1.121	2.368	1.122
920.0	.243	.305	.626	1.321	.626
1365.0	.204	.256	.522	1.086	.522
2200.0	.083	.103	.200	.381	.200

Figure 7 and Table 6 show results calculated by formula (10) Across Ply Modulus $E_{1\psi}(\theta)$ depending on heating temperature θ for angles $\psi = 0$, 15, 30, 45, 60 and 75°. As seen from Figure 7, the effect of a matrix on value of $E_{1\psi}$ is also prevalent for angles $\psi = 0 \ldots 60°$. Value $E_{1\psi}$ for angles ψ from this interval changes very weakly, and only for $\psi > 60°$ function $E_{1\psi}(\theta)$ starts to grow approaching $E_3(\theta)$.

There is another situation for shear modulus $G_{13\psi}$. Value $G_{13\psi}$ reaches its maximum for angle $\psi = 45°$ (8.35 GPa at 295 K and 0.38 GPa at $\theta = 2200$ K), that is higher by four times than for fabric composite at $\psi = 0°$. For angle $\psi = 30°$ this modulus is higher approximately by two times.

§8.2. STRENGTH

8.2.1. ACROSS PLY STRENGTH

Strength condition for fabric 2-D composite in accordance with the developed modulus is determined by relations (14) and (15) from [1]. In order to obtain an expression for ultimate stress $\sigma_{11\psi}$, for which there occurs destruction of BFRC in tension along the Ox_1 axis, it is necessary to substitute the following relation into equation (15):

$$\sigma_{11} = \sigma_{11\psi} \cos^2 \psi;$$
$$\sigma_{13} = \frac{\sigma_{11\psi}}{2} \sin 2\psi; \qquad \sigma_{11\psi} > 0; \tag{11}$$
$$\sigma_{12} = 0.$$

As a result, we obtain:

$$\sigma_{11\psi} = S^+_{1\psi}, \qquad S^+_{1\psi} = \left(\frac{\cos^4 \psi}{S_1^{+2}} + \frac{sin^2 2\psi}{4S_{13}^2} \right)^{-1/2}. \tag{12}$$

Having substituted expression (30) from [1] in place of $S_1^+(\theta)$ and $S_{13}(\theta)$ in equation (12), as a result we obtain a dependence of strength $S^+_{1\psi}$ in tension in the axis Ox_1 direction on temperature θ of heating.

When we derived equation (12), it was assumed that a level of pore gas pressure p is negligibly small. The effect of p will be investigated in detail below.

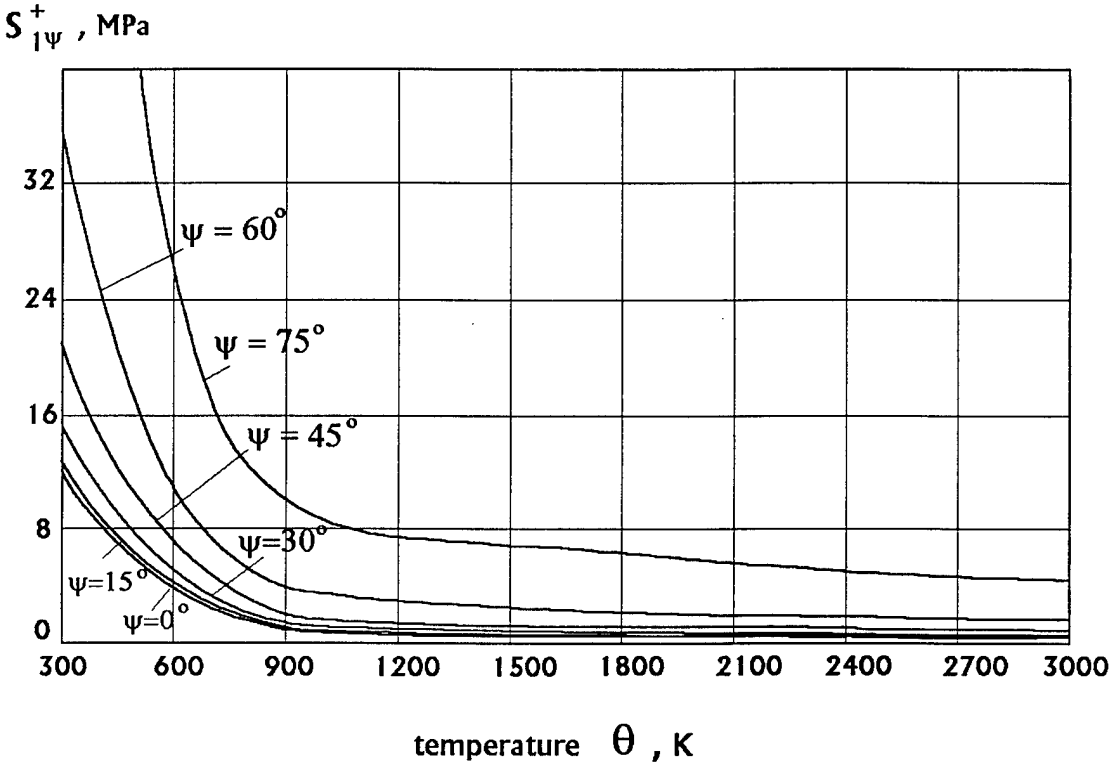

Fig. 9 .

Varying Strength $S^+_{1\psi}$ in Tension along Ox_3 axis
for Carbon/Phenolic BRFC with different bias angles ψ
versus temperature θ of heating at 5 K/s rate.

Tabl. 8.

Varying Strength in Tension along Ox_1 axis for Carbon/Phenolic BRCM with different Bias angles vs temperature of heating

Temperature, K θ	$S^{+}_{1\psi}$ Strength, GPa					
	angle $\psi=0°$	$\psi=15°$	$\psi=30°$	$\psi=45°$	$\psi=60°$	$\psi=75°$
294.0	11.58	12.32	14.92	21.03	36.21	86.92
533.0	4.85	5.15	6.24	8.77	15.04	35.87
922.0	1.08	1.15	1.41	2.02	3.61	9.27
1644.0	.71	.75	.92	1.33	2.42	6.48
3033.0	.46	.49	.60	.88	1.64	4.66

As follows from formula (12), destruction of composite BRFC in tension along the Ox_1 axis occurs due to combined normal separation of fabric layers from each other along the axis Ox_1' and interlayer shear in the inclined plane $(x_1'x_3')$.

Figure 9 shows calculated results of a dependence of strength $\sigma_{11\psi}$ on temperature θ of heating for angles $\psi = 0$, 15, 30, 45, 60 and 75°. with increasing angle ψ, strength $S_{1\psi}^{+}$ grows. However, for angles ψ from the interval from 0° to 30° this increase is equal only to 30 %. Essential growth of the strength (approximately by three times) is for angles $\psi \geq 60°$. Temperature dependences $S_{1\psi}^{+}(\theta)$ for all angles ψ are similar to the temperature dependence of matrix strength $\widetilde{\widetilde{a}}_1(\theta)$ (formula (34) from [1]): under tempeartures from the interval 600 - 900 K there occurs sharp falling down the strength $\sigma_{11\psi}$, after that its value is almost stabilized.

8.2.2. STRENGTH IN TENSION ALONG Ox_3 AXIS

Expression for strength $\sigma_{33\psi}$ of BRFC in tension along the Ox_3 axis can be obtained after substituting the relationships between σ_{ij} and $\sigma_{33\psi}$:

$$\begin{aligned} \sigma_{11} &= \sigma_{33\psi} \sin^2 \psi; \\ \sigma_{33} &= \sigma_{33\psi} \cos^2 \psi; \\ \sigma_{13} &= \frac{1}{2}\sigma_{33\psi} \sin 2\psi \end{aligned} \tag{13}$$

into equation (14) from [1]:

$$\sigma_{33\psi} = S_{3\psi}^{+}; \tag{14}$$

$$S_{3\psi}^{+} = \left(\frac{\sin^4 \psi}{S_1^{+2}} + \frac{\sin^2 2\psi}{4S_{13}} \right)^{-1/2}. \tag{15}$$

This equation defines destruction of composite BRFC by type (C) (delamination of composite). If we substitute relations (13) into the destruction condition by type (A) (15) from [1] (breakage of fabric threads laid in the reinforcing direction Ox_2' or Ox_3), we obtain:

$$\sigma_{33\psi} = S_{3\psi}^{(A)}; \qquad S_{3\psi}^{(A)} = \frac{S_3^{+}}{\cos^2 \psi}. \tag{16}$$

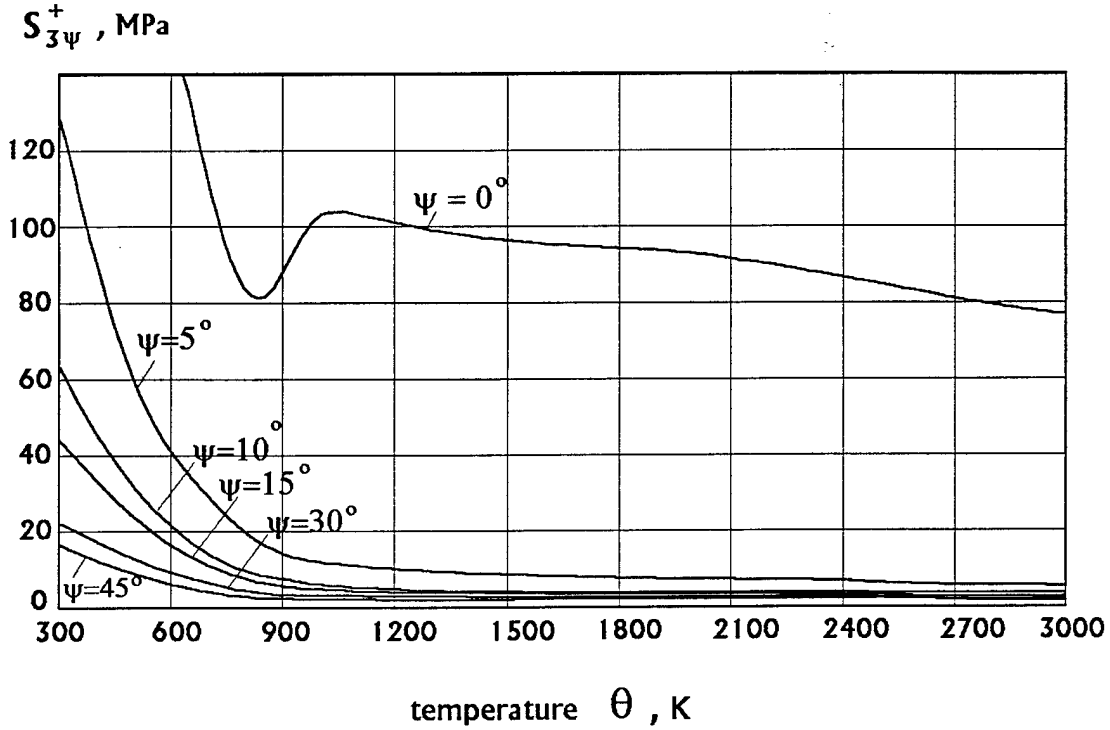

Fig. 10.

Varying Strength $S^+_{3\psi}$ in Tension along Ox_3 axis
for Carbon/Phenolic BRFC with different bias angles ψ
versus temperature θ of heating at 5 K/s rate.

Tabl. 9.

Strength in Tension along Ox_3 axis of Carbon/Phenolic BRCM with different Bias angles

Temperature, K θ	$S^+_{3\psi}$ Strength, MPa					
	angle = 0	ψ = 5°	ψ =10°	ψ = 15°	ψ = 30°	ψ = 45°
295.0	399.7	132.9	66.7	44.7	23.2	16.4
920.0	87.2	12.4	6.2	4.2	2.2	1.5
2475.0	84.9	5.8	2.9	2.0	1.0	0.7
3033.0	76.8	5.3	2.6	1.8	0.9	0.6

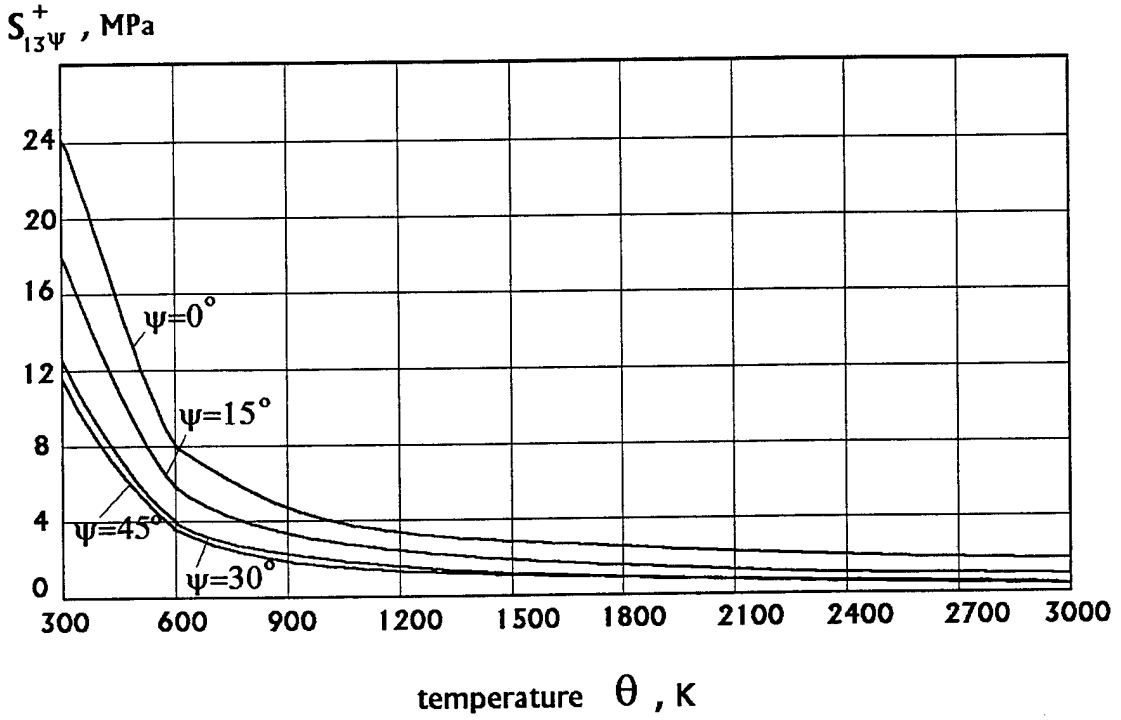

Fig. 11.

Varying Strength $S_{13\psi}$ in Shear in Ox_1x_3 plane
for Carbon/Phenolic BRFC with different bias angles ψ
versus temperature θ of heating at 5 K/s rate.

Tabl. 10

Varying Shear Strength in Ox13 Plane for Carbon/Phenolic BRCM with different Bias angles Ψ vs temperature of heating

Temperature, K θ	$S_{13\Psi}$ Strength, MPa					
	angle $\Psi=0^\circ$	$\Psi=15^\circ$	$\Psi=30^\circ$	$\Psi=45^\circ$	$\Psi=60^\circ$	$\Psi=75^\circ$
294	25.14	18.11	12.92	11.58	12.92	18.10
533	10.33	7.52	5.40	4.85	5.40	7.52
922	2.83	1.80	1.22	1.08	1.22	1.80
1644	2.06	1.21	.79	.71	.79	1.21
3033	1.60	.82	.52	.46	.52	.82

Value of $S_{3\psi}^{(A)}$ calculated from expression (15), as a rule, is essentially higher than $S_{3\psi}^{+}$ determined by formula (14): $S_{3\psi}^{(A)} \geq S_{3\psi}^{+}$, therefore, the destruction condition for BRFC by type (A) is not usually realized. Further, formula (14) for $S_{3\psi}^{+}$ is assumed a main expression for ultimate strength in tension in the Ox_3 axis direction.

Figure 10 shows graphs of dependence of strength $S_{3\psi}^{+}(\theta)$ on temperature θ of heating for different values of angle $\psi = 0, 5, 10, 15, 30, 45°$, calculated by formula (15). Table 9 gives corresponding numerical values of the functions. As seen from these graphs, strength $S_{3\psi}^{+}$ sharply falls down with increasing the angle ψ. For $\psi = 5°$ it decreases by three times under $\theta = 295$ K and almost by 15 times under $\theta = 3033$ K. It can be explained by that for the angle $\psi = 5°$ there occurs a change of a destruction type of fabric composite: if for $\psi = 0°$ the composite destructs due to breakage of fabric fibres and is described by functions S_1^{+} and S_{13} (type (C)). Since strength at breakage across the fabric layers S_1^{+} and at interlayer shear S_{13} is defined, in the main, by properties of the matrix, for angles $\psi \geq 5°$ strength $S_{3\psi}^{+}(\theta)$ behaves itself similarly to strength of the matrix, i.e. sharply decreases in heating up to 800 K, and then is almost stabilized in heating up to 3033 K.

8.2.3. STRENGTH IN SHEAR $S_{13\psi}$

In order to determine strength of BRFC in shear in the plane Ox_1x_3 (in turned axes Ox_i), it is necessary to substitute the following expressions for stresses σ_{ij} for this case of loading into the strength condition (15):

$$\begin{aligned} \sigma_{11} &= -\sigma_{13\psi} \sin 2\psi; \\ \sigma_{33} &= \sigma_{13\psi} \sin 2\psi; \\ \sigma_{13} &= \sigma_{13\psi} \cos 2\psi. \end{aligned} \tag{17}$$

As a result, we obtain that destruction in shear occurs when $\sigma_{13\psi}$ reaches the ultimate value $S_{13\psi}$:

$$\sigma_{13\psi} = S_{13\psi}; \qquad S_{13\psi} = \left(\frac{\sin^2 2\psi}{S_1^{+2}} + \frac{\cos^2 2\psi}{S_{13}^2} \right)^{-1/2}. \tag{18}$$

Temperature dependence of functions $S_{1+}(\theta)$ and $S_{13}(\theta)$, as before, is determined by formulae (30) from [1].

Equation (18) means that destruction of BRFC for all angles ψ occurs due to delamination of the composite, and thus its strength under high temperatures is defined, in the main, by strength of its matrix. This conclusion is verified by calculated results presented in Figure 11 and Table 10. Calculations for the function $S_{13\psi}(\theta)$ were conducted by formula (18) for angles $\psi = 0$, 15, 30 and 45°. Minimal values of strength $S_{13\psi}$ are realized at $\psi = 45°$: at $\theta_0 = 295$ K the strength decreases by two times as compared with the values for $\psi = 0°$, and at $\theta = 3033$ K - almost by four times. Value $S_{13\psi}$ at $\psi = 30°$ is close to the corresponding value at $\psi = 45°$. For angles $\psi = 45 \ldots 75°$ function $S_{13\psi}$ is summetrical: $S_{13\psi} = S_{13\psi}(\psi - \pi/4)$, i.e. with growing angle ψ, value of $S_{13\psi}$ increases.

Chapter IX

RATE OF ABLATION OF CARBON/PHENOLIC BRFC

§9.1. VOLUMETRICAL AND SURFACE ABLATION OF BRFC

Under the action of high-speed hot gas flow on a surface of structures of aerospace vehicles made of composite materials there occurs their ablation, i.e. a loss of mass. In accordance with the developed classification [4, 9], ablation processes of composites are divided into volumetrical ablation (pyrolysis, thermo-decomposition, thermo-oxidative decomposition) and linear (surface) ablation (recession of substance from a surface of composite).

At volumetrical ablation a composite density decreases: $\rho(t) < \rho(0)$, but the volume remains practically a constant $V \approx$ const, and at purely linear ablation the density is not practically change $\rho \approx$ const, but there occurs a decrease of the material volume $V(t) < V(0)$. In reality, there can occur both volumetrical and linear ablation processes in composites simultaneously.

Main quantitative parameters describing ablation processes are: ablation rate (mass or linear, or both of them) and specific heat of ablation.

Volumetrical ablation of 2-D composite in accordance with the developed model is described by mass rates of ablation: J_f of fibre and J_i of matrix, expressions for which are determined by formulae of the Arrhenius type (45) from [1] and by heat of ablation Δe^0 and Δe_f^0 and by gasification coefficients of fibre Γ_f and of matrix Γ_i.

Numerical values of these constants and functions corresponding to Carbon/ Phenolic Generic Composite are given in [1].

Changing reinforcing angle ψ of composite has no effect on characteristics of volumetrical ablation, therefore for BRFC volumetrical ablation is described by the same parameters.

In the present work let us consider in detail formulae for the rate of linear ablation D of BRFC. But in the beginning let us systematize the formulae for calculation of linear rate of ablation of 2-D Fabric Composite.

§9.2. LINEAR RECESSION RATE OF 2-D CARBON/PHENOLIC COMPOSITE

Let us denote $f(\vec{x},t)=0$ equation of a composite surface of ablation $\Sigma(t)$ moving in three-dimensional space with Descartes coordinates Ox_i and basis vectors $\vec{e}_i$, then under the condition on sufficient smoothness of the surface, function $f(\vec{x},t)$ satisfies the following equation [7]:

$$\frac{\partial f}{\partial t}+D\cdot|\nabla f|+\vec{v}_\Sigma\cdot\nabla f=0 \quad \vec{x}\in\Sigma(t),$$

where ∇ is the nabla-operator over coordinates $\vec{x}$, $\vec{v}_\Sigma$ is the velocity of mechanical motion of material points of the compositeon its surface Σ caused by mechanical forces or heat expansion, and D is the normal rate of own motion of the ablation surface D caused by irreversible physico-chemical transformations and:

$$|\nabla f|=(\nabla f\cdot\nabla f)^{1/2}.$$

Velocity $\vec{v}_\Sigma$ is determined from the solution of the general problem on mechanics of motion of solid deformable medium with a mobile boundary, in particular, at small deformations of composite materials, numerical value of $\vec{v}_\Sigma$ can be neglected as compared with D. To calculate the rate D there exist two main approaches: from the point of view of 1) molecular-kinetic theory of gas-fluid media [13] and 2) thermodynamical theory developed, in the main, in our works [5, 19]. Further the second approach will be applied.

In accordance with the developed model of surface ablation processes, the rate of surface ablation D is assumed to consist of a superposition of velocities of different independent ablation processes:

$$D=D_s+D_c+D_f+D_m, \tag{19}$$

where

D_s is the linear rate of evaporation (sublimation) of the composite,

D_c is the linear rate of chemical reaction of separate phases of the composite with reacting gas flow (a main kind of this type of ablation is combustion of carbon phases of the composite: char and carbon fibre in oxygen contained in gas flow),

D_m is the rate of thermomechanical erosion of the composite under the action of high-speed gas flow,

D_f is the linear rate of melting of several phases of the composite, for example, of particles of oxide ceramics Al_2O_3, SiO_2 etc. (For the considered case of Carbon/Phenolic Composite it is assumed that D_f=0.)

For the thermodynamical approach considered here, expressions for rates D_s, D_c, D_m are based on applying the second law of thermodynamics and the assumption on the absence of energy dissipation on surfaces of physico-chemical transformations.

§9.3. COMBUSTION RATE

Combustion process of composite carbon/phenolic material in a hot gas flow containing chemically active components (for examle, air) is a phenomenon of heterogeneous combustion, i.e. a process of chemical reaction of the type:

$$(\text{solid}) + (\text{gas}) \xrightarrow{\theta^\circ C} (\text{gas}). \tag{20}$$

As a solid component of carbon/phenolic composite (without account of special agents) we have carbon C being a main part of chemical composition of the carbonized phenolic matrix and also carbon fibres.

Therefore, further let us consider a multiphase system consisting of N elements ($j = 1, \ldots, N$) wherein $j = 1$ is solid carbon C and the rest $j = 2, \ldots, N$ are mixtures of components of the overrunning gas flow and combustion products. All combustion reactions are assumed to occur on the surface Σ of the composite.

It is follows from the assumptions that:

(a) on the one side of the separation surface Σ (let it be Σ^+) there is only component $j = 1$, on the other side (Σ^-) there are all the rest components $j = 2, \ldots, N$;

(b) if Y_j is the mass concentration of a component in the mixture, then

$$\text{on the surface } \Sigma^+: \; Y_1 = 1, Y_j = 0 \; j = 2, \ldots, N;$$

$$\text{on the surface } \Sigma^-: \; Y_1 = 0, \sum_{j=2}^{N} Y_j = 1. \tag{21}$$

Further we will assume that in the heterogeneous combustion process there occurs n chemical reactions, for which we can write the stoichiometric relations:

$$\sum_{j=1}^{N} \nu_{kj} M_j = 0, \quad k = 1, \dots, n; \tag{22}$$

where ν_{kj} are stoichiometric coefficients, M_j is the molecular mass of the j-th component.

Changing concentrations Y_j of components in a chemical reaction are determined by the balance law of components' mass:

$$\rho_w D_c (0 - Y_1) + I_1 = \dot{m}_1; \tag{23}$$

$$\rho_w D_c (Y_j - 0) + I_j = \dot{m}_j, \quad j = 2, \dots, N; \tag{24}$$

where D_c is the linear rate of combustion of the composite, ρ_w is the density of the composite on the combustion surface: $\rho_w = \rho_1 \varphi_1 + \rho_3 \varphi_3$, I_j is the flow of diffusion of the j-th component from or to the reaction surface Σ, $\dot{m}_j$ is the mass rate of formation of the j-th component.

In relations (23), (24) we take account of assumptions (21) on heterogenity of the conbustion process. From the same conditions (21) it follows that $Y_1 = 1$ and $I_1 = 0$, as there does not occur a diffusion of a solid component, then from relation (23) we obtain:

$$D_c = -\frac{\dot{m}_1}{\rho_w}. \tag{25}$$

This formula allows us to determine the linear rate of combustion of the composite, if the mass rate $\dot{m}_1$ is known.

Mass rates of formation of components $\dot{m}_j$ are determined as follows:

$$\dot{m}_j = M_j \sum_{j=1}^{n} \nu_{jk} U_k, \quad j = 1, \dots, N; \tag{26}$$

where U_k is the mass rate of k-th chemical reaction which is determined by the law of acting masses:

$$U_k = U_k^0 \Pi_{j=1}^{N} Y_j^{\nu_{kj}} \exp\left(-\frac{E_{ak} M_j}{R_a \theta_w}\right), \quad k = 1, \dots, n, \tag{27}$$

here symbol $\Pi_{j=1}^{N}$ means a product of concentrations Y_j of components taking part in the k-th reaction, E_a is the activation energy. Here the law of substance conservation is satisfied for the system as the whole:

$$\sum_{j=1}^{N} \dot{m}_j = 0. \tag{28}$$

Diffusion flows of the j-th component from or to the reaction surface are determined with the help of the so-called Reynolds heat-mass-transfer analogy [13]:

$$I_j = \left(\frac{\alpha}{c_p}\right)(Y_j - Y_{je}), \quad j = 2, \ldots, N, \tag{29}$$

where (α/c_p) is the heat transfer coefficient, Y_{je} is the concentration of the j-th component at the external surface of the boundary layer of the overrunning flow.

With using (29), equations (24) can be written in the form:

$$Y_j = \frac{\dot{m}_j + (\alpha/c_p)Y_{je}}{\rho_w D_c + (\alpha/c_p)}, \quad j = 2, \ldots, N. \tag{30}$$

The equations (30) together with (26) are the system of $(2N-1)$ algebraic equations to determine $(2N-1)$ unknown functions $\dot{m}_1$, $\dot{m}_j$, Y_j $j = 2, \ldots, N$; on solving the system we find the desired linear rate of combustion D_c by formula (25).

Let us consider now in detail a chemical composition of an overrunning flow. Usually under high temperatures (5000 K and higher), the overrunning flow dissociates: besides 'heavy' components O_2, N_2 there are also 'light' ones O, N therein. Let us assume that on the external surface of the boundary layer of the overrunning flow gas consists of five components: its composition is O, O_2 N, N_2, NO (indexes of the components are $j = 2, 3, 4, 5, 6$). On the composite surface Σ^- due to combustion reaction the gas mixture contains also components: CO, CO_2, CN and C_2N_2 $(j = 7, 8, 9, 10)$. At the combustion surface Σ the following chamical reactions run:

$$\begin{aligned} C + O &= CO \qquad \text{reaction } k = 1; \\ C + O_2 &= CO_2 \qquad \text{reaction } k = 2; \\ C + N &= CN \qquad \text{reaction } k = 3; \end{aligned} \tag{31}$$

$$2C + N_2 = C_2N_2 \qquad \text{reaction } k = 4.$$

Chemical composition of such 10-component mixture (component $j = 1$ is carbon C of the solid phase) and chemical reactions (31) allow us to find numerical values of molecular masses M_j, stoichiometric coefficients ν_{kj} and also concentration values Y_{je}, and:

$$Y_{je} = 0 \qquad j = 1, 7 \ldots 10. \tag{32}$$

Number n for such mixture is equal to $n = 4$. Mass rates of chemical reactions U_k (27) are written as follows:

$$U_k = U_k^0 Y_{k+1} \exp\left(-\frac{E_{ak+1} M_{k+1}}{R_a \theta_w}\right) \qquad k = 1, \ldots, 4, \tag{33}$$

and mass rate $\dot{m}_1$ of vanishing carbon due to relations (26) and (33) takes the form:

$$\dot{m}_1 = M_1 \sum_{k=1}^{4} \nu_{1k} U_k^0 Y_{k+1} \exp\left(-\frac{E_{ak+1} M_{k+1}}{R_a \theta_w}\right). \tag{34}$$

Concentrations Y_k contained in this expression can be determined from equation (30) whereinto we should substitute relations (25) and (33):

$$Y_j = \frac{M_j \sum_{k=1}^{4} \nu_{jk} Y_{k+1} U_{k+1}^0 \exp\left(-\frac{E_{ak+1} M_{k+1}}{R_a \theta_w}\right) + (\alpha / c_p) Y_{je}}{M_1 \sum_{k=1}^{4} \nu_{1k} Y_{k+1} U_{k+1}^0 \exp\left(-\frac{E_{ak+1} M_{k+1}}{R_a \theta_w}\right) + (\alpha / c_p)}; \tag{35}$$

$$j = 2, \ldots, N.$$

The equation (35) is the system of nine nonlinear algebraic equations to determine nine concentrations of components $Y_j(\theta_w)$ in the form of functions of the surface temperature θ_w.

Expression for the linear rate of combustion D_c as a function of θ_w is determined by formulae (25) and (34) after finding the concentrations $Y_j(\theta)$ from (35).

In accordance with the method described dabove, numerical calculations were conducted for combustion rate D_c of Carbon/Phenolic Composite. All the constants Y_{je}, M_j, U_k^0 and E_{ak} contained in equations (25), (32) - (35) were taken from data [13].

Figure 12 shows calculated results of linear rate of combustion D_c for 2-D Carbon/Phenolic Composite in the form of dependence $D_c(\theta_w)$ on the surface

temperature for the case of $p = 5$ atm, heat transfer coefficient (α/c_p) was chosen as $(\alpha/c_p) = 2.2$ kg/m$^2\cdot$ s. As seen from Fig.12, the function $D_c(\theta_w)$ has a typical character for combustion processes of carbon materials [20]. We can observe two stages of combustion: kinetic stage when combustion rate D_c sharply increases (temperature interval is from 1000 to 1700 K) and diffusive stage when combustion rate D_c is stabilized at the certain level (temperature interval is from 1700 to 3000 K). In the diffusive regime, the combustion rate magnitude is determined, in the main, by rates of diffusion of oxidizers O_2 and O to the combustion surface Σ and of combustion products CO, CO_2 from the combustion surface Σ of the composite.

Under higher temperatures θ_w of heating a sublimational regime of combustion of the composite starts.

§9.4. SUBLIMATION RATE

Under superhigh temperatures (higher than 3000 K) there occurs evaporation (sublimation) of solid carbon phases of the composite: carbon fibres and carbonized matrix

$$C(\text{solid}) \longrightarrow C(\text{gas}). \tag{36}$$

In this case there is a gaseous component $j = 1$ at the combustion surface Σ^- and the equation of mass balance for component $j = 1$ (of the type (23)) can be rewritten as follows:

$$\rho_w D_s(Y_1 - 1) + \left(\frac{\alpha}{c_p}\right)(Y_1 - 0) = 0, \tag{37}$$

here Y_1 is the concentration of gaseous C at the surface Σ^-; and at the external surface of the boundary layer the concentration of products of physico-chemical transformations, as before, is equal to zero; D_s is the linear rate of sublimation. From (37) we find:

$$Y_1 = \frac{\rho_w D_s}{\rho_w D_s + (\alpha/c_p)}. \tag{38}$$

The rest components of the gas mixture $j = 2, \ldots, N$ at the surface Σ^- for the given case can be considered as inert with respect to the sublimation process: $Y_1 = 1 - \sum_{j=2}^{N} Y_j$.

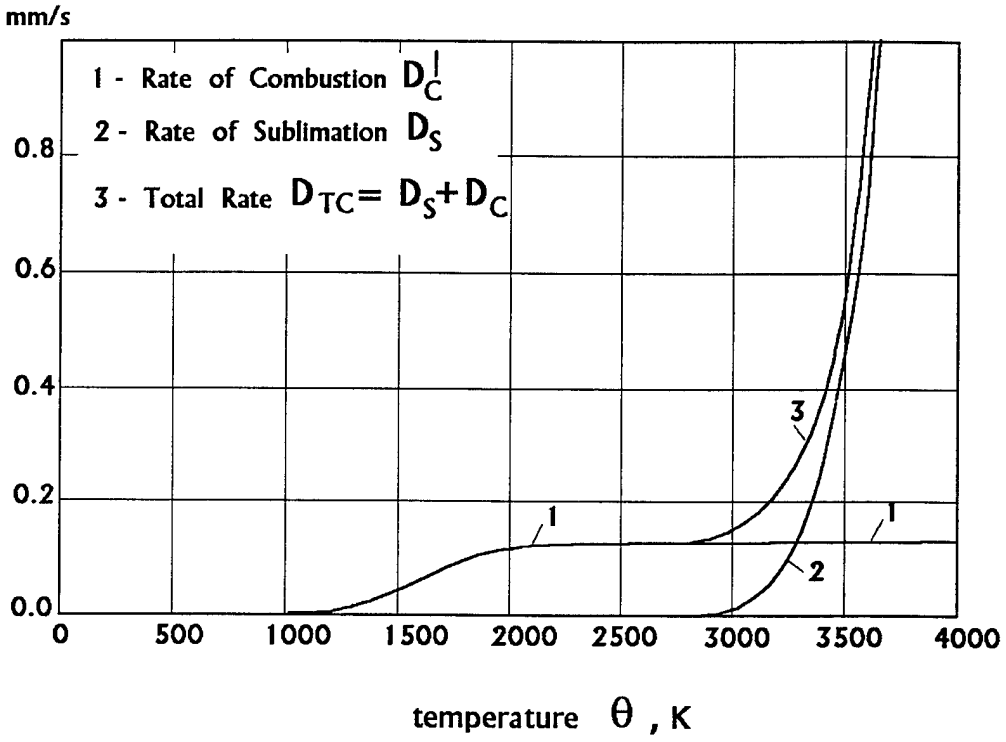

Fig. 12.

Varying Rates of Thermo-chemical (Sublimation D_s and Combustion D_c) Recession of 2-D Carbon/Phenolic Composite versus temperature θ under $p = 5.25$ atm.

Tabl. 11

Relation between Different Parts of Thermal-Chemical Ablation (Combustion and Sublimation) for 2-D Carbon/Phenolic Composite at P_e =5 atm in air

Temperature, K θ	Rate of Recession, mm/s		
	Combustion $\mathcal{D}_c$	Sublimation $\mathcal{D}_s$	Total $\mathcal{D}_{\pi c}$
1500.0	.000	.047	.047
2000.0	.000	.127	.127
3000.0	.010	.136	.146
3200.0	.052	.136	.188
3400.0	.224	.136	.361
3600.0	.828	.136	.964

The sublimation process can be considered as a phase transformation of the first type. For phase transformations of type (36) an expression for the phase transformation rate being, in fact, a linear rate of sublimation D_s is determined by the second law of thermodynamics, if we made the assumption on the absence of sources of energy dissipation on the surface of the phase transformation. In this case, as follows from [19], D_s is determined as:

$$\rho_w D_s = \left(\rho_w \frac{(p_g^* S_n - \sigma_n)}{\left(1 - \frac{\rho_w R_a \theta_w}{p_g^* S_n M_1}\right)} \right)^{1/2} ; \tag{39}$$

$$S_n = \exp\left(-\frac{E_{as} M_1}{R_a \theta_w}\right), \tag{40}$$

where σ_n for the considered case is the partial pressure of the gas phase on the surface $\bar{\Sigma}$:

$$\sigma_n = p_e Y_1; \tag{41}$$

and p_g^* is the constant characterizing the pressure of 'initial state' of the gas phase generated, and for the constant the following relation:

$$\frac{\rho_w R_a \theta_w}{p_g^* S_n M_1} \ll 1$$

is valid, then expression (39) takes the form:

$$\rho_w D_s = \left(\rho_w p_g^* \left(S_n - \left(\frac{p_e}{p_g^*}\right) Y_1 \right) \right)^{1/2}. \tag{42}$$

This equation is similar to the Lengmeur-Knudsen equation.

Two equations (38) and (42) allow us to evaluate the rate D_s and concentration Y_1 in the form of functions of the surface temperature θ_w. The linear rate of sublimation is usually relatively small so that the relation $4 p_g^* S_n (\alpha/c_p)^2/(\rho_w p_e^2) \ll 1$ is satisfied, then equation system (42), (38) admits an approximate solution in the form:

$$\rho_w D_s = \left(\frac{\alpha}{c_p}\right) \left(\frac{p_g^*}{p_e}\right) \exp\left(-\frac{E_{as} M_1}{R_a \theta_w}\right). \tag{43}$$

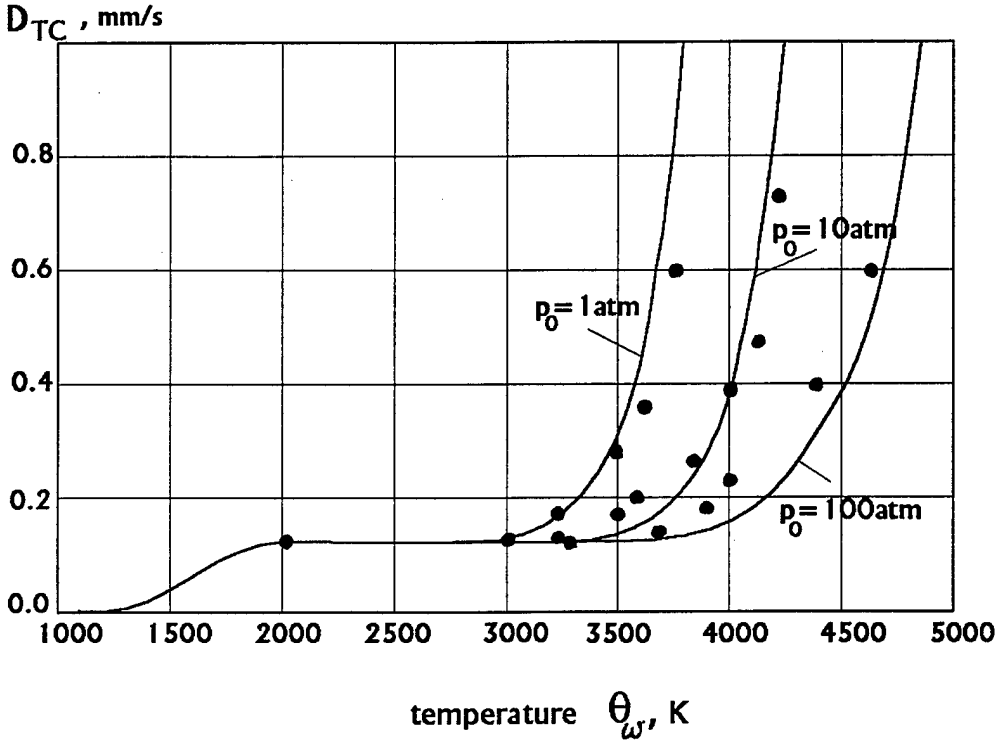

Fig. 13.

Varying Rates of Thermo-chemical (Sublimation D_s and Combustion D_c) Recession D_{TC} of 2-D Carbon/Phenolic Composite versus temperature θ_w and different static pressures: 1, 10, 100 and 500 atm.

Tabl.12

Varying Rates of Thermal-Chemical Ablation of 2-D Carbon/Phenolic Composite on Temperature in air, at different values of static pressure

Temperature, θ_w, K	$\mathcal{D}_{TC}$ Rate of Recession, mm/s					
	P_e=1 atm		10 atm		100 atm	
	theory	experim.	theory	experim.	theory	experim.
2000.0	.13	.15	.13	.15	.13	.15
3000.0	.14	.15	.14	.15	.14	.15
3200.0	.15	.19	.14	.15	.14	.15
3400.0	.22	.22	.14	.19	.14	.15
3600.0	.43	.30	.17	.20	.14	.15
3800.0	1.07	.60	.23	.26	.15	.20
4000.0	2.80	3.00	.40	.40	.16	.25
4200.0			.82	.72	.20	.30
4400.0			1.77	2.10	.30	.40
4600.0					.50	.60
4800.0					.88	1.50
5000.0					1.58	2.30

As follows from this equation, dependence of D_s on pressure p_e of the surroundings is inversely proportional. This expression will be consider further as a sublimation rate for Carbon/Phenolic Composites. Constants p_g^* and E_{as} in (43) are determined in experiments and are equal to:

$$\frac{E_{as}}{R_a M_1} = 80 \cdot 10^3 \ \frac{1}{\mathrm{K}}; \qquad p_g^* = 10^9 \ \frac{\mathrm{N}}{\mathrm{M}^2}. \tag{44}$$

Figure 12 shows a dependence of function $D_s(\theta_w)$ on the surface temperature θ_w of Carbon/Phenolic Composite determined by equation (44). Figure 12 also shows a dependence of summarized thermochemical rate of ablation D_{TC}:

$$D_{TC} = D_s + D_c \tag{45}$$

of Carbon/Phenolic Composite on temperature θ_s for the case when $p_e = p_0' = 5$ atm. As seen from this figure, in heating up to 3000 K only kinetic and diffusive regimes of combustion of the composite are realized in air and $D_c \approx 0$, and under higher temperatures ($> 3000K$) there occurs a sublimation regime wherein the ablation rate D_{TC} sharply increases due to fast growing the sublimation rate D_s.

It is well known that the sublimation rate depends on total pressure p_e of gas flow: with increasing pressure p_e the rate D_s lowers. Figure 13 gives calculated results of the rate of thermochemical ablation $D_{TC}(\theta_w)$ for three values of pressure $p_e = 1$, 10 and 100 atm and corresponding experimental data from work [20].

Numerical results of the calculations and experiments are presented in Table 14. As seen from the table and Fig.13, formula (44) describes the dependence of D_s on pressure p_e not only qualitatively but allows to obtain a sufficient accuracy of quantitative description.

§9.5. THERMO-MECHANICAL ABLATION RATE

9.5.1. GENERAL RELATIONS

Thermo-mechanical ablation means the process of mechanical crumbling off (erosion) of particles from a surface of composite by a hot high-speed flow.

The cause of thermo-mechanical ablation can be main acting factors: (1) overrunning gas flow (with velocity $\vec{V}$), the boundary layer of which moves along the ablation surface Σ of the composite with velocity $\vec{V}_\Sigma$:

$$\vec{V}_\Sigma = \vec{V} - V_n\vec{n}, \tag{46}$$

where $V_n = \vec{V} \cdot \vec{n}$ is the normal component of velocity $\vec{V}$, and (2) internal flow of gaseous products of pyrolysis of the matrix which moves through pores towards the external surface Σ of the composite and 'breaks up' a thin nonstrong coke layer of the composite preventing partially from gas filtration. Therefore, the rate of thermo-mechanical ablation D_m can be represented as a sum of rates D_e and D_i of these two processes:

$$D_m = D_e + D_i, \tag{47}$$

where D_e will be called a rate of external thermo-mechanical erosion, and D_i - a rate of internal thermo-mechanical erosion.

From the definition of thermo-mechanical erosion it follows that rates D_e and D_i should depend on characteristics of resistance to the force action of external and internal gas flows, i.e. on strength of the composite. However, the composite strength depends, generally speaking, on the direction of mechanical force action, hence, the linear rate of thermo-mechanical ablation also depends on the direction of motion of a gas flow with respect to principal orthotropy axes of the composite. It is a main distinction of rate D_m from rate of thermo-chemical ablation D_{TC} which is independent of both the direction of flow motion and orientation of orthotropy axes of the composite.

Thus, linear rate of thermo-mechanical ablation D_m should depend on some tensors $\underset{\sim}{a}^{(\varkappa)}$ $\varkappa = 1, \ldots, n$, characterizing a type of anisotropy of a composite material (ositropic, transversally isotropic, orthotropic etc.), and on the orientation of anisotropy axes with respect to the ablation surface Σ, i.e., in fact, on normal vector $\vec{n}$ to the surface:

$$D_e = D_e\left(\vec{n}, \underset{\sim}{a}^{(\varkappa)}, \vec{V}_\Sigma, \theta_w\right); \tag{48}$$

$$D_i = \left(\vec{n}, \underset{\sim}{a}^{(\varkappa)}, \theta_w\right), \quad \varkappa = 1, \ldots, n. \tag{49}$$

Besides that, rate of carring off D_e depends, evidently, on the surface temperature θ_w and also on both rate and direction of motion of hot gas flow $\vec{V}_\xi$ along the ablation surface Σ that is presented in formula (48).

Since the function D_m is scalar, arguments in (48), (49) should also be scalar invariants of the values $\vec{n}$, $\underset{\sim}{a}^{(\varkappa)}$, $\vec{V}_\Sigma$. Let us consider the following invariants:

$$a^{(\varkappa)} = \vec{n} \cdot \underset{\sim}{a}^{(\varkappa)} \cdot \vec{n},$$

$$p_\Sigma = \rho_{ge} \vec{V}_\Sigma \cdot \vec{V}_\Sigma = \rho_{ge} V_\Sigma^2; \qquad \varkappa = 1, \ldots, n. \tag{50}$$

Here we assumed that all tensors $\underset{\sim}{a}^{(\varkappa)}$ are of the second rank, and ρ_{ge} is the gas density on the external surface of the boundary layer of the overrunning flow (scalar).

Number of invariants n, as it was shown in [21], is not more than 6 ($n \leq 6$).

Hence, rates D_e and D_i can be presented in the form of function of two invariants $a^{(\varkappa)}$ and $p^{(\varkappa)}$:

$$D_e = D_e \left(a^{(\varkappa)}, p_\Sigma, \theta_w \right); \tag{48'}$$

$$D_i = D_i \left(a^{(\varkappa)}, \theta_w \right); \qquad \varkappa = 1, \ldots, n. \tag{49'}$$

Now let us assume that in (48'), (49') the dependence on arguments $a^{(\varkappa)}$ is only linear:

$$D_e = \sum_{\varkappa=1}^{n} D_{e\varkappa} (p_\Sigma, \theta_w)\, a^{(\varkappa)}; \tag{51}$$

$$D_i = \sum_{\varkappa=1}^{n} D_{i\varkappa} (\theta_w) a^{(\varkappa)}; \tag{52}$$

and investigate the effect of the type of anisotropy on the rates of thermo-mechanical ablation D_e and D_i.

9.5.2. ISOTROPIC COMPOSITES

For isotropic materials, for example, nonreinforced matrices, composites reinforced by dispersed particles or reinforced chaotically by short fibres, number $n = 1$, and tensor $\underset{\sim}{a}^{(1)}$ is single and invariants (50) have the form:

$$n = 1, \quad \underset{\sim}{a}^{(1)} = \underset{\sim}{\delta}, \quad a^{(1)} = \vec{n} \cdot \delta \cdot \vec{n} = 1; \tag{53}$$

and expressions (51), (52) for D_e and D_i take the form:

$$D_e = D_{Me} = D_{e1}(p_\Sigma, \theta_w); \tag{54}$$

$$D_i = D_{Mi} = D_{i1}(\theta_w); \tag{55}$$

where $\underset{\sim}{\delta}$ is the Kronecker tensor with components δ_{ij} in the Ox_i axes. Thus, as it should be expected, for isotropic media, rates of thermo-mechanical ablation D_{Me} amd D_{Mi} are independent of direction of the normal $\vec{n}$ and are determined only by the surface temperature θ_w and invariant $p^{(1)}$ which, in fact, is a velocity head of the gas flow on the ablation surface Σ.

Formulae (54) and (55) establish only on what arguments the rates D_{Me} and D_{Mi} of matrix ablation are dependent. Further content of the paragraph is devoted to determination of the functions $D_{Me}(p_\Sigma, \theta_w)$ and $D_{Mi}(\theta_w)$.

RATE OF INTERNAL EROSION OF MATRIX D_{Mi}

Expression for rate D_i is determined on the basis of joint solving the heat-cunductivity, filtration equations and kinetic equation describing the pyrolysis process in quasistatic approximation ($\frac{\partial}{\partial t} \to 0$) and has the form:

$$\frac{\partial \varphi_2}{\partial \bar{x}} = \frac{J_m^0}{\rho D_i}\varphi_2 \exp\left(-\frac{E_{am}}{R\theta}\right), \qquad 0 \le \bar{x} < +\infty;$$

$$\frac{\partial \theta}{\partial \bar{x}} + \frac{k_m}{\rho_m c_m D_i}\frac{\partial^2 \theta}{\partial \bar{x}^2} = 0;$$

$$\frac{\partial \rho_g(1-\varphi_2)}{\partial \bar{x}} + \frac{K}{D_i}\frac{\partial^2 p_g}{\partial \bar{x}^2} + \rho\frac{\partial \varphi_2}{\partial \bar{x}} = 0; \tag{56}$$

$$p_g = p_e; \quad \theta = \theta_w, \quad \bar{x} = 0; \qquad \theta = \theta_0, \quad \varphi_2 = \varphi_2^0, \quad \bar{x} = +\infty;$$

$$\frac{\partial \rho_g(1-\varphi)}{\partial \bar{x}} = 0, \qquad \bar{x} = \bar{x}^*;$$

where θ_0 and $\varphi_2^0 = 1$ are the temperature and polymer phase concentration of the cold material; $\bar{x}$ - mobile coordinate connected to the ablation surface: $\bar{x} = x - x_D$ (Fig. 20a), ρ_g - density of the gas phase, J_m^0 - pre-exponential multiplier, K - gas permeabliity coefficient of the material matrix.

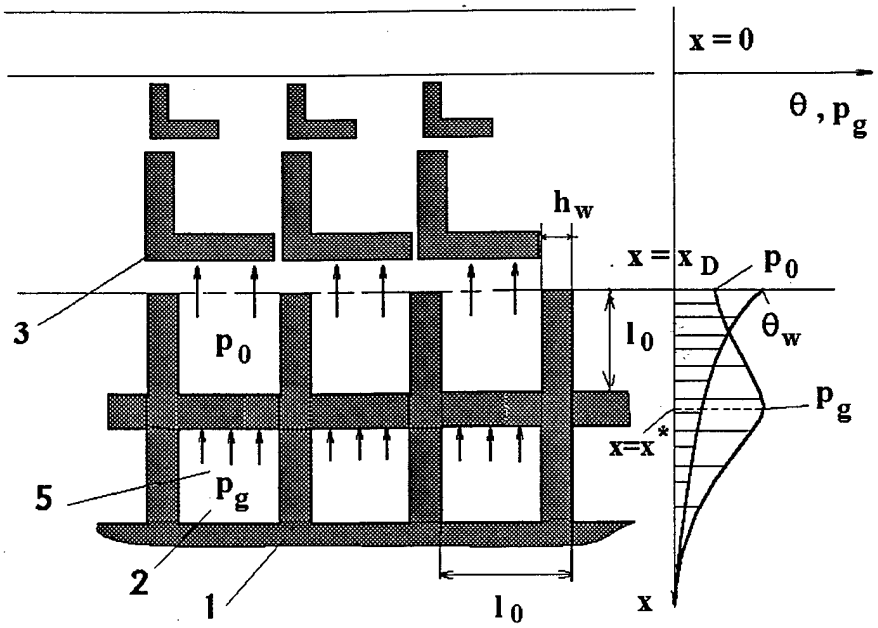

(a)

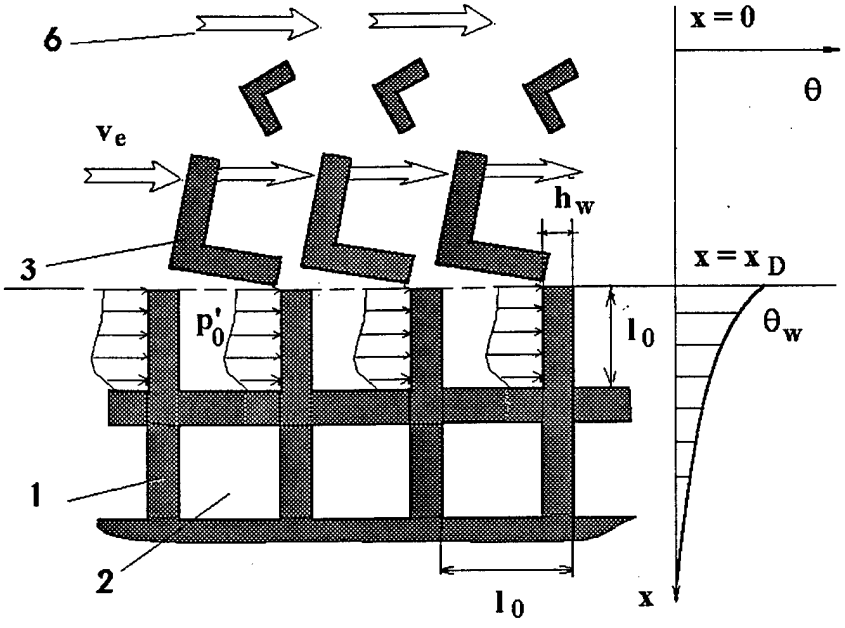

(b)

Fig. 20.

Models of processes of thermo-mechanical erosion of composites for calculations of linear ablation rates:
a) Model of internal erosion of a matrix for calculation of rate D_{Mi}
b) Model of external erosion of a matrix for calculation of rate D_{Me}
1 - matrix (solid phase), 2 - pore, 3 - dispresed particles of matrix in gas flow, 4 -fibre, 5 - pore gas pressure, 6 - overrunning hot gas flow.

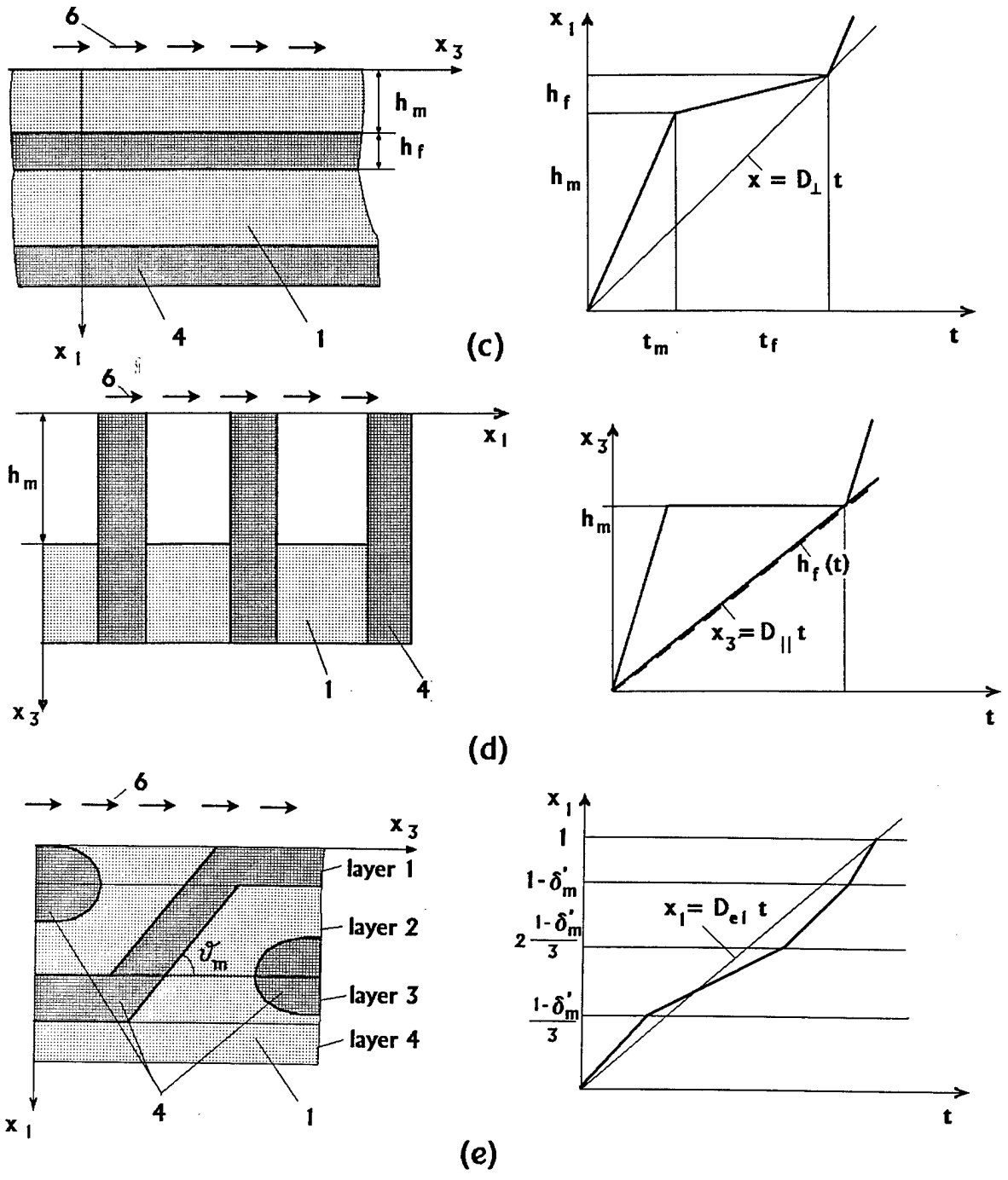

Fig. 20.

Models of processes of thermo-mechanical erosion of composites
for calculations of linear ablation rates:
c) Model of external erosion of unidirectional composite for calculation of rate $D_\perp$
d) Model of external erosion of unidirectional composite for calculation of rate $D_{||}$
e) Model of external erosion of fabric composite for calculation of rate D_{e1}
1 - matrix (solid phase), 2 - pore, 3 - dispresed particles of matrix in gas flow,
4 -fibre, 5 - pore gas pressure, 6 - overrunning hot gas flow

A typical graph of dependence of pore gas pressure p_g on coordinate $\bar{x}$ for ablative matrix has a local maximum (Fig. 20a). The presence of this maximum is a typical peculiarity of heating of materials, wherein there can occur a thermo-decomposition, that was established by direct numerical solving the equations (56) of internal heat-mass-transfer [1, 6]. In order to find an approximate analytical solution of system (56), a boundary condition for the filtration equation of the problem (56), with using the existence of local extremum of function $p(\bar{x})$ at a certain point $\bar{x}^*$, was formulated in the form: $\partial p/\partial \bar{x} = 0$ at $x = \bar{x}^*$. At the same point $\bar{x}^*$ a thermo-decomposition process only starts, therefore we can assume that $\varphi_2(\bar{x}^*) \approx 1$. Solution of the third equation of system (56) is sought within the domain $0 \leq \bar{x} \leq \bar{x}^*$.

Then solution of the system (56) has the form:

$$\frac{\partial p_g}{\partial \bar{x}} = \frac{D_i}{K}(1-\varphi_2)(\rho_m - \rho_g), \quad 0 \leq \bar{x} \leq \bar{x}^*;$$

$$\varphi_2 = \exp\Big(-\frac{J_m^0}{\rho_m D_i} I(\bar{x})\Big), \quad 0 \leq \bar{x} < +\infty; \tag{57}$$

$$\theta - \theta_0 = \theta_W \exp\big(-\frac{\rho_m c_m D_i}{k}\bar{x}\big),$$

where

$$I(\bar{x}) \equiv \int_{\bar{x}}^{\infty} \exp\,\big(-\frac{E_{am}}{R\theta(\bar{x}')}\big) d\bar{x}'. \tag{58}$$

Herein it is taken into account that usually $\rho_g \ll \rho$ for composite materials and $1 - \varphi_2(\bar{x}^*) \ll 1$.

To determine integral I the following approximation is used:

$$\exp\,\big(\frac{\rho_m c_m D_i \bar{x}}{k}\big) \longrightarrow \big(1 + \frac{\rho_m c_m D_i \bar{x}}{k}\big).$$

In particular, we obtain that

$$I(0) = \frac{k_m R_a \theta_w}{E_{am}\rho_m c_m D_i} \exp\,\Big(-\frac{E_{am}}{R\theta_w}\Big). \tag{59}$$

If $\varphi_2 = \varphi_w$ denotes a value of solid phase concentration of the matrix at the ablation surface $\bar{x} = 0$, then from equation (59) at $y = 0$ we obtain the expression for combustion rate D_i:

$$D_i = -\frac{J_m^0 I(0)}{\rho_m \ln\,\varphi_w}. \tag{60}$$

In accordance with the considered model, ablative material at its external surface of combustion has a regular structure (Fig. 20a) in the form of cells with wall thickness h_w and cavity dimension l_0 connected to φ_w by the relation:

$$\left(1+\frac{h_w}{l_0}\right)^{-3} = 1-\varphi_w. \tag{61}$$

Pyrolise process leads to descreasing wall thickness h_w. However, the value $h_w = 0$ can not be reached, as at a certain value of h_w there occurs mechanical destruction of the walls under the action of bending stresses σ in the wall caused by pore pressure p_g of pyrolytical gases.

An idealized scheme of a stress state of each the bulge of the ablation surface can be represented as cantilever bending of a beam by uniform pressure p_g. When the bending stress exceeds the strength limit of the matrix in tension, there occurs breaking-off a surface particle and its carrying-off to the gas flow.

The considered idealized model of erosion assumes that at each the elementary destruction a shape of a dispersed particle and a shape of the residual ablation surface remain self-similar (Fig. 20a).

The value of h_w for which there occurs destruction of the next layer of the matrix surface is determined by the formula for bending stresses:

$$\left(\frac{h_w}{l_0}\right)^2 = \frac{6(p_g-p_e)}{\sigma_{mT}}, \tag{62}$$

where σ_{mT} is the ultimate stress in tension (strength) of the matrix under temperature θ_w.

Expression for pressure difference $(p_g - p_e)$ near the ablation surface can be found with the help of linearized formula (57):

$$p_g - p_e = \frac{D_i}{K}\rho_m(1-\varphi_w)l_0, \tag{63}$$

where it was taken into account that at the combustion surface gas density in pores ρ_{gw} is much less than density of solid phase $\rho_{gw} \ll \rho_m$.

On substituting formula (63) into (62) and then (62) into (61), the equation for φ_w can be derived:

$$\varphi_w = 1-\left(1+\left(\frac{6D_i\rho_m l_0}{K\sigma_{mT}}(1-\varphi_w)\right)^{1/2}\right)^{-3}. \tag{64}$$

As a rule, $(6D_i\rho l_0)/(K\sigma_0) \gg 1$, therefore, solution of equation (64) can be represented in the form:

$$1 - \varphi_w = \left(\frac{K\sigma_{mT}}{6D_i\rho l_0}\right)^{3/5}. \tag{65}$$

Since $\varphi_w < 1$, we can make one more approximation, namely

$$\ln\ \varphi_w = \left(\frac{K\sigma_{mT}}{6D_i\rho_m l_0}\right)^{3/5}. \tag{66}$$

On substituting formula (59) and (66) into (60), the final expression for the erosion rate D_i can be found:

$$D_{Mi} = D_i = \left(\frac{k_m J_m^0}{\rho_m c_m}\right)^{\omega} \left(\frac{6\rho_m l_0}{k\sigma_{mT}}\right)^{2\omega-1} \cdot \left(\frac{R_a\theta_w}{E_a}\right)^{\omega} \exp\left(-\frac{E_a\omega}{R_a\theta_w}\right); \quad \omega = 5/7. \tag{67}$$

RATE OF EXTERNAL EROSION OF MATRIX D_{Mi}

Unlike internal erosion when material particles at the surface destruct under the action of internal forces (intrapore pressure), ablation surface particles' destruction (erosion) at the presence of an external high-speed flow occurs due to the action of local pressure p_Σ onto bulging parts of the ablation surface (Fig. 20b).

A scheme of mechanical destruction of an matrix surface under the action of an external flow is analogous to the scheme of internal erosion, therefore formulae (58) - (62) also take place but instead of the pressure difference $p_g - p_e$ we should consider the pressure head p_Σ:

$$\left(\frac{h_w}{l_0}\right)^2 = \frac{6p_\Sigma}{\sigma_{mT}}. \tag{68}$$

On substituting formula (68) into (62) and then into (61), we find the expression for function φ_w:

$$-\ln\ \varphi_w = \chi\left(\frac{p_\Sigma}{\sigma_{mT}}\right) \equiv -\ln\Big(1 - \big(1 + (\frac{6p_0'}{\sigma_{mT}})^{1/2}\big)^{-3}\Big), \tag{69}$$

Then from equations (59), (60) and (69) we obtain the expression for D_{Me}:

$$D_{Me} = \frac{1}{\rho_m}\left(\frac{J_m^0 k_m}{c_m\chi(p_s/\sigma_{mT})}\right)^{1/2} \cdot \left(\frac{R\theta_w}{E_{am}}\right)^{1/2} \exp\left(-\frac{E_{am}}{2R\theta_w}\right). \tag{70}$$

9.5.3. TRANSVERSALLY ISOTROPIC COMPOSITES

For transversally isotropic media which have only one axis, for example Ox_3', of transverse isotropy (they are, for example, unidirectionally reinforced composites), a number $n = 2$, there are two tensors $\underset{\sim}{a}^{(\varkappa)}$ and invariants (50) have the form:

$$n = 2, \quad a_{ij}^{(2)} = \delta_{i3}\delta_{j3}; \quad a_{ij}^{(1)} = \delta_{i1}\delta_{j1} + \delta_{i2}\delta_{j2};$$

$$a^{(2)} = n_3^2, \quad a^{(1)} = n_1^2 + n_2^2, \tag{71}$$

and expressions (51), (52) for the rate D_e take the form:

$$D_e = D_{\|}(p_\Sigma, \theta_w)n_3^2 + D_\perp(p_\Sigma, \theta_w)(n_1^2 + n_2^2). \tag{72}$$

As follows from formula (72), for transversally isotropic composites there exist two different functions: $D_{\|}$ - rate of external erosion of surface Σ being orthogonal to the Ox_3 axis of transverse isotropy and $D_\perp$ - rate of external erosion of surface Σ of the composite being orthogonal to axis Ox_1 or Ox_2.

RATE OF THERMO-MECHANICAL EROSION OF FIBRES

Although fibres without matrix are not independent constructional material, but theoretically we can consider separately a process of thermo-mechanical erosion a hypothetic material, properties of which are coincident with properties of monofibres. This hypothetic material is transversally isotropic, as many fibres, in particular carbon fibres, are anisotropic: properties along and across fibres can be very essentially different. Rate of thermo-mechanical erosion of fibres is determined similarly to formulae (72), (74):

$$D_{ef} = D_{f\perp}(p_\Sigma, \theta_w)(n_1^2 + n_2^2) + D_{f\|}(p_\Sigma, \theta_w)n_3^2. \tag{73}$$

The concept of the hypothetic material of 'fibres' allows us for determination of rates $D_{f\perp}$, $D_{f\|}$ to use the models developed for a matrix, therefore formulae

for these rates have the form similar to (70):

$$D_{f\perp}(p_\Sigma, \theta_w) = \frac{1}{\rho_f}\left(\frac{J_f^0 k_f}{c_f \chi(p_\Sigma/\sigma_{f\perp})}\right)^{1/2}\left(\frac{R_a\theta_w}{E_{af}}\right)^{1/2}\exp\left(-\frac{E_{af}}{R_a\theta_w}\right); \qquad (74)$$

$$D_{f\parallel} = D_{f\perp}\left(\frac{\chi(p_\Sigma/\sigma_{f\perp})}{\chi(p_\Sigma/\sigma_f)}\right)^{1/2}, \qquad (75)$$

where σ_f and $\sigma_{f\perp}$ are strength of monofibres in the longitudinal and perpendicular directions; k_f, ρ_f, c_f are heat-physical characteristics of the fibres; J_f^0 and E_{af} are the pre-exponential multiplier and activation energy of the process of thermo-oxidative decomposition of carbon fibres.

RATES OF EXTERNAL EROSION $D_\perp$ and $D_\parallel$ OF UNIDIRECTIONAL COMPOSITES

Rate of external thermo-mechanical erosion $D_\perp$ in formulae (72) can be determined with the help of the model presented in Fig. 20c in the form of a multilayer material consisting of periodically repeated layers of a matrix and hypothetic material of fibres. Let thicknesses of the layers be h_m and h_f, t_m and t_f be times during which there occurs a complete recession of one layer of the matrix and fibre, respectively

$$t_m = h_m/D_{me}\,, \quad t_f = h_f/D_{f\perp} \qquad (76)$$

and let us introduce ablation rate $D_\perp$ of the whole multilayer material

$$D_\perp = \frac{h_m + h_f}{t_m + t_f}, \qquad (77)$$

then from (76) and (77) we obtain:

$$D_\perp = \left(\frac{1-\delta_m}{D_{f\perp}} + \frac{\delta_m}{D_{me}}\right)^{-1}, \qquad (78)$$

where $\delta_m = h_m/(h_f + h_m)$ is the relative thickness of matrix interlayer between the layers of fibres in the unidirectional composite. It is the desired formula that connects ablation rates of matrix D_{me} and fibres $D_{f\perp}$.

Rate of thermo-mechanical erosion $D_{\|}$ on the surface Σ being orthogonal to the Ox_1 axis under the action of a flow across the direction of laying the fibres can be determined with the help of the following model. Let us consider a multilayer material consisting of periodically repeated layers of matrix and fibres. Unlike the case considered above, herein the matrix and fibres' layers are oriented across the direction of motion of the gas flow (Fig. 20d). Mechanical erosion of matrix and fibres in this multilayer material occurs simultaneously but with different rates: $D_{me} > D_{f\|}$,therefore for the same time t_f a thickness of matrix carried off h_m is more than h_f, where $h_m = D_{me}t_f$; $h_f = D_{f\|}t_f$. There appears a nonsmooth surface Σ of ablation: 'holes' forms in the places of the matrix carried off. However, when the thickness h_f reaches the certain value, recession of the matrix comes to a halt, as erosional action of the flow within the 'hole' eases towards its depth. The recession process of the matrix is resumed, when the thickness h_f of the fibre carried off reaches value of h_m (this model is presented in Fig. 20c). Hence, a total rate of recession of the multilayer material $D_{\|}$ will be close numerically to the value of recession rate of the fibre:

$$D_{\|} = D_{f\|}. \tag{79}$$

9.5.4. FABRIC COMPOSITES

Fabric composites, for which directions of warp and fill have the same rights, can be consider as transversally isotropic with a plane of isotropy being coincident with the plane of laying the fabric. Let the Ox_1 axis be coincident with the normal to the plane. Then for such the composite, number $n = 2$ and tensors $\underset{\sim}{a}^{(\varkappa)}$ have the following form in the coordinate system Ox_i:

$$n = 2, \quad a_{ij}^{(2)} = \delta_{i2}\delta_{j2} + \delta_{i3}\delta_{j3}, \quad a_{ij}^{(1)} = \delta_{i1}\delta_{j1};$$

$$a^{(2)} = n_2^2 + n_3^2, \quad a^{(1)} = n_1^2, \tag{80}$$

and expressions (51) and (52) for rates of internal and external erosion have the form:

$$D_e = D_{e1}(p_\Sigma, \theta_w)n_1^2 + D_{e2}(p_\Sigma, \theta_w)(n_2^2 + n_3^2); \tag{81}$$

$$D_i = D_{i1}(\theta_w)n_1^2 + D_{i2}(\theta_w)(n_2^2 + n_3^2), \tag{82}$$

where D_{e1} is the rate of external erosion of the composite surface being orthogonal to the Ox_1 axis under the action of the flow onto the surface; D_{e2} is the rate of external erosion of the composite surface Σ being orthogonal to axis Ox_2 or Ox_3 under the action of the flow onto the surfaces respectively, and $D_{\|}$ is the rate of internal erosion on the surface orthogonal to the Ox_1 axis and D_{i2} - on the surfaces orthogonal to axes Ox_2 and Ox_3.

RATE OF EXTERNAL EROSION

To determine the erosion rate D_{e1} let us consider a model of a multilayer material consisting of periodically repeated four layers (see Fig. 20e): the first and third layers are represented by unidirectional composite with perpendicular (with respect to the flow direction) laying its fibres, their recession rate is coincident with $D_{\perp}$; the fourth layer is an interlayer of the matrix between the fabric layers, its erosion rate is D_{Me} and relative thickness is δ'_m, and the second layer is considered as unidirectional composite turned by angle ϑ_m with respect to the ags flow direction. Erosion rate of the second layer D_{ϑ} is evaluated with the help of formulae (72) and (73), in which we should assume $n_2 = 0$, $n_3 = \sin\vartheta_m$, $n_1 = \cos\vartheta_m$:

$$D_{\vartheta} = D_{\|}\sin^2\vartheta_m + D_{\perp}\cos^2\vartheta_m. \tag{83}$$

A total rate of recession of four-layer material D_1 is determined by the method of summing up, as it was shown for rate $D_{\perp}$ (78) of unidirectional composite:

$$D_{e1} = \left(\frac{2(1-\delta'_m)}{3D_{\perp}} + \frac{1-\delta'_m}{D_{\vartheta}} + \frac{\delta'_m}{D_M}\right)^{-1}. \tag{84}$$

Erosion rate D_{e2} on the surface orthogonal to the Ox_3 axis under the action of flow along the Ox_1 axis on the basis of conclusions given above for rate $D_{\|}$ of unidirectional composite and up to the certain accuracy can be considered as equal to rate $D_{f\|}$:

$$D_{e2} = D_{\|} = D_{f\|}. \tag{85}$$

RATE OF INTERNAL EROSION

Rates of internal erosion D_{i1} and D_{i2} can be determined in the similar way as it was made for ablative matrices with the only difference that in place of matrix strength σ_{mT} we should substitute strength of fabric composite in tension S_1^+ and S_2^+, respectively:

$$D_{i1} = D_{im}\left(\frac{\sigma_{mT}}{S_1^+}\right)^{2\omega-1}, \quad D_{i2} = D_{im}\left(\frac{\sigma_{mT}}{S_2^+}\right)^{2\omega-1}. \tag{86}$$

9.5.5. BIAS-REINFORCED FABRIC COMPOSITES

Rates $D_{\psi 1}$ and $D_{i\psi 1}$ of internal and external thermo-mechanical erosion of BRFC with angle ψ in the Ox_1x_3 plane can be readily evaluated with the help of formulae (81) and (82) for fabric composite. In these formulae we should assume $n_2 = 0$, $n_1 = \cos\psi$, $n_3 = \sin\psi$:

$$D_{e\psi 1} = D_{e1}\cos^2\psi + D_{e2}\sin^2\psi; \tag{87}$$

$$D_{i\psi 1} = D_{i1}\cos^2\psi + D_{i2}\sin^2\psi. \tag{88}$$

Total rate $D_{\psi 1}$ of thermo-mechanical erosion of BRFC is determined as follows:

$$D_{\psi 1} = D_{e\psi 1} + D_{i\psi 1}. + D_c + D_s. \tag{89}$$

9.5.6. CALCULATED RESULTS

Figure 14 shows calculated results for different components of thermo-mechanical erosion of 2-D composite: ablation rate of matrix D_M, unidirectional composite $D_{\|}$ and $D_{\perp}$ and also D_{e1}, D_{e2} and D_{i1} - as functions of surface temperature θ_w. As seen from the figure, the rate of thermo-mechanical ablation of matrix D_M is essentially higher than the rate of ablation of fibres $D_{\|}$ and $D_{\perp}$, but rates of

ablation of fabric composite D_{e1} and D_{e2} are close to the ablation rate of fibres in their numerical values.

Difference of rates $D_{\|}$ and $D_{\perp}$ is equal approximately to 30 % under $\theta_w = 3000$ K, and difference of rates D_{e1} and D_{e2} of fabric composite in different directions is just higher, approximately 60 %.

It is explained by that a matrix in fabric composite plays a greater role than in unidirectional composite.

As follows from Fig.14, magnitude of the internal erosion rate D_{i1} is also sufficiently high: it is equal approximately to 25 % of the external thermo-mechanical erosion rate D_{e1}.

Table 13 gives the correponding numerical values of the functions.

§9.6. COMPARISON OF THEORETICAL AND EXPERIMENTAL RESULTS ON ABLATION RATE

To verify an adequacy of the developed model of linear ablation we conducted a comparison of numerical results of the total linear rate of ablation D_1 on the surface orthogonal to the Ox_1 axis and of experimental data for Generic 2-D Carbon/Phenolic Fabric Composites from work [5]. Velocity head was chosen $p'_0 = 5$atm, pressure p_Σ - equal to p'_0: $p_\Sigma = p'_0 = 5$ atm. Rate D_1 was determined in the form of function of surface temperature θ_w:

$$D_1 = D_c + D_s + D_{m1}, \tag{90}$$

$$D_{m1} = D_{e1} + D_{i1};$$

and constants contained in the expression for D_1

$$J_i^0,\ E_{ai},\ \Gamma_i,\ J_f^0,\ E_{af},\ \Gamma_f; \tag{91}$$

$$k_m,\ c_m,\ \rho_m,\ k_f,\ c_f,\ \rho_f,\ K_0;$$

$$\sigma_\perp^0,\ \bar{\sigma}_f^0,\ \sigma_{f\perp},\ S_{1+},\ S_{2+},$$

and also $\delta_m = 0.1,\ \ l_0 = 10^{-3}$ m

were determined before in [1].

It should be noted that formulae (86) - (90) allow us to determine the rate of thermo-mechanical ablation D_M of 2-D composite with using only mechanical and heat-physical constants (91) without any empirical formulae for recession rates of matrix and fibres.

Figure 15 shows calculated results of different rates of ablation for 2-D carbon/Phenolic Composite: external thermo-mechanical erosion rate D_{e1}, internal erosion rate D_{i1} and also linear rate of combustion D_c, sublimation D_s and total rate of recession D_1. As seen from this figure, under temperatures 1200 - 2000 K a main contribution into recession rate D_1 is of combustion rate D_c and external thermo-mechanical erosion D_{e1}. Under temperatures 2000 - 3000 K diffusive combustion rate D_c is stabilized, and D_{e1} continues to grow. Under these temperatures internal erosion rate D_{i1} also becomes essential. Under temperatures 3000 - 4000 K there occurs a sublimation of carbon components of the composite and its rate gives a main contribution to the ablation rate D_1 of the composite.

Points in Figure 15 indicate experimental values of ablation rate D_1 from [5]. Under $\theta_w = 3000$ K experimental values of D_1 are in the interval from 0.5 to 0.67 mm/s, and theoretical values are equal to 0.6 mm/s. Thus, the accuracy of modelling of the process of linear ablation of 2-D Carbon/Phenolic Composite is sufficiently high: it predicts the magnitude of D_1 falling within the domain of spread in experimental data.

Figure 16 shows a dependence of thermo-mechanical erosion coefficient ϵ

$$\epsilon = \frac{D_{m1}}{D_1} \tag{92}$$

on temperature θ_w at different values of velocity head p_0'. It is seen, that at initial period of heating under 900 - 1200 K values of ϵ are the closest to 1, as recession is determined, in the main, by mechanical ablation. Under temperatures 1200 - 2000 K, as mentioned above, an essential contribution is of combustion rate D_c, therefore, values of ϵ decrease to 0.4 - 0.6. Since under temperatures 2000 - 3000 K diffusive combustion rate D_c is stabilized, value of ϵ anew grows up to 0.6 - 0.8. And, finally, when sublimation process starts within the interval $\theta_w = 3000$ - 4000 K, value of the thermo-mechanical erosion coefficient falls down practically to zero.

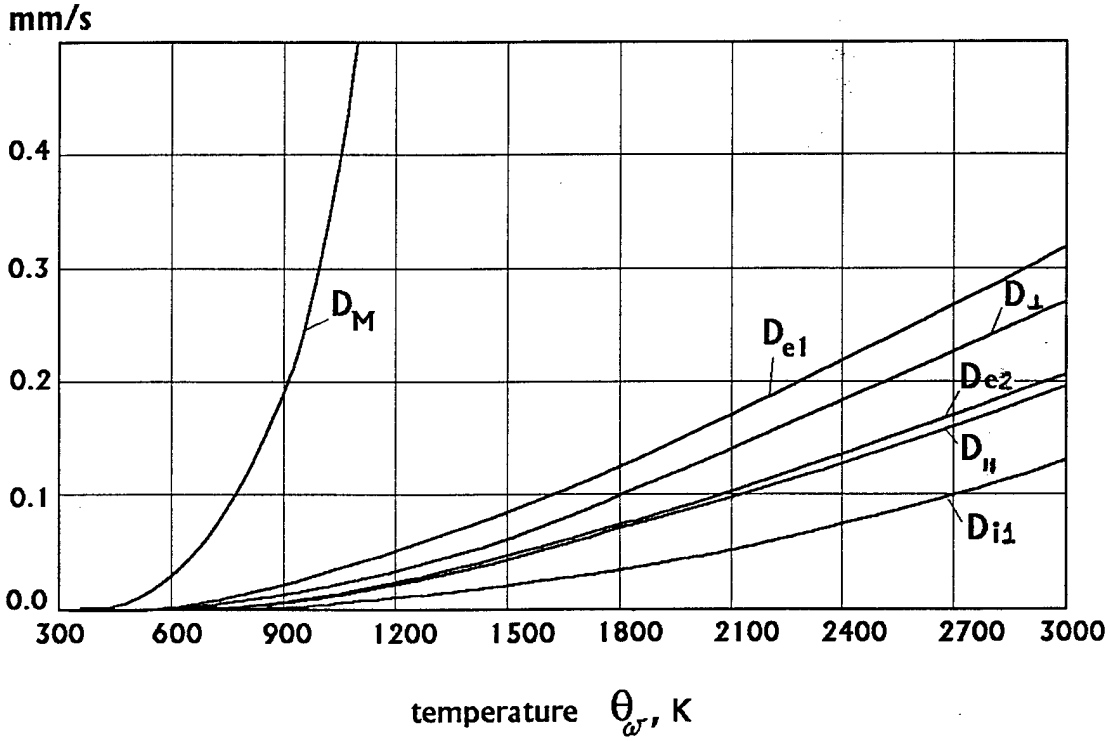

Fig. 14.

Varying Rates of Thermo-mechanical Recession of Phenolic Matrix (D_m), Unidirectional Composite ($D_\perp$) and ($D_{//}$) and 2-D Fabric Composite (D_{e1}, D_{e2}) and Internal Erosion Rate D_{i1} of 2-D Carbon/Phenolic Composite versus temperature θ at p_o'= 5.25 atm.

Tabl. 13

Rates of Thermo-Mecanical Ablation :

1. Exteranl T-M Erosion for Phenolic Matrix D_{Me} ,
2. Exteranl T-M Erosion for Unidirectional Carbon/Phenolic Composite along Fibers $D_{\parallel}$,
3. Exteranl T-M Erosion for Unidirectional Carbon/Phenolic Composite Across Fibers $D_{\perp}$,
4. Exteranl T-M Erosion for 2-D Textile Carbon/Phenolic Composite along Fabric D_{e2} ,
5. Exteranl T-M Erosion for 2-D Textile Carbon/Phenolic Composite Across Ply Fabric D_{e1} ,
6. Internal T-M Erosion for 2-D Textile 2-D Textile Carbon/Phenolic Composite D_{i1} .

Temperature, K θ_w	Rates of Recession, mm/s					
	D_{Me}	$D_{\parallel}$	$D_{\perp}$	D_{e2}	D_{e1}	D_{i1}
295.0	.000	.000	.000	.000	.000	.000
1000.0	.327	.013	.018	.014	.021	.003
1500.0	1.509	.047	.063	.049	.077	.018
2000.0	3.386	.094	.125	.097	.153	.049
2500.0	5.640	.145	.193	.150	.237	.091
3000.0	8.061	.197	.263	.205	.322	.140

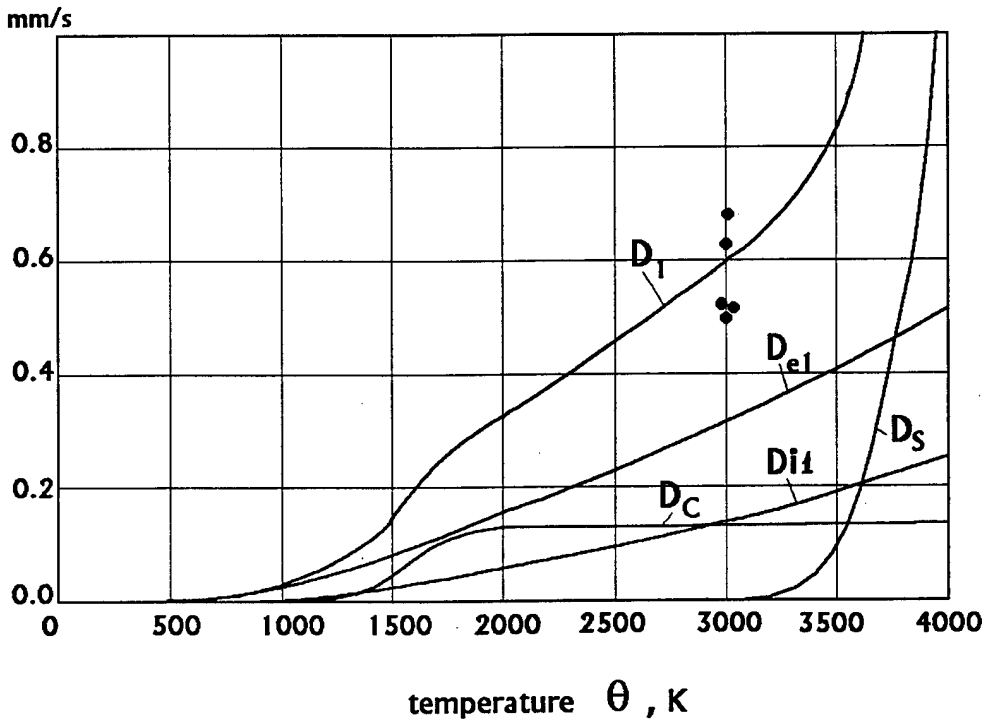

Fig. 15.

Varying Rates of Thermo-mechanical (D_{e1} and D_{it}) and Thermo-chemical Ablation (D_c and D_s) and total rate of ablation D_1 of 2-D Carbon/Phenolic Composite versus temperature θ at $p = 5.25$ atm in air. Solid curves - calculated results, points - experimental data of D_1 [5].

Tabl. 14

Relation Between Rates of Thermal-Mechanical and Thermo-chemical Ablation of 2-D Carbon/Phenolic Composite at P_o'=5 atm in air

Temperature θ_w K	Rate of Recession, mm/s				
	Sublimation D_S	Combustion D_c	External T-M erosion D_{e1}	Internal T-M erosion D_{i1}	Total D_1
1500.0	.000	.047	.077	.018	.142
2000.0	.000	.127	.154	.049	.329
2500.0	.000	.135	.238	.091	.464
3000.0	.002	.136	.324	.140	.603
3500.0	.084	.136	.409	.196	.824
4000.0	1.449	.136	.491	.254	2.331

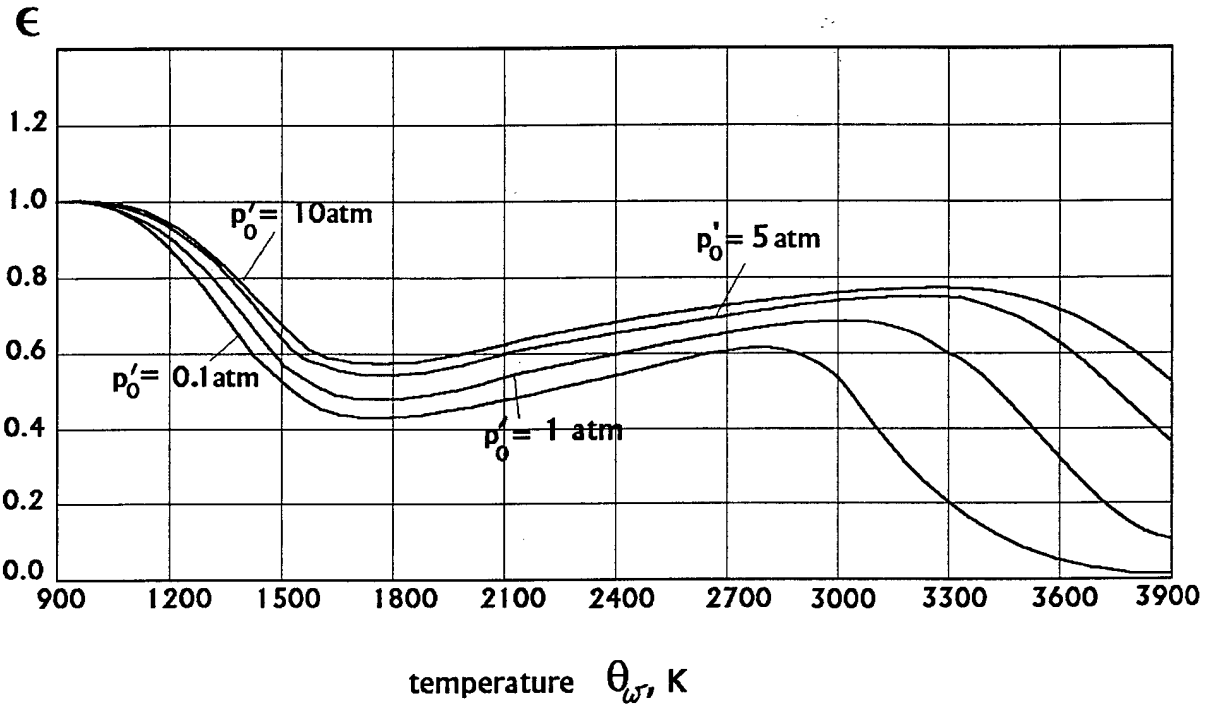

Fig. 16.

Varying Coefficient of Thermo-mechanical Erosion ϵ of 2-D Carbon/Phenolic Composite versus temperature θ_w at different values of valocity head in air.

Tabl.15

Varying Coefficient of Thermal-Mechanical Erosion of 2-D Carbon/Phenolic Composite on Temperature at different values of Velosity Head in air

Temperature, K θ_w	Coefficient ϵ				
	P_o'=0.01	0.1	1.	5	10 atm
1500.0	.514	.548	.595	.641	.665
2000.0	.447	.479	.525	.572	.597
2500.0	.541	.579	.623	.665	.688
3000.0	.171	.527	.681	.730	.750
3500.0	.007	.069	.410	.680	.745
4000.0	.000	.005	.059	.259	.416

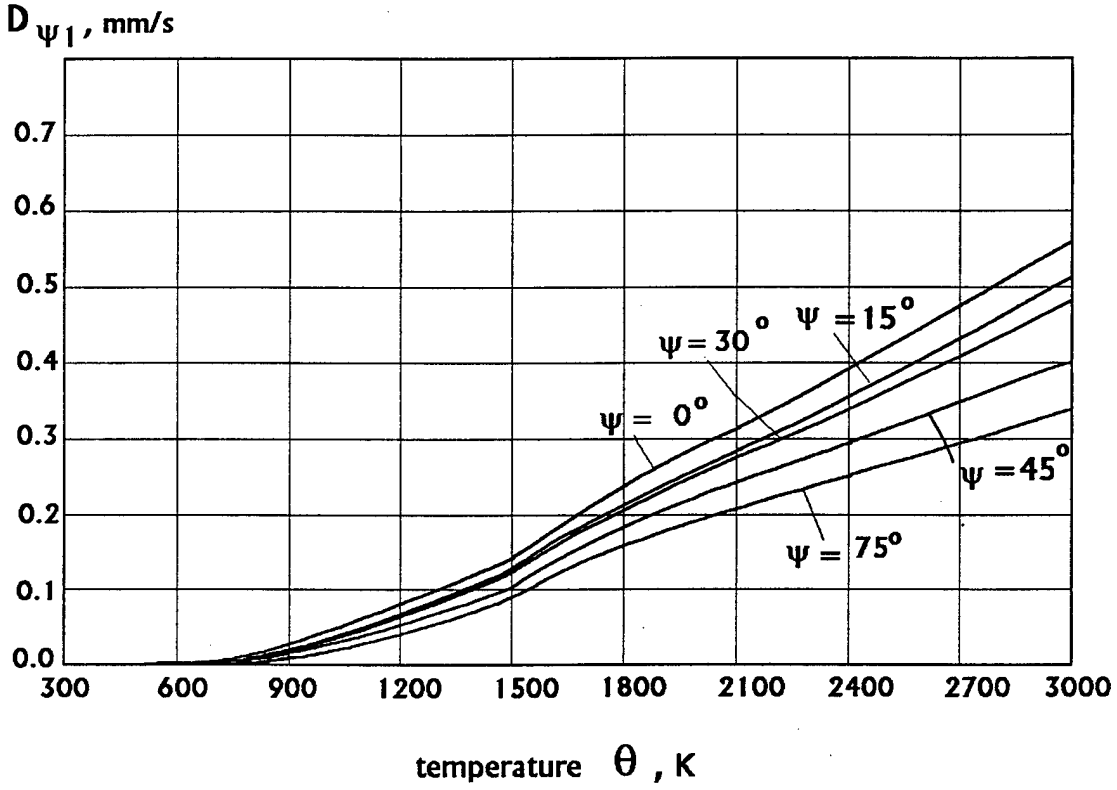

Fig. 17.

Varying Ablation Rates of Carbon/Phenolic Composite versus temperature θ at different bias angles ψ and $p_0' = 3$ atm in air.

Tabl.16

Varying of Total Ablation Rates of Carbon/Phenolic BRCM vs Temperature for different values of angle ψ at P =3 atm in air

Temperature, K θ_w	Rate of Recession $\mathcal{D}_{\psi 1}$ mm/s					
	angle ψ =0°	ψ=15°	ψ=30°	ψ=45°	ψ=60°	ψ=75
1500.0	.138	.135	.126	.114	.101	.092
2000.0	.280	.273	.255	.231	.206	.188
2500.0	.403	.393	.365	.327	.289	.26
3000.0	.531	.517	.479	.427	.375	.33
3500.0	.737	.719	.671	.606	.540	.492
4000.0	2.176	2.155	2.097	2.019	1.940	1.882

With increasing the velocity head p'_0, value of the coefficient ϵ also grows (see Fig.16).

The corresponding numerical values are given in Table 15.

Figure 17 shows calculated results of the total rate of recession $D_{\psi 1}$ of composite BRFC for $p'_0 = 3$ atm ($p_\Sigma = p'_0 = 3$ atm) as a function of surface temperature θ_w for different values of angle $\psi = 0$, 15, 30, 45, 60, 75°.

Heat-transfer coefficient (α/c_p) was assumed to be equal to $(\alpha/c_p) = 1.1$ kg/m$^2\cdot$ s. As seen from Figure 17, with increasing angle ψ the recession rate $D_{\psi 1}$ of BRFC lowers within all the temperature θ_w interval. Under $\theta_w = 3000$ K values of rate $D_{\psi 1}$ are equal to 0.53, 0.48 and 0.34 for angles 0°, 30° and 75°, respectively. Thus, for small angles ψ (0° - 30°) lowering the ablation rate is not very essential ($\approx$ 10 % as compared with angle $\psi = 0°$), and only for greater angles (60° - 75°) this lowering is equal approximately to 35 %.

The corresponding numerical values $D_{\psi 1}$ are given in Table 6.

§9.7. CALCULATION OF HEAT FLUX ON ABLATIVE SURFACE

To determine true temperature of ablative surface θ_w of composite under the action of overrunning hot gas flow, it is necessary to take account of processes of heat and mass transfer occuring on this surface.

Total heat flux q_e to the ablative surface of the composite, which is consumed for warming up the material, consists of the following components:

$$q_e = q_e^0 - q_R - q_{bl} - q_w - q_{sub} + q_{cs} + q_{cg}, \tag{93}$$

where

$q_e^0 = (\alpha/c_p)(H_r - H_0)$ - convective heat flux to the 'cold wall' supplied from the heated boundary layer to the composite surface Σ,

$q_w = (\alpha/c_p)(H_w - H_0)$ - convective heat flux carried off from the surface Σ heated up to temperature θ_w into the surroundings,

$q_R = \varepsilon_w \sigma_{SB} \theta_w^4$ - radiational heat flux carried off from the surface Σ at the expense of own radiation of the surface,

$q_{bl} = \gamma_{bl}(\rho_g v_g)_w(H_r - H_w)$ - convective heat flux carried off from the heated surface Σ at the expense of injection into the boundary layer of gaseous products of thermo-decomposition of phenolic matrix,

$q_{sub} = \rho_w D_s \Delta Q_{sub}$ - heat flux carried off from the composite surface Σ at the expense of physico-chemical process of sublimation of the composite,

$q_{cs} = \rho_w D_c Y_1 \Delta Q_{com}$ - heat flux supplied to the composite surface Σ at the expense of exothermal process of combustion of solid phases of the composite in the oxidizing overrunning flow,

$q_{cg} = \gamma_{bl}(\rho_g v_g)_w D_c \sum_i \Delta Y_i \Delta Q_i$ - heat flux supplied to the composite surface Σ at the expense of exothermal process of combustion of gaseous products of thermo-decomposition of polymer binder injected into the boundary layer.

There is a following notation:

(α/c_p) - heat-transfer coefficient between the composite surface Σ and boundary layer of hot gas;

H_r - enthalpy of the overrunning flow;

$H_w = c\theta_w$ - enthelpy of the composite surface heated;

$H_0 = c\theta_0$ - enthalpy of the 'cold wall';

σ_{SB} - Stefan-Boltsman constant;

ε_w - degree of blackness of the heated surface;

γ_{bl} - injection coefficient $(0 < \gamma_{bl} < 1)$;

ΔQ_{sub} - heat of sublimation of carbon phases of the composite;

ΔQ_{com} - heat of combustion of solid phases of the composite (absolute value);

ΔQ_i - combustion heat of gaseous products of phenolic matrix thermo-decomposition (absolute value);

Y_1 - mass concentration of carbon component on the composite surface Σ;

ΔY_i - changing mass concentrations of chemical components in the mixture of gaseous products of thermo-decomposition of phenolic matrix at combustion on the surface Σ;

$(\rho_g v_g)_w = -(K\nabla p_g)_w \cdot \vec{n}$ - mass rate of injection of gaseous products of phenolic matrix thermo-decomposition into the boundary layer,

$(\nabla p_g)_w$ - pore pressure gradienton the ablation surface Σ.

To conduct numerical calculations, we use the following values of constants:

$$(\alpha/c_p) = 1.1 \text{ kg/m}^2 \cdot \text{s}; \quad q_e^0 = 12 \text{ MW/m}^2; \quad \theta_0 = 295K;$$

$$\varepsilon_w = 0.8; \quad \gamma_{bl} = 0.4; \quad \Delta Q_{sub} = 20 \text{ MJ/kg};$$

$$\Delta Q_{com} = 9.8 \text{ MJ/kg}; \quad Y_1 = 1.$$

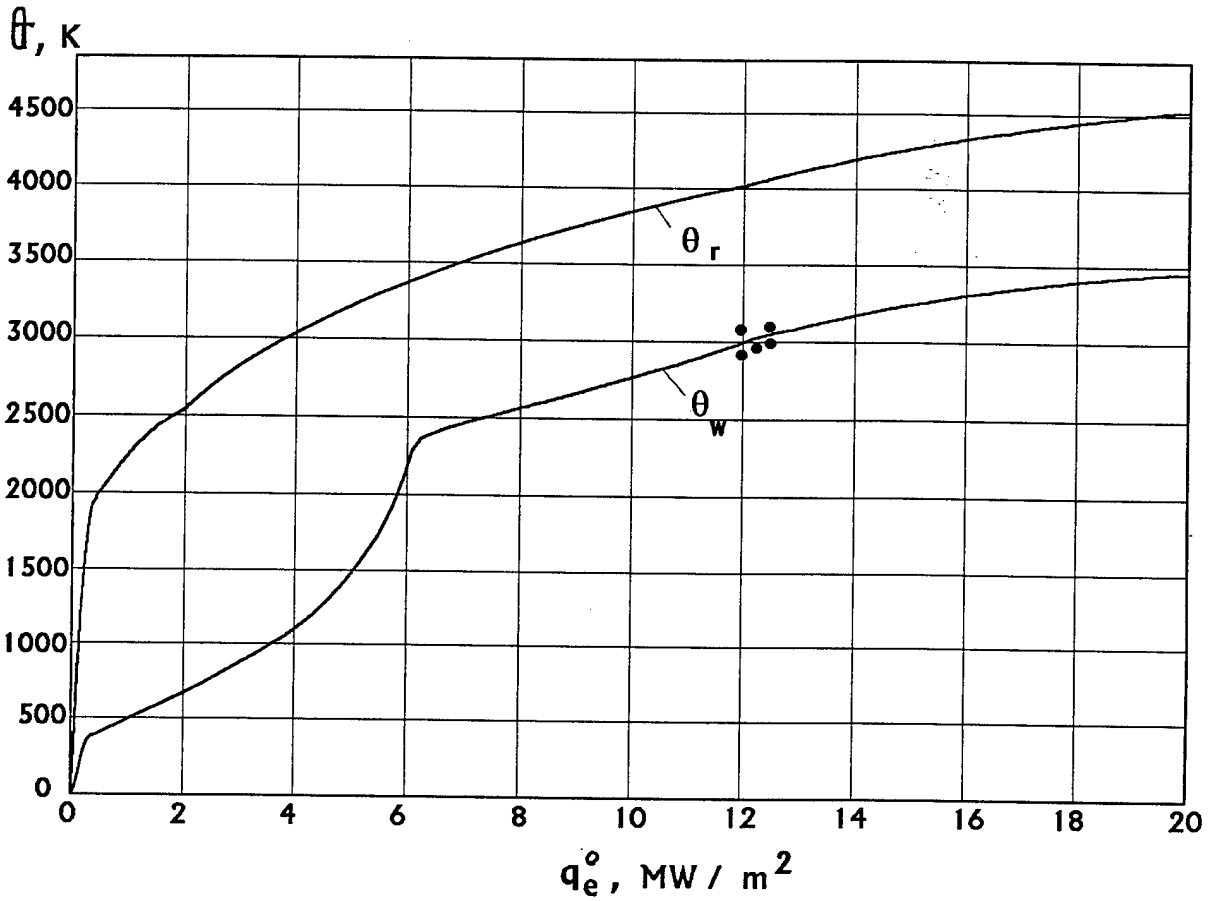

Fig. 18.

Dependence of equilibrium temperature θ_r and
true temperature of the surface θ_w (•)
of 2-D Carbon/Phenolic Composite on Cold Wall Convective Heat Flux q_e°.
Solid curves - calculated results, points - experimental data[5].

Tabl. 17

Varying of Equilibrium and True Temperatures of Ablation Surface vs Cold Wall Heat Flux q_e°

Heat flux, MW/m2 q_e°	Temperature θ, K	
	Equilibrium Temperature θ_r	True Temperature θ_w
6.8	3484	2430
7.6	3582	2531
10.2	3856	2813
12.6	4065	3029
16.0	4315	3257

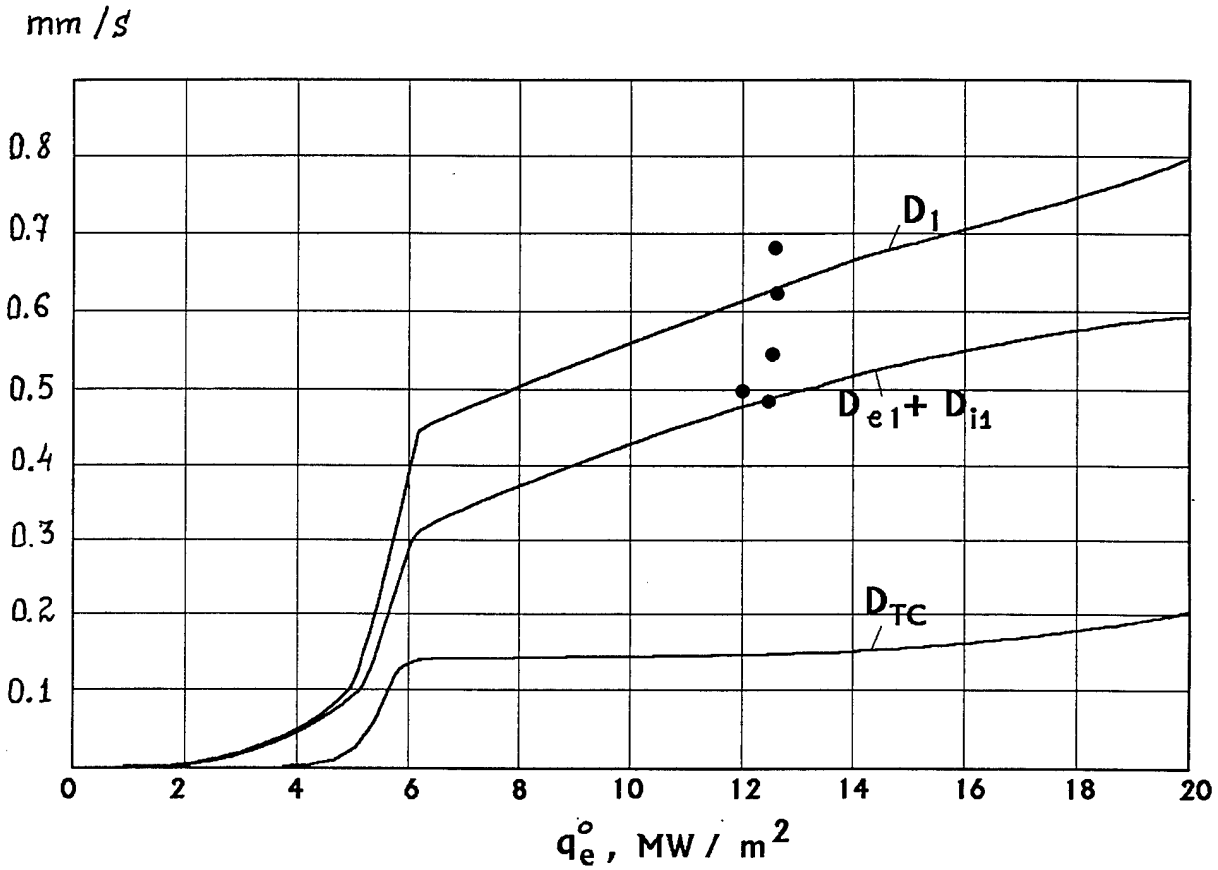

Fig. 19.

Varying Rates of Thermo-mechanical ($D_{e.1} + D_{i1}$), Thermo-chemical (D_{TC}) and total D_1 Ablation of 2-D Carbon/Phenolic Composite versus Heat Flux q_e^o at $p_o' = 5$ atm in air. Solid lines - calculated results, • - experiments [5].

Tabl. 18

Varying Rates of Thermal-Mechanical and Thermo-Chemical Ablation of 2-D Carbon/Phenolic Composite on Heat Flux q_e°, at P_o'=5 atm in air

HEAT FLUX, MW/m2	Rate of Recession, mm/s		
q_e°	Thermo-Chemical Ablation D_{TC}	Thermo-Mechanical Ablation D_{m1}	Total Ablation D_1
4.0	.001	.047	.049
6.8	.135	.336	.471
7.6	.135	.360	.496
10.2	.137	.429	.566
12.0	.139	.467	.606
16.0	.158	.531	.689

Chapter X

CALCULATION OF INTERNAL HEAT-MASS-TRANSFER AND THERMOSTRESSES IN A CYLINDRICAL SHELL MADE OF BRFC UNDER THE ACTION OF A HIGH-TEMPERATURE GAS FLOW

The aim of the present Chapter is to conduct calculations of fields of temperature θ, pore gas pressuure p, volumetrical phase concentrations φ_i, and also thermostresses caused by nonuniform heating and volumetrical ablation in a cylindrical shell (Figure 1) made of Bias-Reinforced Carbon/Phenolic Composite under the action of a high-temperature gas flow onto the shell.

§10.1. MATHEMATICAL PROBLEM STATEMENT

A general statement of the mathematical problem on coupled calculation of internal heat-mass-transfer and thermostresses in ablative composite materials has been formulated in [1] and also in our previous works [6-9]. Let us apply this model for calculation of a cylindrical shell made of BRFC (Figure 1).

Let us consider further a cylindrical coordinate system $Or\vartheta z$ and assume that the axes of the system are coincident with the axes of the coordinate system Ox_i considered above and rotated by angle ψ about principal orthotropy axes Ox_i' of the composite.

Let us consider a hollow cylinder of ablative material BRFC subjected to intensive heating on the external side. Convective heat fluxes q_e and pressures p_e are uniformly distributed on the lateral surface.

There is a total pressure of overrunning flow $p_e = p_{e0} + p_0'$ at the external surface of the cylinder $r = R_0$, where p_{e0} is the static pressure of quiescent atmosphere, p_0' is the velocity head of gas $p_0' = \rho_{ge} v_{e3}^2$, ρ_{ge} is the density of gas flow on the composite surface, $v_{e3} = V_3$ is the component of gas velocity $\vec{V}$ at the external surface of the boundary layer (in the Oz axis direction). Projection of the flow velocity vector $\vec{V}$ on the cylinder surface $r = R_D$ (ablation surface Σ) is

determined from (46) as: $V_{\Sigma 1} = V_{\Sigma 2} = 0$; $V_{\Sigma 3} = V_3 = v_{e3}$. Pressure p_Σ from (50) is determined as follows: $p_\Sigma = \rho_{ge} V_3^2 = p_0'$. At the internal surface of the cylinder $r = R_1$ a pressure is assumed to be equal to static pressure p_{e0}.

Both the ends of the cylindrical shell $z = 0$ and $z = L$ are assumed to be free from stresses, i.e. $\sigma_z = -p_{e0}$ at $z = 0, L$. The ends are assumed to be hermetic and heat-insulated.

Let us state the following problem: to determine parameters of internal heat-mass-transfer in an ablating structure and to find stresses in the structure caused by external heating and ablation (volumetric and surface).

Conditions of the problem allow to use a statement in terms of stresses (see item [1]).

In the scope of these assumptions a solution of the problem is sought in the form of functions depending on radius r and t. Stresses are determined as follows:

$$\sigma_r = \frac{F}{r} + \varphi_g p; \quad \sigma_\vartheta = F' + \varphi_g p; \quad \sigma_{rz} = 0; \tag{94}$$

$$\sigma_z = -p_{e0},$$

where F is the stress function, and $F' \equiv \partial F / \partial r$.

Constitutive relations (12) from [1] have the following form for the considered problem:

$$\varepsilon_r = \overset{\circ}{\varepsilon}_{11\psi} + \frac{\sigma_r + \widetilde{f}_{1\psi p}}{E_{1\psi}} - \frac{\nu_{12\psi}}{E_1}(\sigma_\vartheta + \widetilde{f}_{2\psi p}) - \frac{\nu_{13\psi}}{E_{1\psi}}(\widetilde{f}_{3\psi p} - p_{e0});$$

$$\varepsilon_\vartheta = \overset{\circ}{\varepsilon}_{22\psi} - \frac{\nu_{12\psi}}{E_{2\psi}}(\sigma_r + \widetilde{f}_{1\psi p}) + \frac{\sigma_\vartheta + \widetilde{f}_{2\psi p}}{E_{2\psi}} - \frac{\nu_{23}}{E_{2\psi}}(\widetilde{f}_{3\psi p} - p_{e0}); \tag{95}$$

$$\varepsilon_z = \overset{\circ}{\varepsilon}_{33\psi} - \frac{\nu_{13\psi}}{E_{1\psi}}(\sigma_r + \widetilde{f}_{1\psi p}) - \frac{\nu_{23\psi}}{E_{2\psi}}(\sigma_\vartheta + \widetilde{f}_{2\psi p}) + \frac{1}{E_{3\psi}}(\widetilde{f}_{3\psi p} - p_{e0}).$$

Elasticity moduli $E_{i\psi}$ and Poisson ratios $\nu_{ij\psi}$ are expressed by formulae (10), heat deformations $\overset{\circ}{\varepsilon}_{ii\psi}$ – by formulae (7) and coefficients of phase interaction $\widetilde{f}_{i\psi}$ – by the formulae:

$$f_{1\psi} = f_1 \cos^2 \psi + f_3 \sin^2 \psi;$$

$$f_{3\psi} = f_1 \sin^2 \psi + f_3 \cos^2 \psi; \tag{96}$$

$$f_{2\psi} = f_2,$$

where functions f_i depend on composite porosity φ_g and are expressed as follows:

$$f_1 = f_m = \frac{\varphi_g/(1-\varphi_1^0)}{1-(\varphi_g/(1-\varphi_g^0))^{2/3}+\varphi_g/(1-\varphi_1^0)};$$

$$f_2 = \left(\zeta(1-\sqrt{\varphi_1^0})+1-\zeta\right) f_m; \tag{97}$$

$$f_3 = \left((1-\zeta)(1-\sqrt{\varphi_1^0})+\zeta\right) f_m.$$

Here φ_1^0 is the volumetric concentration of fibres in the composite, ζ is the ratio of the fibres' number, per unit volume of the composite, directed along the weft to the fibres' number directed along the fabric warp.

To determine function F we have the equation of compatibility of deformations:

$$\frac{\partial \varepsilon_\vartheta}{\partial r} + \frac{\varepsilon_\vartheta - \varepsilon_r}{r} = 0,$$

into which we should substitute relation (95). As a result, we obtain the equation of the second order for F:

$$\frac{\partial^2 F}{\partial r^2} + \left(\frac{\partial}{\partial r}\left(\frac{1}{E_{2\psi}}\right) + \frac{1}{rE_{2\psi}}\right) E_{2\psi}\frac{\partial F}{\partial r} - \left(\frac{\partial}{\partial r}\left(\frac{\nu_{12\psi}}{rE_{1\psi}}\right) + \frac{1-\nu_{12\psi}}{E_{1\psi}r}\right) E_{2\psi}F +$$
$$+ \left(\frac{\partial \mathring{\varepsilon}'_{22\psi}}{\partial r} + \frac{\mathring{\varepsilon}_{22\psi} - \mathring{\varepsilon}_{11\psi}}{r}\right) E_{2\psi} + E_{2\psi}\frac{\partial}{\partial r}\left(\left(-\nu_{12\psi}\widetilde{f}_{1\psi} + \widetilde{f}_{2\psi} - \nu_{23\psi}\widetilde{f}_{3\psi}\right)\frac{1}{E_{2\psi}}\right) +$$
$$+ \frac{1}{r}\left(-\nu_{12\psi}\widetilde{f}_{1\psi} + \widetilde{f}_{2\psi} - \nu_{23}\widetilde{f}_{3\psi} - \frac{E_{2\psi}}{E_{1\psi}}\left(\widetilde{f}_{1\psi} - \nu_{12\psi}\widetilde{f}_{2\psi} - \nu_{13\psi}\widetilde{f}_{3\psi}\right)\right) = 0. \tag{98}$$

Heat-mass-transfer equations have the form:

$$\rho_1 \frac{\partial \varphi_a}{\partial t} = -J_1;$$

$$\rho_2 \frac{\partial y_i}{\partial t} = -J_i;$$

$$\frac{\partial}{\partial t}(\rho_g \varphi_g) = \frac{1}{r}\frac{\partial}{\partial r}\left(RK_{11}r\frac{\partial}{\partial r}(\varphi_g \rho_g \theta)\right) + \sum_{i=1}^{3} J_i\Gamma + J_f\Gamma_f; \tag{99}$$

$$\rho c\frac{\partial \theta}{\partial t} = \frac{1}{r}\frac{\partial}{\partial r}\left(k_{11\psi}r\frac{\partial \theta}{\partial r}\right) + c_g RK_{11}\frac{\partial}{\partial r}(\varphi_g\rho_g\theta)\frac{\partial \theta}{\partial r} - \sum_{i=1}^{3} J_i\Delta e^0 - J_f\Delta e_1^0.$$

Boundary and initial conditions for the set of equations (98), (99) are:

$$r = R_1: \quad F = -R_1 p_{e1}; \quad R\rho_g\theta = p_{e1}; \quad k_{11}\theta' = q_{e1}; \tag{100}$$

$$r = R_D(t): \quad F = -R_D p_{e2}, \quad R_a\rho_g\theta = p_{e2}, \quad k_{11}\theta' = q_{e2};$$

$$t = 0: \quad \varphi_a = \varphi_1^0, \quad y_i = y_{i0}, \quad \rho_g = \rho_{g0}, \quad \theta = \theta_0, \tag{101}$$

here R_1 is the internal radius of the cylinder, $R_D(t)$ is the external radius decreasing with time due to linear ablation of the composite:

$$R_D = R_2 - \int_0^t D_{\psi 1}(\tau)d\tau, \tag{102}$$

where R_2 is the external radius of the cylinder at initial time $t = 0$, $D_{\psi 1}$ is the total rate of linear ablation of BRFC calculated by formula (89).

Heat flux q_{e1} carried off from the internal surface $r = R_1$ of the shell is determined by convective heat transfer and ragiation:

$$q_{e1} = \alpha_{T1}(\theta - \theta_{e1}) + \varepsilon\sigma_{SB}\theta^4, \tag{103}$$

here α_{T1} is the coefficient of heat transfer from the internal surface, θ_{e1} is the temperature of the surrounding air inside the cylinder, σ_{SB} is the Stefan-Boltsman coefficient, ε is the degree of blackness of the internal surface.

Heat flux q_{e2} supplied to the external recessive surface $r = R_D(t)$ of the composite shell is calculated by the relations (93):

$$q_{e2} = q_e. \tag{104}$$

The equation system (98) - (99) with conditions (100) - (101) is the mathematical statement of the problem on determination of functions F, φ_a^0, y_i, ρ_g and θ depending on coordinate r and time t. On determining a value of stress function F, stresses σ_r and σ_ϑ in the cylindrical composite shell can be found by formulae (94).

Pore gas pressure p is determined by the formula:

$$p = R_a\rho_g\theta. \tag{105}$$

§10.2. DAMAGE PARAMETERS

In accordance with the model developed, fabric ablative composites and BRFC have four main types of destruction (A), (B), (C) and (D) (see [1]). For the cylindrical shell made of BRFC two types of destruction are possible: (A) - breakage of threads laid in Warp and Fill Directions of Fabric Ox_1' and Ox_3' and (C) - delamination of the composite.

Destruction of the type (A) starts when damage parameter $z_2(r,t)$ reaches value 1 within a certain zone with coordinate $r = r_2^*$ at time t_2^*:

$$z_2(r_2^*, t_2^*) = 1; \tag{106}$$

this parameter, from relations (14) of [1] and equations (14), (16) of the present work, is determined by the formula:

$$z_2(r,t) = \frac{\sigma_\vartheta(r,t)}{S_{3\psi}^+(r,t)} \max\ \{1, \frac{S_{3\psi}^+}{S_{3\psi}^{(A)}}\}. \tag{107}$$

As it was noted in Chapter VIII, for angles $\psi \geq 5°$ the condition $S_{3\psi}^+/S_{3\psi}^{(A)} \leq 1$ is usually satisfied, therefore from (107) it follows that

$$z_2(r,t) = \frac{\sigma_\vartheta}{S_{3\psi}^+} \qquad \text{at } \psi \geq 5°. \tag{108}$$

At the same time for fabric 2-D composites with angle $\psi = 0°$ the condition $S_{3\psi}^+/S_{3\psi}^{(A)} \geq 1$ is satisfied, and, thus, damage parameter z_2 takes the form:

$$z_2(r,t) = \frac{\sigma_\vartheta \cos^2\psi}{S_3^+} \qquad \text{at } \psi = 0°. \tag{109}$$

These expressions for z_2 at different angles ψ will be used in calculations below.

Destruction by the type (C) starts when damage parameter $z_1(r,t)$ reaches value 1 within a certain zone of the cylinder with coordinate $r = r_1^*$ at time t_1^*:

$$z_1(r_1^*, t_1^*) = 1, \tag{110}$$

which from equations (15) of [1] and (12) of §8.2 is determined by the formula:

$$z_1(r,t) = \frac{\sigma_r(r,t)}{S_{1\psi}^+(r,t)}. \tag{111}$$

Expression (111) is valid for all angles ψ from 0° to 90°, and at $\psi = 0°$ we have $S^+_{1\psi} = S^+_1$.

§ 10.3. METHOD OF NUMERICAL SOLUTION OF THE PROBLEM

The peculiarity of the problem statement given above consists in that a domain of its resolution is variable: it is interval $R_1 \le r \le R_D(t)$. For numerical solving the problem within variable domains we need to reconstruct difference schemes or finite-element grids at each time step that usually leads to an appearance of calculation instability and lowering the accuracy of calculated results. To avoid this, we developed the method of passage to mobile coordinates [6]. For the problem considered, this method consists in the following.

Let us introduce a mobile coordinate x:

$$x = a(t)r + b(t), \tag{112}$$

where functions $a(t)$ and $b(t)$ are determined by the formulae:

$$a(t) = \frac{R_2 - R_1}{R_D(t) - R_1}, \quad b(t) = -\frac{R_1(R_2 - R_D(t))}{R_D(t) - R_1}. \tag{113}$$

The transformation of coordinates (112), (113) reduces the mobile domain $R_1 \le r \le R_D(t)$ to the non-mobile $R_1 \le x \le R_2$.

The equation system (98) - (99) in the mobile coordinate system is written as follows:

$$\dot{\varphi}_a - D_{\psi 1}\xi\varphi'_a = -J_f/\rho_f;$$

$$\dot{y}_i - D_{\psi 1}\xi y'_i = -J_i/\rho_2;$$

$$(\varphi_g\rho_g)^\bullet - D_{\psi 1}\xi(\varphi_g\rho_g)' = \frac{a^2}{x-b}(R_a K_{11}(x-b)(\rho_g\theta)')' + \varphi_2^0\sum_{i=1}^{3} J_i\Gamma_i + \varphi_1^0 J_f\Gamma_f;$$

$$\rho c\dot{\theta} - \rho c D_{\psi 1}\xi\theta' = \frac{a^2}{x-b}(k_{11\psi}(x-b)\theta')' + c_g a^2 R - aK_{11}\theta'(\rho_g\theta)' -$$

$$\varphi_2^0\Delta e^0\sum_{i=1}^{3} J_i\Gamma_i - \Delta e_f^0\varphi_1^0 J_f\Gamma_f, \tag{114}$$

and compatibility equation is:

$$F'' + \left(\frac{1}{x-b} - \frac{E'_{2\psi}}{E_{2\psi}}\right) F' - \left(\frac{1-\nu_{12\psi}}{(x-b)E_{1\psi}} + \left(\frac{\nu_{12\psi}}{(x-b)E_{1\psi}}\right)'\right) E_{2\psi} F +$$

$$+ \left(\overset{\circ}{\varepsilon}{}'_{22\psi} + \frac{\overset{\circ}{\varepsilon}_{22\psi} - \overset{\circ}{\varepsilon}_{11\psi}}{x-b}\right) E_{2\psi} + E_{2\psi}\left(\frac{1}{E_{2\psi}}\left(-\nu_{12\psi}\widetilde{f}_{1\psi} + \widetilde{f}_{2\psi} - \nu_{23\psi}\widetilde{f}_{3\psi}\right)\right)' +$$

$$+ \frac{1}{x-b}\left(\nu_{12\psi}\widetilde{f}_{1\psi} + \widetilde{f}_{2\psi} - \nu_{23\psi}\widetilde{f}_{3\psi} - \frac{E_{2\psi}}{E_{1\psi}}\left(\widetilde{f}_{1\psi} - \nu_{12\psi}\widetilde{f}_{2\psi} - \nu_{13\psi}\widetilde{f}_{3\psi}\right)\right) = 0.$$

Here derivative with respect to coordinate x is $(') = \partial/\partial x$. Boundary (100) and initial (101) conditions remains their forms in coordinates x, t excepting the heat conditions:

$$x = R_1: \qquad a k_{11\psi}\theta' = q_{e1};$$

$$x = R_2: \qquad a k_{11\psi}\theta' = q_{e2}. \tag{116}$$

Expressions for stresses are transformed in the similar way:

$$\sigma_r = \frac{aF}{x-b} + \varphi_g p,$$

$$\sigma_\vartheta = aF' + \varphi_g p. \tag{117}$$

Additional function $\xi = \xi(x,t)$ is introduced by equation:

$$\xi = \frac{R_2 - R_1}{(R_D - R_1)^2}\left(\frac{x-b}{a} - R_1\right). \tag{118}$$

Here all unknown functions F, θ, ρ_g, φ_a, y_i depend on arguments x and t.

Equation system (114) - (116) has been solved numerically with the help of step-by-step method and difference implicit absolutely stable scheme. To solve the systems of linear algebraic equations arising in applying the difference method, we use the procedure of matrix sweeping.

§10.4. CALCULATED RESULTS. INITIAL DATA.

In accordance with the method described above, numerical calculations were conducted to determine a thermomechanical behaviour of a cylindrical shell made

of Carbon/phenolic BRFC. Characteristics of the composite were given the same as they were presented in chapter VII - IX of the present report and in [1]. Conditions of heating were chosen according to [11]:

heat flux to the cold wall	$q_e^0 = 12$ MW/m^2;
total pressure of gas flow on the external surface of the shell	$p_{e2} = 3$ atm;
pressure on the internal surface of the shell	$p_{e1} = 1$ atm.

Besides that, we assume the following values of heat characteristics of the flow:

heat-transfer coefficient with hot gas flow	$(\alpha/c_p) = 2.2$ kg/m$^2 \cdot$ s;
heating time	$t = 7 \ldots 10$ s;
chemical composition of gas at external surface of boundary layer	corresponds to standard composition of air at $\theta = 295K$
heat-transfer coefficient from internal surface of the shell	$\alpha^T = 10$ W/(m$^2 \cdot$ K);
degree of blackness	$\varepsilon_w = 0.8$.

Geometrical dimensions of the shell:

thickness	12 mm;
internal radius	125 mm;
Bias angle ψ	0° and 30°.

Numerical calculations were conducted for two angles $\psi = 0°$ and 30°.

10.4.1. THE EFFECT OF ABLATION ON THERMOMECHANICAL BEHAVIOUR OF A SHELL OF BRFC

At first let us describe results for $\psi = 30°$.

Figure 21 shows changing characteristics of BRFC corresponding to these conditions of heating: temperature θ_w of ablating surface $r = R_D(t)$, linear rate of ablation $D_{\psi 1}$ and temperature θ_s of the internal surface of the shell $r = R_1$ depending on time t of heating. As seen from Fig.21, temperature θ_w of the ablating surface quickly (during 0.1 - 0.2 s) comes to a quasistationary regime and does not practically change during all the time of heating being at the level of $\approx$ 3000 K. The same character has function $D_{\psi 1}(t)$: its quasistationary magnitude is equal to 0.62 mm/s for angle $\psi = 30°$ under the given conditions of heating.

Temperature of the internal surface θ_s starts to differ essentially from initial temperature $\theta_0 = 295$ K only in $t \approx 6$ s and at time $t = 7$ s is equal to 414 K (Fig.21).

Figure 22 shows distributions of temperature $\theta(r,t)$ versus the shell thickness for different times $t = 0.5$, 1, 3, 5 and 7 s. As seen from this figure, during heating time t the external surface of the shell $r = R_D(t)$ is carried off and temperature profile $\theta(r,t)$ is displaced in the direction of internal surface $r = R_1$.

Corresponding distributions of pore gas pressure $p(r,t)$ versus the shell thickness are given in Figure 23. As seen from this figure, the level of pore gas pressure for the shell with angle $\psi = 30°$ is sufficiently high and is equal to $p_{max} = 40 - 100$ atm. Distribution of pore pressure $p(r,t)$ versus coordinate r has a typical peak, maximum of which p_{max} corresponds to the temperature value $\theta(r,t)$ of the shell and $\theta(r,t) \approx 600$ K (see Figs. 22 and 23). This peakis displaced, as the composite is warmed up, towards the internal surface $r = R_1$ of the shell, and a maximum value of pore pressure $p_{max}(t)$ increases with time from 40 atm at $t = 0.5$ s to $\approx$ 100 atm at $t = 7$ s.

Distributions of volumetric concentration of polymer phase of the matrix $\varphi_2(r,t)$ versus the shell thickness are shown in Figure 24 for different times. As seen fron thi figure, within the warmed zone, where $\theta(r,t) \geq 600$ K, value of $\varphi_2(r,t)$ sharply falls down from initial value $\varphi_2^0 = 0.35$ to 0. Value $\varphi_2(r,t) = 0$ corresponds to the domain of composite coked completely. The width of the domain during

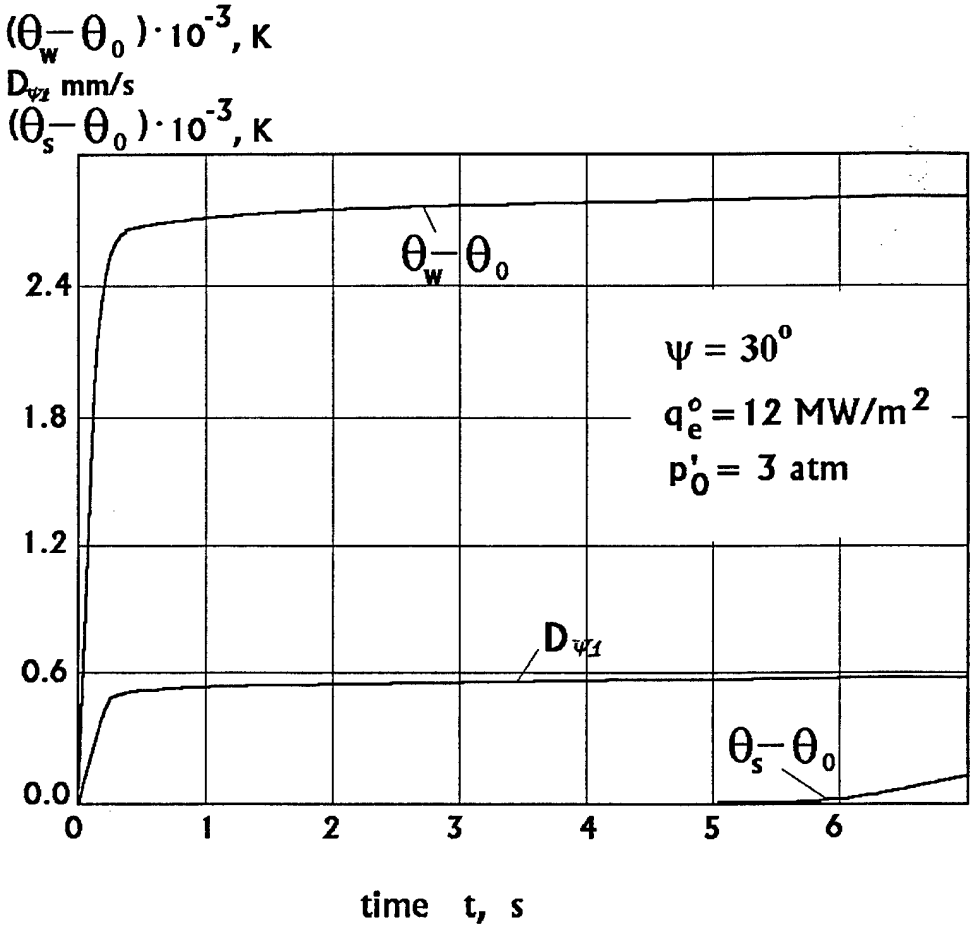

Fig. 21.

Varying external surface temperature θ_w, temperature θ_s on the internal surface $R = r_1$ and recession rate $D_{\psi 1}$ versus duration of heating t of the shell made of BRFC with $\psi = 30°$.

Tabl. 19

Varying of True Temperature of Surface, Rate of Recession and Temperature of Internal Surface of BRFC with $\varphi = 30°$ vs Time of Heating

Time t,s	Temperature θ_w , K	Rate of Recession $D_{\varphi 1}$ mm/s	Temperature θ_s ,K
.1	2143.0	.000	294.0
.2	2911.6	.390	294.0
.3	2972.7	.602	294.0
.4	2988.9	.620	294.0
.5	3004.3	.625	294.0
.6	3014.1	.630	294.0
.7	3024.6	.633	294.0
.8	3030.9	.636	294.0
.9	3036.5	.638	294.0
1.0	3041.3	.640	294.0
1.2	3049.1	.643	294.0
1.4	3055.4	.645	294.0
1.6	3060.5	.647	294.0
1.8	3066.5	.649	294.0
2.0	3070.2	.650	294.0
2.2	3073.2	.652	294.0
2.4	3076.0	.652	294.0
2.6	3078.3	.653	294.0
2.8	3080.5	.654	294.0
3.0	3082.4	.655	294.0
3.2	3084.2	.655	294.0
3.4	3085.8	.656	294.0
3.6	3087.3	.657	294.1
3.8	3088.6	.657	294.2
4.0	3092.1	.657	294.4
4.2	3092.9	.658	294.7
4.4	3094.0	.659	295.3
4.6	3095.0	.659	296.2
4.8	3095.9	.660	297.8
5.0	3096.8	.660	300.3
5.2	3097.6	.660	304.1
5.4	3098.4	.660	309.7
5.6	3099.1	.661	317.7
5.8	3099.8	.661	329.1
6.0	3100.5	.661	344.6
6.2	3101.1	.661	365.5
6.4	3101.7	.662	393.0
6.6	3102.3	.662	428.6
6.8	3102.9	.662	473.7
7.0	3103.4	.662	530.0
7.2	3103.9	.662	599.4
7.4	3104.4	.663	684.2

Tabl. 20

Varying of True Temperature of Surface, Rate of Recession and Temperature of Internal Surface of BRFC with $\psi = 0°$ vs Time of Heating

Time t,s	Temperature θ_ω , K	Rate of Recession $D_{\psi 1}$ mm/s	Temperature θ_S ,K
.1	2143.0	.000	294.0
.2	2911.6	.363	294.0
.3	2972.7	.558	294.0
.4	2988.9	.574	294.0
.5	3004.3	.579	294.0
.6	3014.1	.583	294.0
.7	3024.6	.586	294.0
.8	3030.9	.589	294.0
.9	3036.5	.591	294.0
1.0	3041.3	.593	294.0
1.2	3049.1	.595	294.0
1.4	3055.4	.598	294.0
1.6	3060.5	.599	294.0
1.8	3066.5	.601	294.0
2.0	3070.2	.603	294.0
2.2	3073.2	.604	294.0
2.4	3076.0	.604	294.0
2.6	3078.3	.605	294.0
2.8	3080.5	.606	294.0
3.0	3082.4	.607	294.0
3.2	3084.2	.607	294.0
3.4	3085.8	.608	294.0
3.6	3087.3	.608	294.0
3.8	3088.6	.609	294.0
4.0	3092.1	.609	294.0
4.2	3092.9	.610	294.0
4.4	3094.0	.610	294.0
4.6	3095.0	.611	294.0
4.8	3095.9	.611	294.0
5.0	3096.8	.611	294.0
5.2	3097.6	.612	294.0
5.4	3098.4	.612	294.0
5.6	3099.5	.612	294.0
5.8	3099.8	.612	294.0
6.0	3100.5	.613	294.1
6.2	3101.1	.613	294.2
6.4	3101.7	.613	294.3
6.6	3102.3	.613	294.6
6.8	3102.9	.613	295.1
7.0	3103.4	.614	295.9
7.2	3103.9	.614	297.4
7.4	3104.4	.614	299.8

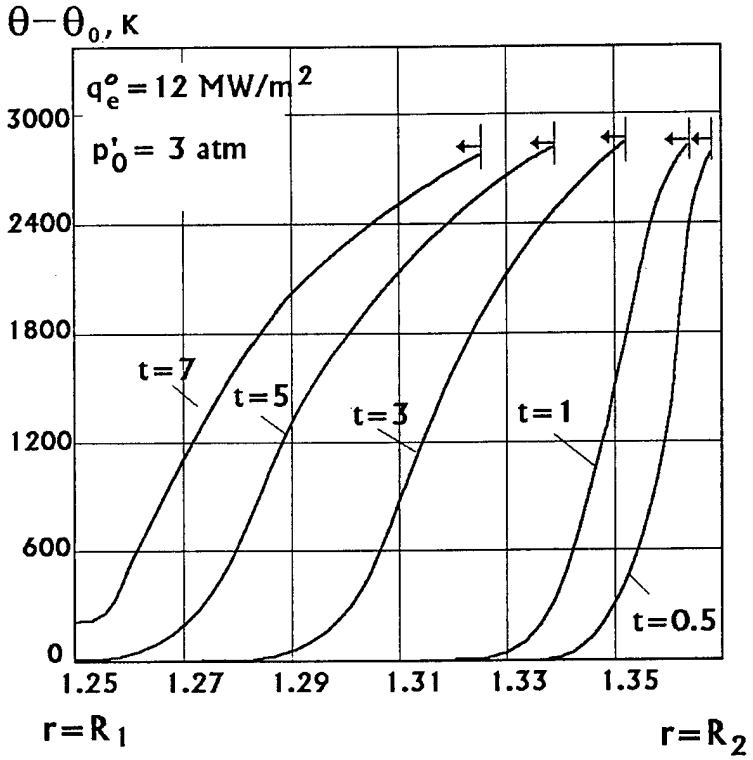

Fig. 22.

Distribution of temperature θ versus thickness
of the cylindrical shell of BRFC at different times $t = 0.5$, 1, 3, 5, 7 s
(r - radius of the shell). Symbol $\leftarrow$ shows a location
of the carried off surface of the shell $r_2 = R_D(t)$ at times t.

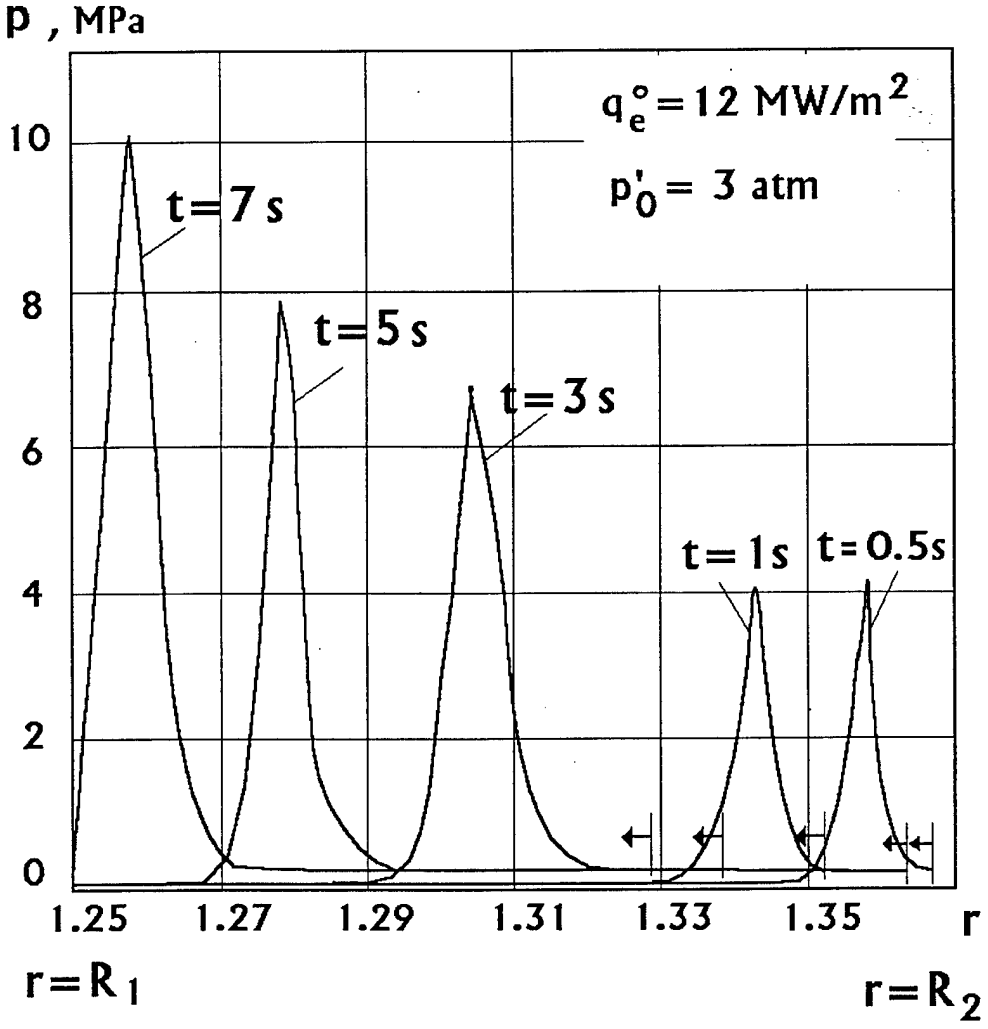

Fig. 23.

Distribution of pore gas pressure p versus thickness of the cylindrical shell of BRFC at different times t (r - radius of the shell). Symbol $\leftarrow$ shows a location of the carried off surface of the shell $r_2 = R_D(t)$ at times t.

warming up grows and becomes equal to 3.5 mm at $t = 7$ s, while the thickness of the composite layer carried off is equal to ≈ 4 mm at the same time moment.

Figure 25 shows distributions of tangential stresses $\sigma_\vartheta(r,t)$ versus the shell thickness at different times t of heating. At initial times, when $t \leq 0.2$ s and ablation process of the composite (volumetric and surface) is not yet realized, heat deformation $\overset{\circ}{\varepsilon}_{22\psi}$ of the composite is positive, that leads to the appearance of compressive (negative) values of stresses σ_ϑ. As the composite is warmed up, for $t \geq 0.5$ s near the external surface $r = R_D$ a volumetrical ablation starts that leads to the appearance of negative values of heat deformations $\overset{\circ}{\varepsilon}_{22\psi}$, thus there appears a shrinkage which, in its turn, causes an appearance of tensile (positive) values of tangential stresses σ_ϑ. For the case, within the domain of relatively low temperatures, where $\theta(r,t) \leq 1500$ K, there are compressive stresses σ_ϑ. This stress profile $\sigma_\vartheta(r,t)$ is displaced towards the internal surface of the cylinder, as the composite is warmed up. A maximum level of tensile stresses σ_ϑ grows max $\sigma_\vartheta \approx 60$ MPa. However, further, near the external ablating surface, stresses σ_ϑ start to decrease (approximately from $t = 2$ s) and go anew into the domain of negative values (at $t = 7$ s $\sigma_\vartheta(R_D,t) = -15$ MPa). This phenomenon is caused by peculiarities of heat deformation $\overset{\circ}{\varepsilon}_{22\psi}$ of the type of Carbon/Phenolic composite, for which under temperatures $\theta \geq 2400$ K the shrinkage is replaced by heat expansion that leads to the appearance anew of negative values of σ_ϑ within the domain adjioned immediately to the ablating surface of the composite. Therefore, at $t \geq 5$ s a profile of tangential stresses $\sigma_\vartheta(r,t)$ has two domains of negative values (where temperatures are relatively low: $295K \leq \theta \leq 1500K$ and are very high $\theta \geq 2400$ K) and one domain of positive values (where temperature is equal to 1500 K $\leq \theta \leq$2400 K). The appearance of thermal stresses of such type is a specific feature of the considered class of Carbon/Phenolic Composite.

The most dangerous stresses, from the point of view of destruction, are tensile stresses σ_ϑ. The degree of danger is characterized by the damage parameter z_2: the closer its value is to 1, the closer stress σ_ϑ is to ultimate strength σ of the composite FRFC in tension under the given tenperature θ. Distributions of the damage parameter $z_2(r,t)$ versus the shell thickness for different times t are shown in Figure 26. Functions $z_2(r,t)$ have a typical peak at $t \geq 2$ s, which moves towards the internal surface of the cylinder, while the composite is warmed up. Value of

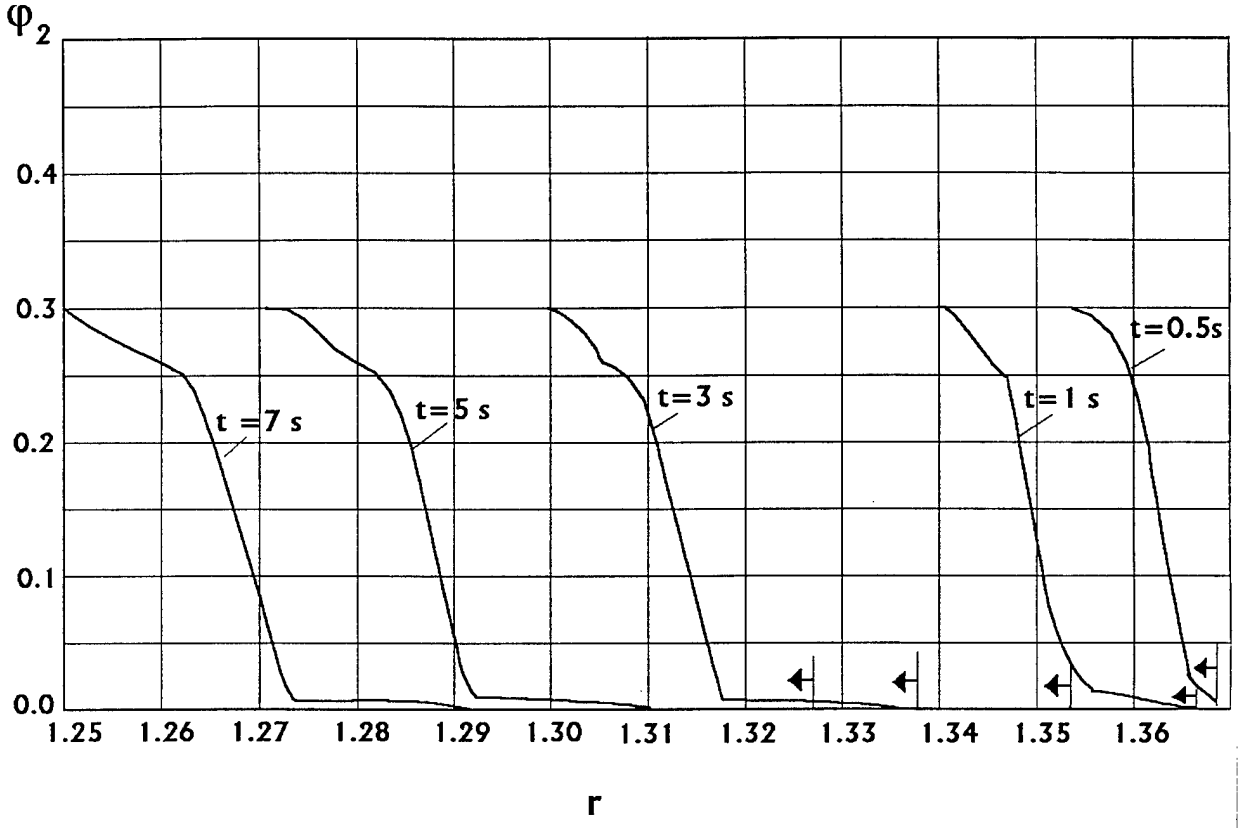

Fig. 24.

Distribution of volumetric content of polymer phase φ_2
versus thickness of the cylindrical shell of BRFC at different times t
(r - radius of the shell). Symbol $\leftarrow$ shows a location
of the carried off surface of the shell $r_2 = R_D(t)$ at times t.

z_2 reaches its maximum at the top of this peak and becomes equal to 0.40 - 0.75. And absolute maximum of value z_2 equal ≈ 0.75 is at time $t \approx 1$ s, when minimal values of $\overset{\circ}{\varepsilon}_{22\psi}$ are realized at the ablating surface (shrinkage reaches its maximum value). Apparently, this time moment for the considered type of BRFC is the most dangerous from the point of view of possible destruction of the shell by the type (A).

Besides tangential stresses, radial thermostresses σ_r prove to be also very essential in the cylindrical shell of BRFC. Fihure 27 shows distributions of stresses $\sigma_r(r,t)$ versus the shell thickness for different times t. During initial time period of heating ($t \leq 0.2$ s), when the process of volumetric ablation has no time to be realized, heat deformation $\overset{\circ}{\varepsilon}_{11\psi}$ is positive and stresses σ_r are also positive (i.e. tensile). The process of volumetric ablation near the heated surface at $t \geq 0.5$ s leads to the appearance of shrinkage deformations ($\overset{\circ}{\varepsilon}_{11\psi} < 0$) and compressive stresses σ_r within the shell (Fig. 27). However, pore gas pressure p also has an essential effect on a character of radial stresses σ_r. Within the zone of the heated composite (at $\theta \geq 600$ K), as it was mentioned above, there appears a peak of pore pressure. This peak causes the appearance of a peak (local maximum) of radial stresses σ_r. Value of stresses σ_r at the top of the peak can be both positive and negative. As seen from Fig.27, at times $t = 0.5$ and 7 s maximum of stresses σ_r is positive, i.e. σ_r are tensile within the domain ($\sigma_r \approx 0.4$ MPa), and at time $1 < t < 7$ s the σ_r stress peak is negative (min $\sigma_r \approx$ -1.5 MPa). and the σ_r stress peak is displaced towards the internal surface, while the composite is warmed up.

Danger of stresses σ_r from the point of view of possible destruction of composite BRFC by the type (C) (delamination) is described by damage parameter z_1. Distributions of damage parameter $z_1(r,t)$ versus the shell thickness for different times are shown in Figure 28. As seen from this figure, a character of distribution of parameter z_1 has a peak form. An appearance of peaks is caused by the presence of peaks of pore gas pressure p. As follows from the calculated results, maximum value of z_1 is very high: 0.5 - 0.95; it means that a state of composite BRFC is close to destruction by type (C) (due to delamination).

Let us note another peculiarity. For composites BRFC with $\psi > 0°$ for non-zero stresses σ_r there appear not only normal stresses σ_{11} but also stresses of interlayer shear σ_{13}, which also raise a danger of delamination of the composite.

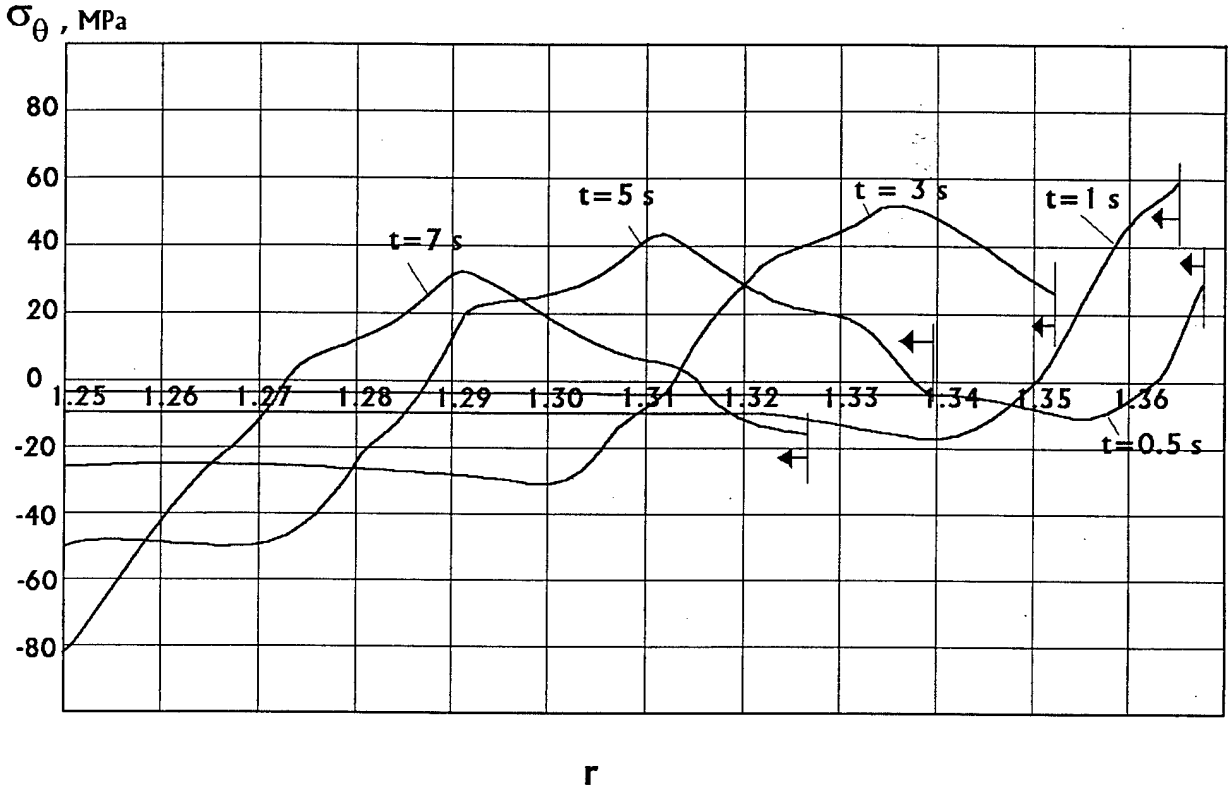

Fig. 25.

Distribution of tangential stresses σ_θ versus thickness of the cylindrical shell of BRFC at different times t (r - radius of the shell). Symbol $\leftarrow$ shows a location of the carried off surface of the shell $r_2 = R_D(t)$ at times t.

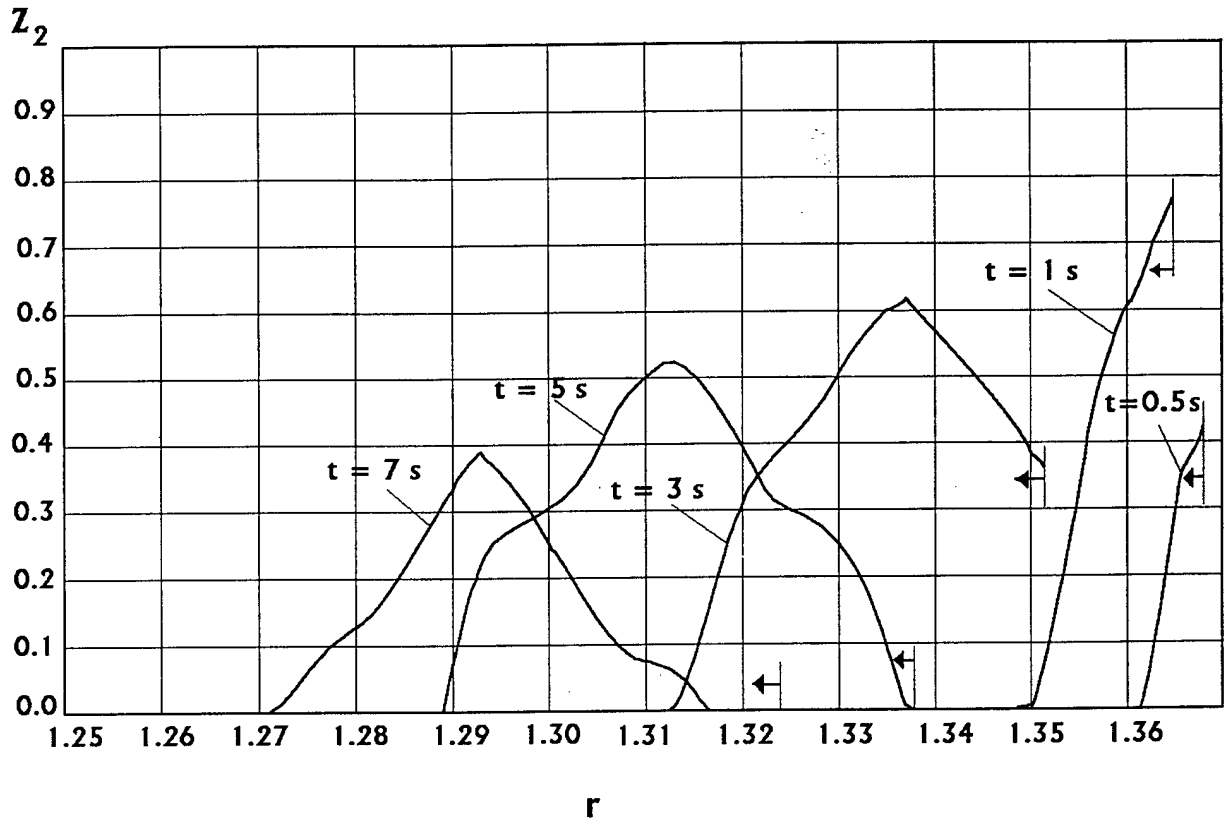

Fig. 26.

Distribution of damage parameter z_2 versus thickness of the cylindrical shell of BRFC at different times t (r - radius of the shell). Symbol $\leftarrow$ shows a location of the carried off surface of the shell $r_2 = R_D(t)$ at times t.

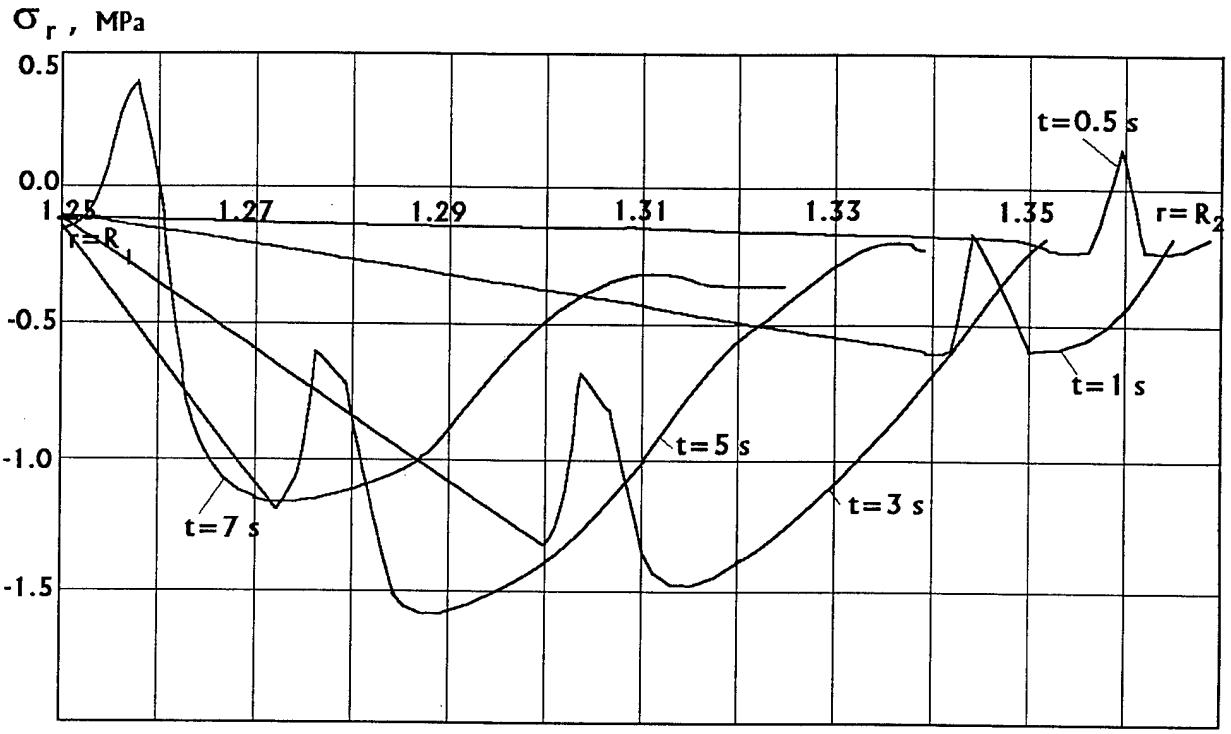

Fig. 27.

Distribution of stresses σ_r versus thickness
of the cylindrical shell of BRFC at different times t
(r - radius of the shell).

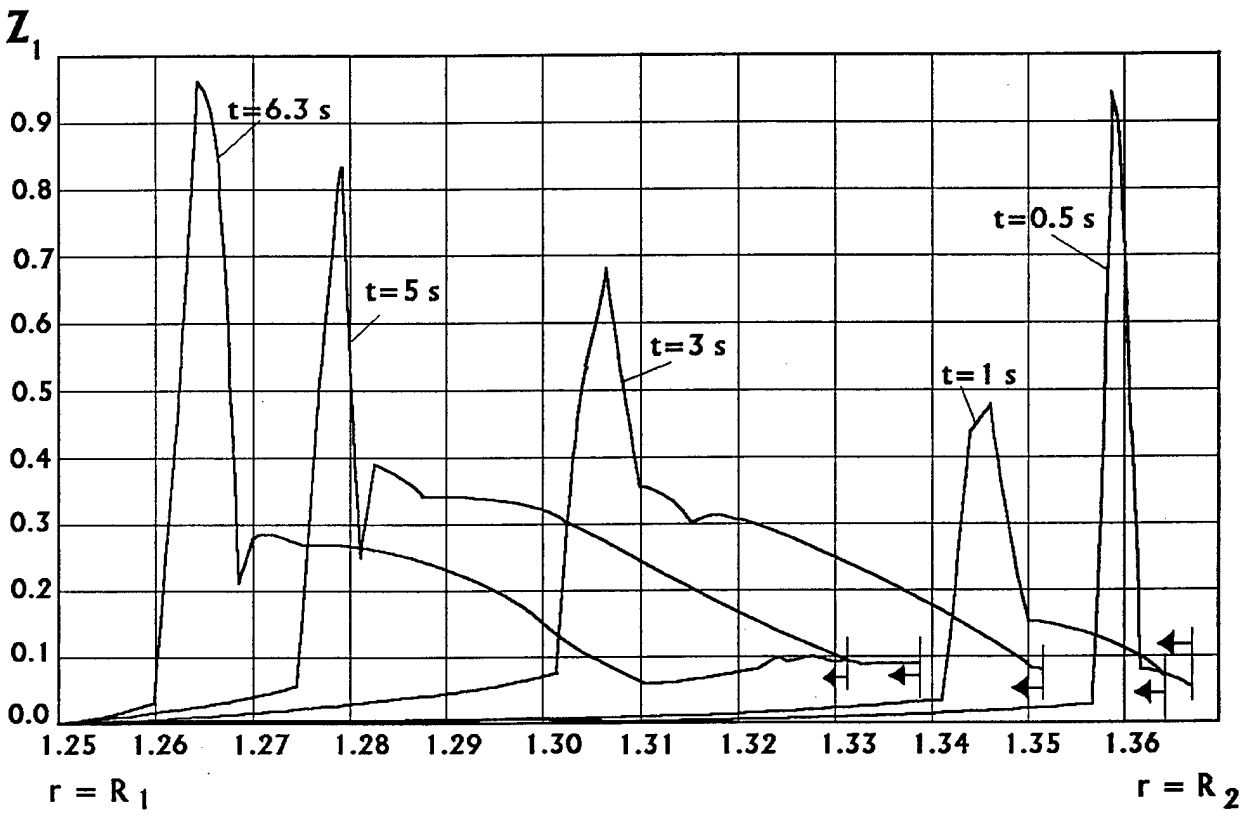

Fig. 28.

Distribution of damage parameter z_1 versus thickness of the cylindrical shell of BRFC at different times t (r - radius of the shell). Symbol $\leftarrow$ shows a location of the carried off surface of the shell $r_2 = R_D(t)$ at times t.

It is due to this that in Figure 28 function $z_2(r,t)$ has a 'plateau' on the right side of the main peak of values, this plateau is of a sufficiently high level of values: $z_1 = 0.20$ - 0.35.

Values of parameter z_1 reaches their maximum near the ablating surface $r = R_D$ at t =0.5 s and at final time of calculation $t = 7$ s near the internal surface of the shell $r = R_1$. Hence, the appearance of delaminations within a structure of the considered type is possible near both the external and internal surfaces of the shell.

10.4.2. THE EFFECT OF ANGLE ψ

Let us investigate now the effect of angle ψ on a thermomechanical behaviour of the shell of BRFC under the action of a high-temperature gas flow.

Calculations being similar to the above-described ones were conducted for a composite with angle $\psi = 0°$, i.e. for 2-D fabric composite, layers of which are laid perpendicularly to the normal vector to the lateral surface of the shell. Calculations in Figs. 29 - 32 correspond to this case.

Figure 29 shows distributions of temperature $\theta(r,t)$ versus the shell thickness under the same conditions of heating as in Fig.22. As seen from the figure, warming up the shell for case $\psi = 0°$ is lower: at $t = 7$ s temperature of the internal surface does not practically change $\theta_s = 295$ K. It is connected with that heat conductivity of composite k_{11} for $\psi = 0°$ is less than $k_{11\psi}$ at $\psi = 30°$ (see Figures 2, 3).

Lower warming up the composite makes it possible that gases generating in pores at volumetric ablation have time to filtrate and outcome partially into the surroundings. Therefore the level of pore pressure (see Fig. 30) for $\psi = 0°$ is lower than for $\psi = 30°$. Maximum values of p are equal to 45 and 100 atm, respectively.

Lowering the level of pore pressure p leads to decreasing peaks of radial stresses σ_r (Fig. 31) and damage parameter z_1 (Fig. 32). Maximum values of parameter z_1 for $\psi = 0°$ does not exceed 0.1, i.e. a danger of the appearance of delaminations in a composite with $\psi = 0°$ proves to be lower, in spite of higher strength of composite BRFC with $\psi = 30°$.

At the same time the effect of angle ψ on a character of tangential stresses

σ_ϑ and damage parameter z_2 is not essential practically; maximum level of values of parameter z_2 is also equal 0.75. Hence, the main cause of possible destruction of 2-D composite with $\psi = 0°$ is cracking of fibres near the ablating surface (type (A)).

It should be mentioned, that the composite with $\psi = 30°$ has a less linear rate of recession: $D_{\psi 1} = 0.57$ mm/s as compared with $D = 0.61$ mm/s for $\psi = 0°$ (see Table 23) and also a less mass rate of recession $\dot{m}$ (see Figs. 33 and 34) and less dimensionless rate of recession $\bar{G}$. Mass rate $\dot{m}$ is determined as follows:

$$\dot{m} = \frac{\partial \Delta m}{\partial t},$$

where

$$\Delta m(t) = m_0 - m(t),$$

is a loss of specific mass of the composite, where m_0 and $m(t)$ are determined as follows:

$$m_0 = \rho_0 (R_2 - R_1);$$

$$m(t) = \frac{1}{R_D(t) - R_1} \int_{R_1}^{R_D(t)} \rho(r) r dr,$$

here $\rho = \sum_{i=1}^{3} \rho_i \varphi_i$ is the density of the composite.

Dimensionless rate $\bar{G}$ is determined as follows:

$$\bar{G} = \frac{\dot{m}}{(\alpha / c_p)}.$$

In spite of that ablation rate (linear $D_{\psi 1}$, mass $\dot{m}$ and dimensionless $\bar{G}$) of composite BRFC with $\psi = 30°$ is less than for angle $\psi = 0°$, temperature of the internal surface θ_s proves to be higher (at $t = 7$ s it is equal to 414 and 293 K, respectively). There appears a natural question: what variant is more effective.

If we estimate these variants with the help of well-known criterion - effective enthalpy I_{eff} determined as

$$I_{eff} = \frac{q_e^0}{\dot{m}},$$

then we obtain

$$I_{eff} = 12.27 \text{ MJ/kg} \quad \text{at} \quad \psi = 0°;$$

$$I_{eff} = 12.95 \text{ MJ/kg} \quad \text{at} \quad \psi = 30°;$$

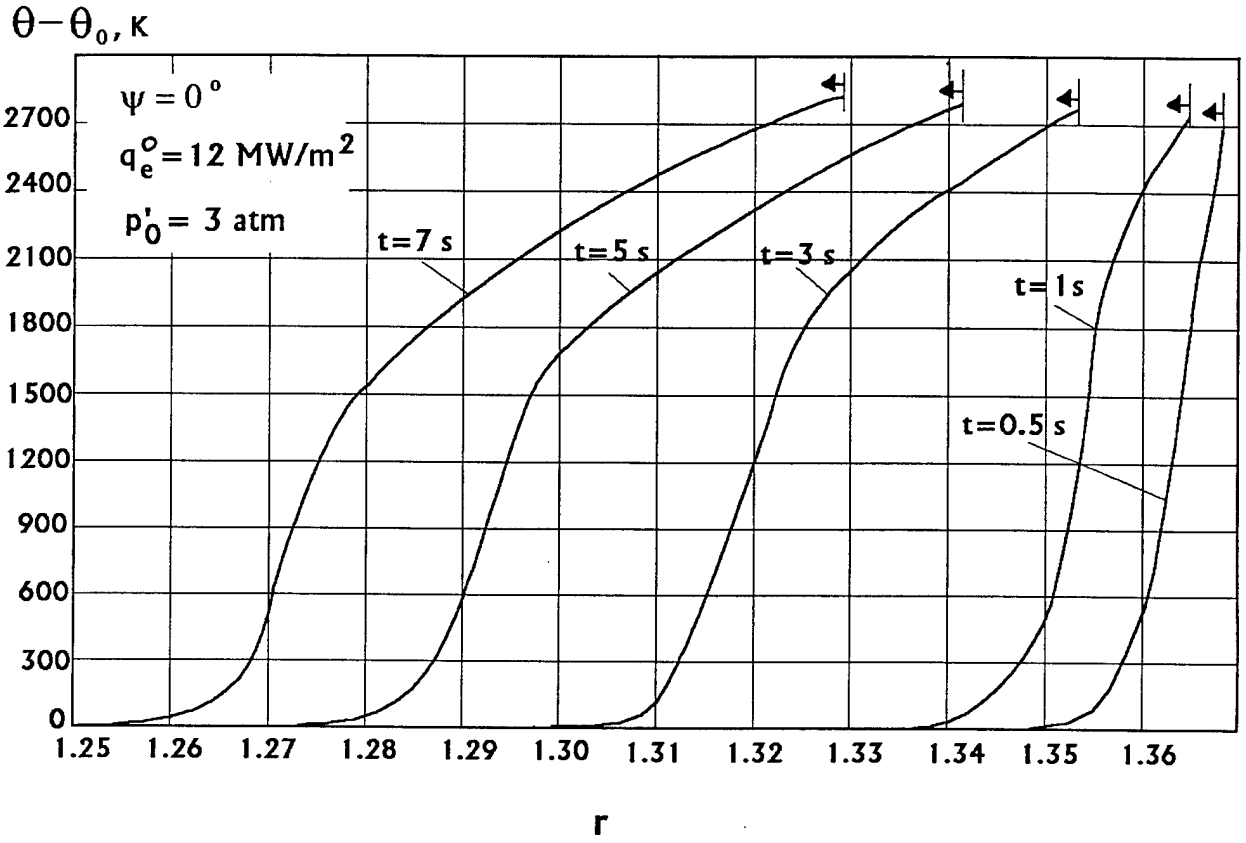

Fig. 29.

Distribution of temperature θ versus thickness of the cylindrical shell of BRFC at different times t and $\psi = 0°$ (r - radius of the shell). Symbol $\leftarrow$ shows a location of the carried off surface of the shell $r_2 = R_D(t)$ at times t.

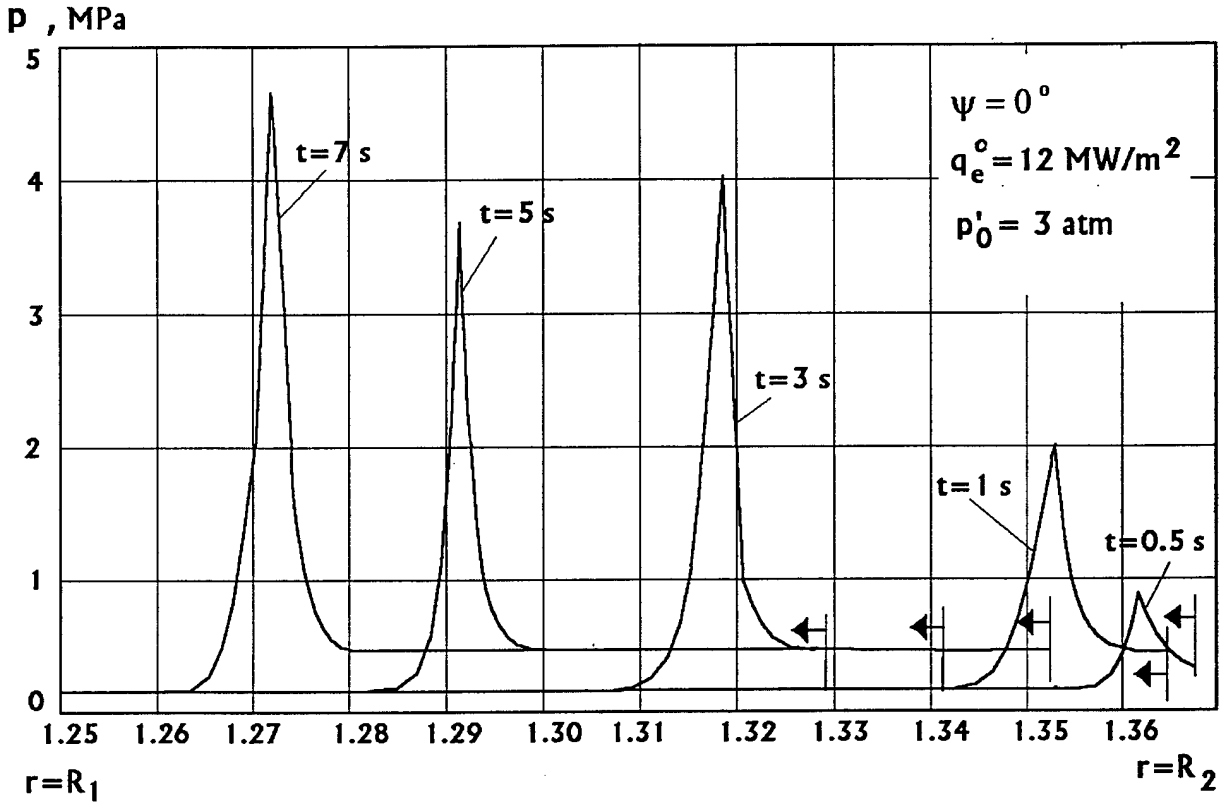

Fig. 30.

Distribution of pore gas pressure p versus thickness of the cylindrical shell of BRFC at different times t and $\psi = 0°$ (r - radius of the shell). Symbol $\leftarrow$ shows a location of the carried off surface of the shell $r_2 = R_D(t)$ at times t.

i.e. variant with $\psi = 30°$ would be considered more effective. However, this criterion does not take into account that temperature θ_s is higher for $\psi = 30°$. In fact, it is a deficiency of the criterion of effective enthalpy.

More convenient criterion for such situations is another one: the criterion of dimensionless parameter of efficiency Di introduced in [5]:

$$\mathrm{Di} = \frac{q_e^0 t}{\rho_0 c (R_2 - R_1)^2 \theta_s}.$$

In accordance with this criterion:

$$\mathrm{Di} = 15.5 \quad \text{for} \quad \psi = 0°;$$

$$\mathrm{Di} = 11.0 \quad \text{for} \quad \psi = 30°;$$

i.e. composite BRFC with $\psi = 0°$ proves to be more effective.

If one have no requests to composite BRFC differing from requests considered in the present work, then the criterion on efficiency Di is more preferable as compared with I_{eff}, and, hence, BRFC with $\psi = 0°$ should be considered as more effective.

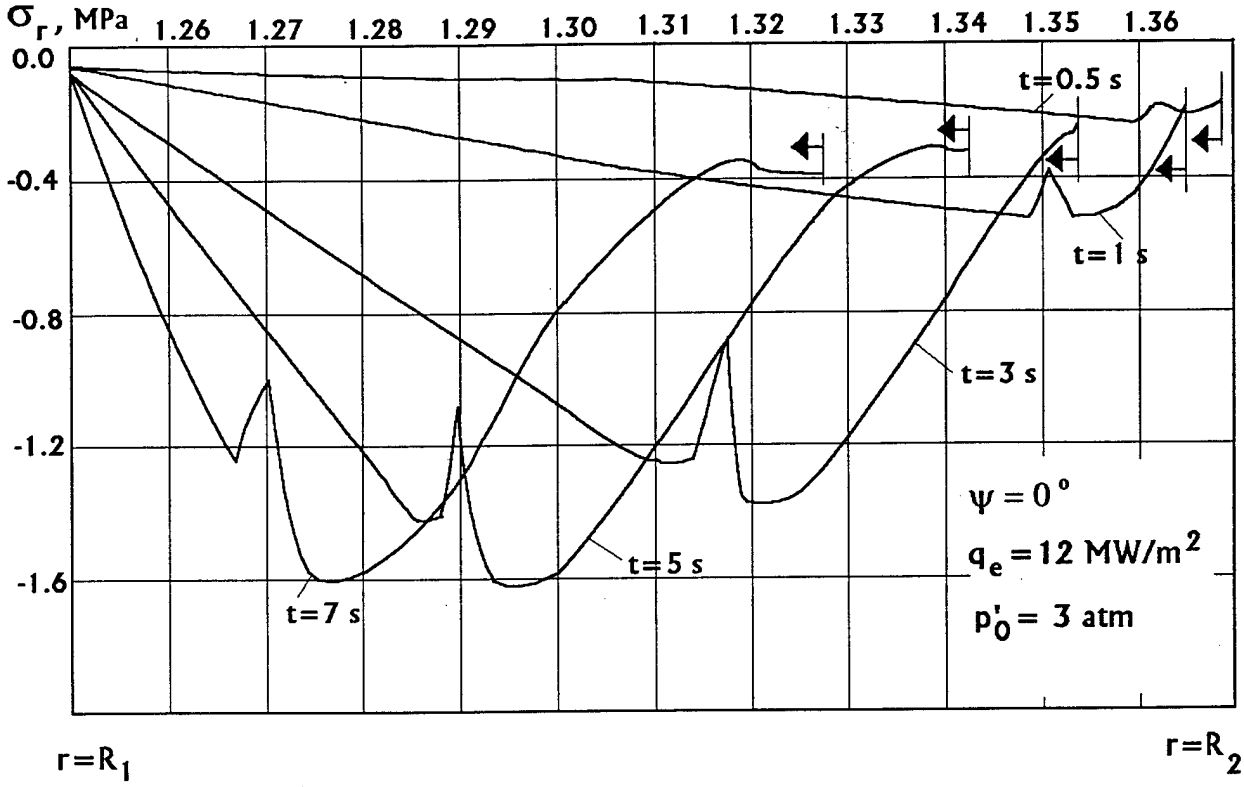

Fig. 31.

Distribution of stress σ_r versus thickness
of the cylindrical shell of BRFC at different times t and $\psi = 0°$
(r - radius of the shell). Symbol $\leftarrow$ shows a location
of the carried off surface of the shell $r_2 = R_D(t)$ at times t.

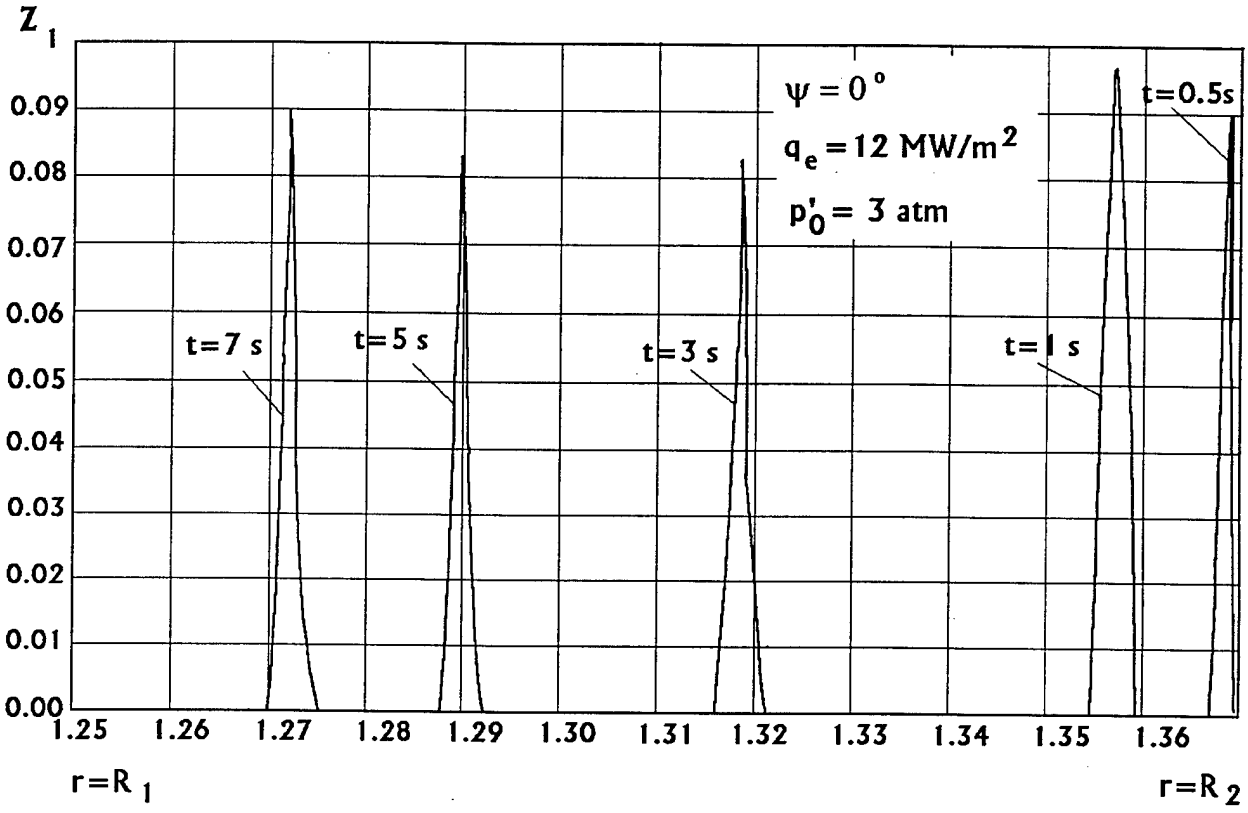

Fig. 32.

Distribution of damage parameter z_1 versus thickness of the cylindrical shell of BRFC at different times t and $\psi = 0°$ (r - radius of the shell). Symbol $\leftarrow$ shows a location of the carried off surface of the shell $r_2 = R_D(t)$ at times t.

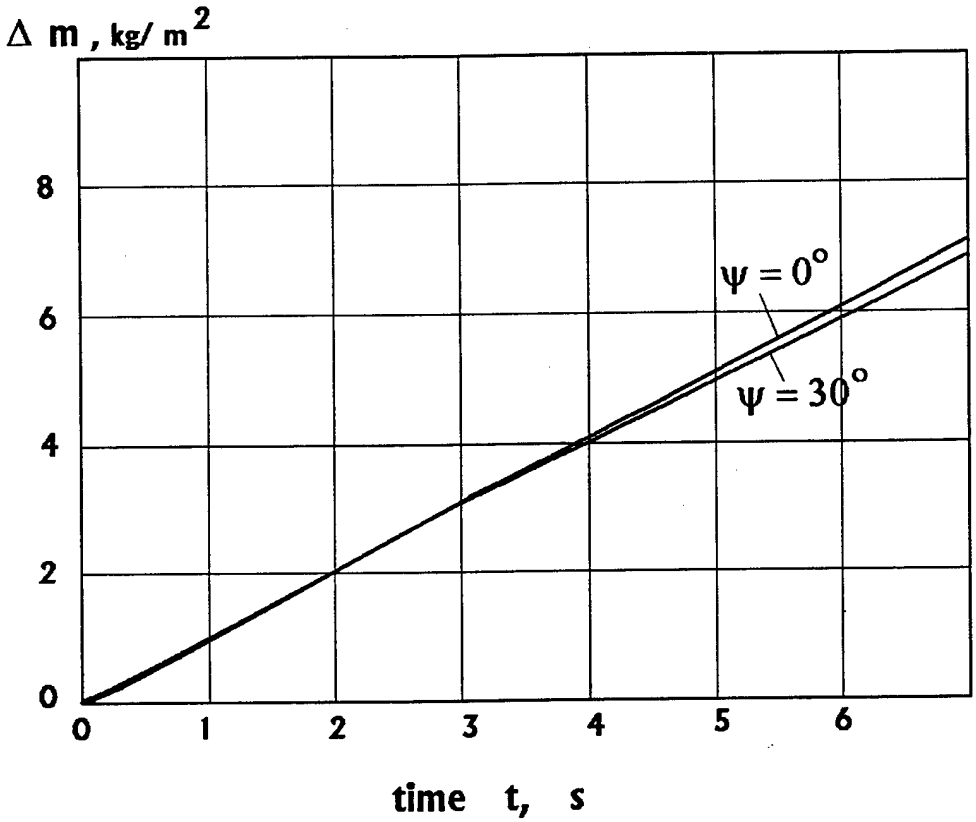

Fig. 33.

Dependence of mass loss Δm of BRFC
on time t of heating.

Tabl. 21

Varying of Loss mass, Mass Ablatiom Rate and Dimensionless Mass Ablation Rate on Heating Time t of BRFC with φ=0°

Time t,s	Loss of mass Δ m, kg/m2	Mass Ablation Rate $\dot{m}$ kg/(m2·s)	Dimensionless Mass Ablation Rate $\bar{G}$
.1	.0	.000	.000
.2	.1	.783	.356
.3	.2	.977	.444
.4	.3	.990	.450
.5	.4	1.061	.483
.6	.5	1.093	.497
.7	.6	1.093	.497
.8	.8	1.093	.497
.9	.9	1.069	.486
1.0	1.0	1.089	.495
1.2	1.2	1.080	.491
1.4	1.4	1.067	.485
1.6	1.6	1.050	.477
1.8	1.8	1.048	.476
2.0	2.0	1.048	.476
2.2	2.2	1.037	.471
2.4	2.4	1.026	.469
2.6	2.7	1.023	.466
2.8	2.9	1.023	.465
3.0	3.1	1.016	.462
3.2	3.3	.998	.458
3.4	3.5	.997	.454
3.6	3.7	.997	.453
3.8	3.9	.991	.450
4.0	4.1	.987	.449
4.2	4.3	.983	.447
4.4	4.4	.981	.446
4.6	4.6	.970	.441
4.8	4.8	.969	.441
5.0	5.0	.963	.438
5.2	5.2	.954	.434
5.4	5.4	.954	.434
5.6	5.6	.946	.430
5.8	5.8	.942	.429
6.0	6.0	.942	.428
6.2	6.2	.928	.422
6.4	6.4	.928	.422
6.6	6.5	.928	.422
6.8	6.7	.927	.421

Tabl. 22

Varying of Loss mass, Mass Ablatiom Rate and Dimensionless Mass Ablation Rate on Heating Time t of BRFC with φ=30°

Time t,s	Loss of mass Δm, kg/m2	Mass Ablation Rate $\dot{m}$ kg/(m2·s)	Dimensionless Mass Ablation Rate $\bar{G}$
.1	.0	.000	.000
.2	.1	.886	.403
.3	.3	1.207	.549
.4	.4	1.221	.555
.5	.5	1.231	.560
.6	.6	1.220	.555
.7	.7	1.216	.553
.8	.9	1.216	.553
.9	1.0	1.196	.544
1.0	1.1	1.201	.546
1.2	1.3	1.183	.538
1.4	1.6	1.169	.531
1.6	1.8	1.155	.525
1.8	2.0	1.143	.520
2.0	2.3	1.129	.513
2.2	2.5	1.113	.506
2.4	2.7	1.107	.503
2.6	2.9	1.103	.502
2.8	3.2	1.099	.500
3.0	3.4	1.088	.494
3.2	3.6	1.075	.488
3.4	3.8	1.070	.487
3.6	4.0	1.068	.486
3.8	4.2	1.059	.481
4.0	4.4	1.046	.475
4.2	4.6	1.046	.475
4.4	4.9	1.042	.474
4.6	5.1	1.031	.468
4.8	5.3	1.025	.466
5.0	5.5	1.023	.465
5.2	5.7	1.015	.461
5.4	5.9	1.008	.458
5.6	6.1	1.006	.457
5.8	6.3	.997	.453
6.0	6.5	.996	.453
6.2	6.7	.990	.450
6.4	6.9	.983	.447
6.6	7.1	.982	.446
6.8	7.3	.977	.444
7.0	7.4	.978	.444

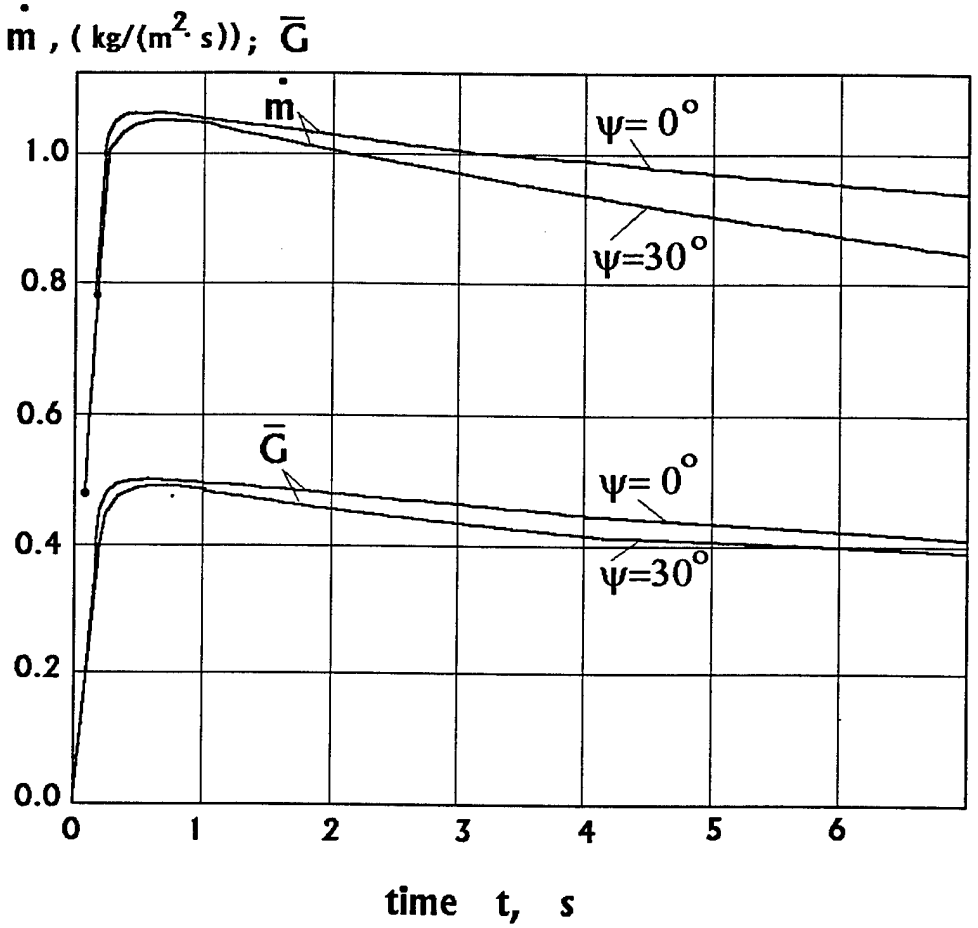

Fig. 34.

Dependence of mass recession rate $\dot{m}$ (kg/(m^2· s)) and dimensionless recession rate $\bar{G}$ of BRFC on time t of heating.

Tabl. 23

Varying of Recession Rate, Temperature of Ablation Surface and Temperature of Internal Surface vs Heating Time t of BRFC with $\varphi = 0°$

Time t,s	Rate of Recession $D_{\varphi 1}$ mm/s	Temperature of Ablation Surface θ_w,K	Temperature of Internal Surface θ_3,K
.1	.000	2142	294
.2	.363	2911	294
.3	.558	2972	294
.4	.574	2988	294
.5	.579	3004	294
.6	.583	3014	294
.7	.586	3024	294
.8	.589	3030	294
.9	.591	3036	294
1.0	.593	3041	294
1.2	.595	3049	294
1.4	.598	3055	294
1.6	.599	3060	294
1.8	.601	3066	294
2.0	.602	3070	294
2.2	.604	3073	294
2.4	.604	3075	294
2.6	.605	3078	294
2.8	.606	3080	294
3.0	.607	3082	294
3.2	.607	3084	294
3.4	.608	3085	294
3.6	.608	3087	294
3.8	.609	3088	294
4.0	.609	3092	294
4.2	.610	3092	294
4.4	.610	3093	294
4.6	.611	3094	294
4.8	.611	3095	294
5.0	.611	3096	294
5.2	.612	3097	294
5.4	.612	3098	294
5.6	.612	3099	294
5.8	.612	3099	294
6.0	.613	3100	294
6.2	.613	3101	294
6.4	.613	3101	294
6.6	.613	3102	294
6.8	.613	3102	295
7.0	.613	3102	295

Tabl. 24

Varying of Recession Rate, Temperature of Ablation Surface and Temperature of Internal Surface vs Heating Time t of BRFC with ψ=30°

Time t,s	Rate of Recession $D_{\psi 1}$ mm/s	Temperature of Ablation Surface θ_w,K	Temperature of Internal Surface θ_s,K
.1	.000	2142	293
.2	.344	2911	293
.3	.520	2972	293
.4	.536	2988	293
.5	.540	3004	293
.6	.544	3014	293
.7	.547	3024	293
.8	.549	3030	293
.9	.551	3036	293
1.0	.553	3041	293
1.2	.555	3049	293
1.4	.557	3055	293
1.6	.559	3060	293
1.8	.561	3066	293
2.0	.562	3070	293
2.2	.563	3073	293
2.4	.563	3075	293
2.6	.564	3078	293
2.8	.565	3080	293
3.0	.565	3082	293
3.2	.566	3084	293
3.4	.566	3085	293
3.6	.567	3087	293
3.8	.567	3088	293
4.0	.568	3092	293
4.2	.569	3092	293
4.4	.569	3093	293
4.6	.569	3094	294
4.8	.570	3095	294
5.0	.570	3096	296
5.2	.570	3097	297
5.4	.570	3098	300
5.6	.571	3099	304
5.8	.571	3099	310
6.0	.571	3100	318
6.2	.571	3101	328
6.4	.571	3101	342
6.6	.572	3102	361
6.8	.572	3102	384
7.0	.572	3103	414

Chapter XI

THE EFFECT OF INCLINATION ANGLE ON PROPERTIES OF CARBON/PHENOLIC BRFC

Table 25 shows summary results of all calculations conducted for the present report for properties of Carbon/Phenolic BRFC at two angles $\psi = 0$ and 30°. The purpose of the table is to investigate the effect of inclination angle ψ on properties of composites and on a thermo-mechanical behaviour of a cylindrical shell made of BRFC under external heating.

In the last column of the table there are relative changes (in %) of values of the functions at passage from angle $\psi = 0°$ to $\psi = 30°$. Sign 'plus' means an increase of values, 'minus' means a decrease.

Tabl. 25

	temperature	$\varphi = 0°$	$\varphi = 30°$	$\frac{V_{30} - V_0}{V_0} \cdot 100$
1. Across Ply Thermal Conductivity $k_{11\varphi}$, (W/m K)	295 K	.65	1.10	+69
	3000 K	5.72	10.40	+82
2. Longitudinal Thermal Conductivity $k_{33\varphi}$, (W/m K)	295 K	2.25	2.00	-11
	3000 K	25.00	19.76	-21
3. Across Ply Thermal Expansion $\mathring{\varepsilon}_{11\varphi}$, %	600 K	1.30	.976	-25
	3000 K	-10.60	-8.05	-20
4. Longitudinal Thermal Expansion $\mathring{\varepsilon}_{33\varphi}$, %	295 K	.01	.014	+40
	3000 K	.14	-2.568	
5. Across Ply Elastic Modulus $E_{1\varphi}$, GPa	295 K	6.79	5.34	-21
	3000 K	0.23	0.24	+4
6. Longitudinal Elastic Modulus $E_{3\varphi}$, GPa	295 K	60.23	4.44	-92
	3000 K	30.00	0.22	-99
7. Shear Elastic Modulus $G_{13\varphi}$, GPa	295 K	1.679	4.189	+150
	3000 K	.083	.200	+141
8. Strength in Tension along Ox_1, $S^+_{1\varphi}$, MPa	295 K	11.58	14.92	+29
	3000 K	.46	.60	+30
9. Strength in Tension along Ox_3, $S^+_{3\varphi}$, MPa	295 K	399.70	23.20	-94
	3000 K	76.80	.90	-99
10. Shear Strength $S_{13\varphi}$, MPa	295 K	25.14	12.92	-49
	3000 K	1.60	.52	-55
11. Linear Ablation Rate $\mathcal{D}_{\varphi 1}$, mm/s	3000 K, $p'_0 = 3$ atm, $(\alpha/c_p) = 2.2$	.61	.57	-6.5
12. Temperature $\theta_s - \theta_0$ (K) of internal 'cold' surface after t= 7 s of heating	$q^0_e = 12$ MW/m, $h = 12$ mm	0	119	
13. Temperature θ_ω of ablation surface, K	= 12 MW/m, $p'_0 = 3$ atm, $(\alpha/c_p) = 2.2$	3102	3102	
14. Mass ablation rate $\dot{m}$, kg/(m² s)	- " -	.978	.927	-5.5
15. Dimensionless mass ablation rate $\bar{G}$	- " -	.44	.42	-4.8
16. Maximal value of damage parameter z_1 in cylindrical shell	- " -	.1	.95	+850
17. Maximal value of damage parameter z_2 in cylindrical shell	- " -	.75	.75	0
18. Maximal value of radial thermal stresses in cylindrical shell σ_r, MPa	- " -	-0.25	.4	
19. Maximal tangential thermal stresses in cylindrical shell σ_θ, MPa	- " -	57	57	0
20. Maximal value of pore pressure p, MPa	- " -	4.5	10	+122
21. Effective enthalpy I_{eff}, MJ/kg	- " -	12.27	12.95	+5.5
22. Dimensionless parameter	- " -	15.5	11.	-29

CONCLUSIONS

1. In the present Report the model developed before on thermo-mechanical processes of ablation for Carbon/Phenolic Bias-Reinforced Composites under high temperatures has been modified.

2. Calculations have been conducted for heat-physical characteristics of BRFC (heat conductivity, heat expansion (shrinkage)) for different inclination angles ψ; as initial data we have used experimental results obtained in [11].
   It is established that for $\psi = 30°$ Across Ply Conductivity is higher by 70 - 80 % than for BRFC with $\psi = 0°$. Due to this, temperature on the internal wall of the cylindrical shell with angle $\psi = 30°$ under external heating by flux $q_e^0 = 12$ MW/m^2 will be higher ($\theta_s - \theta_0 \approx 0$ and 119 °C, respectively, at time $t = 7$ s of heating).
   It is also established that Longitudinal Thermal Expansion $\overset{\circ}{\varepsilon}_{22\psi}$ being the cause of appearance of tangential stresses in the cylindrical shell for $\psi = 0$ and 30° is practically the same.
   At the same time heat deformation $\overset{\circ}{\varepsilon}_{33\psi}$ essentially increases in its absolute magnitude, but its role for the problem on heating of a cylindrical shell is not considerable.

3. With the help of the modified model, calculations have been conducted for thermo-mechanical characteristics (elastic moduli, strength) of BRFC for different inclination angles ψ. It has been established that for values ψ =0 and 30° Across Ply Elastic Modulus $E_{1\psi}$ and Longitudinal Elastic Modulus $E_{2\psi}$ are practically the same within all the temperature interval, only longitudinal modulus E_3 decreases that has no essential effect on the problem of heating a cylindrical shell.
   Increasing angle ψ from 0° to 30° leads to growing Strength $S_{1\psi}^{+}$ in Tension along Ox_3 axis by 30 % and Shear Elastic Modulus $G_{13\psi}$ by 150 %.

4. With the help of the model, numerical calculations of linear rate of ablation of BRFC have been conducted for different angles ψ. Comparison with experimental values taken from scientific literature data for $\psi = 0°$ has shown a good accuracy of prediction of the linear ablation rate with the help of the model. It has been set that

a contribution of thermo-mechanical erosion into the total linear rate of ablation is very essential: for considered conditions of heating ($q_e^0 = 12$ MW/m^2, $p_0' = 3$ atm) it is equal to 50 - 70 %.

It has been also established that an increase of angle ψ from 0° to 30° leads to decreasing the summarized linear rate of ablation $D_{1\psi}$ by 7 %, the mass rate of ablation $\dot{m}$ by 6 %, dimensionless rate of recession $\bar{G}$ by 5 %; while temperature of the heated surface θ_w does not change practically.

5. With the help of the model, calculations have been conducted for thermo-stresses and internal heat and mass transfer in a cylindrical shellmade of BRFC with angles $\psi = 0°$ and 30° under external convective heating with parameters $q_e^0 = 12$ MW/m^2 and $p_0' = 3$ atm.

   It has been established that temperature on the internal nonheated surface of the composite grows with increasing angle ψ, and maximum of pore gas pressure p also increases (more by two times).

6. Increasing angle ψ has no effect practically on a level of tensile tangential stresses σ_θ near the external surface of the cylindrical shell: their maximum is equal approximately to 57 MPa, that ensures value of damage parameter equal to $z_2 \approx 0.75$. At the same time the increase of angle ψ from 0° to 30° leads to sharp increasing radial stresses σ_r within the shell: their maximal values become positive (tensile) and equal to ≈ 0.4 MPa, and value of damage parameter z_1 grows up to 0.95, i.e. approaches practically the ultimate magnitudewhen there occurs a destruction of the composite by the delamination type.

   The main cause of growth of damage parameter z_1 at ψ =30° is higher pore gas pressure than for $\psi = 0°$ and the appearance of stresses of interlayer shear at inclined location of the fabric layers in the composite.

7. Thus, the mathematical model developed of coupled thermo-mechanical processes of ablation of composites under the action of high-temperature gas flows allows us:

   • to perform calculations of heat-physical and thermo-mechanical characteristics of fabric 2-D composites, including BRFC, taking as initial data only properties of the matrix, fibres and parameters of their geometrical interlocaltion;

   • to conduct calculations of ablation rates (mass and linear) of composites under the action of high-speed hot gas flows, including account of both thermo-chemical processes (combustion, sublimation, pyrolysis) and thermo-mechanical processes (internal and external mechanical erosion of different types). Here for calculations of

ablation rates of composite we have no need to know ablation rates of its matrix and fibres: they can be determined with the help of the same heat-physical and mechanical properties of the matrix and fibres;

• to conduct calculations of thermo-stresses and parameters of internal heat and mass transfer in structures of ablative composites under the action of gas flows;

• to optimize an internal structure and composition of ablative composites in order to obtain the best characteristics and the highest efficiency of the materials.

8. Verification of the developed model has shown that:

• the model ensures a quite satisfactory accuracy of prediction of the characteristics of ablative composites: the best estimations are at room, high and superhigh temperatures, the worst – at elevated temperatures (294 - 600 K); the best prediction is realized for elastic moduli, strength, gas permeability and heat capacity, the worst – for heat expansion and heat conductivity, it is explained by the absence of sufficiently reliable data on thermal expansion and conductivity of matrix and fibres;

• the model ensures a good accuracy of prediction of linear and mass rates of composite ablation under the action of gas flows, that is achieved at the expense of sufficiently detailed modelling of thermo-mechanical erosion processes of composites giving a main contribution into the ablation process at great values of velocity head of the flow p'_0.

The limited scope of experimental data does not allow us to conduct more detailed verification of the model, in particular for different values of velocity head p'_0 and heat flux q_e^0.

9. To continue the work in future, we suggest on the basis of the present model to develop a method of optimal designing of composition and internal structure of ablative composite materials. This method will allow us to select such composition of composite materials (matrix, one, two, three or more fillers) and such structure (angles of reinforcing, volumetric content of different fillers etc.) which would ensure a creation of ablative composites with the best characteristics and the highest efficiency in composition of structures under the concrete conditions of heating. It should be noted that development of criteria of what material can be considered as more effective will be the most important problem in this work. For example, under the certain conditions of heating, material with higher heat conductivity and smaller rate of ablation can prove to be more effective, and under other conditions of heating the most effective material can have opposite properties.

REFERENCES

1. 'Verification of Model for Heat-Mechanical Processes in Ablating Composites'. First progress report F61708-96-W0227, 1996.

2. 'Development of Models for Heat-Mechanical Processes in Thermal Protection Made of Ablating Composites', Report No.1 on the contract SPC-94-4104, 1995.

3. 'Development of Models for Heat-Mechanical Processes in Thermal Protection Made of Ablating Composites', Report No.2 on the contract SPC-94-4104, 1995.

4. 'Development of Models for Heat-Mechanical Processes in Thermal Protection Made of Ablating Composites', Report No.3 on the contract SPC-94-4104, 1995.

5. Dimitrienko, Iou.I., , Efremov, G.A. and Chernyavsky, S.A., 'Optimum Design of Erosion-Stable Heatshield Composite Materials'. *Applied Composite Materials*, v.4, N 1, pp.35-52 (1997).

6. Dimitrienko Iou.I. Thermal stresses and heat-mass-transfer in ablating composite materials. *J.Heat and Mass Transfer*, vol.38, N 1, 1995, pp.139-146.

7. Dimitrienko Iou.I., Effect of Finite Deformations on Internal Heat-Mass-Transfer in Elastomer Ablative Materials, *Int. Journal of Heat Mass Transfer*, vol. 40, No.3, 1997, pp.699-709.

8. Dimitrienko Iou.I., Internal Heat-Mass-Transfer and Stresses in Thin-Walled Structures of Ablating Materials, *Int. Journal of Heat Mass Transfer*, vol.40, No.7, 1997, pp.1701-1711.

9. Dimitrienko Yu.I., Thermal Stresses in Ablative Composite Thin-Walled Structures under Intensive Heat Flows, *Int. Journal of Engineering Science*, vol.35, N 1, 1997, pp.15-31.

10. Dimitrienko, Iou.I., , Efremov, G.A., Chernyavsky, S.A. and Medvedev, Yu.V., 'Theory and Synthesis of Advanced Thermal–Protective Composite Materials', *Applied Composite Materials*, v. 2, N 6, pp.367-384 (1995).

11. 'Mechanical and Thermal Data Package for Generic 2-D Carbon Phenolic Composites. Wright Pat. AFB. Information materials, 1996.

12. Dimitrienko Iou.I., Efremov G.A., Epifanovsky I.S. Reusable Re-entry Vehicles with Reclaimable Ablating Thermal Protection. Preprints of 19th Int.Symp. on Space Technology and Science May 1994, Yokohama, Japan, 94-b-26.

13. Polezhaev Yu.V., Yurevich. Thermal Protection. Moscow, Energia, 1976 (in Russian).

14. Dimitrienko Yu.I., Thermomechanical Behaviour of Composite Materials and Structures under High Temperatures. 1. Materials. *Composites. Part A: Applied Science and Manufacturing.* 1997 (in print).

15. Dimitrienko Yu.I., Thermomechanical Behaviour of Composite Materials and Structures under High Temperatures. 2. Structures. *Composites. Part A: Applied Science and Manufacturing.* 1997 (in print).

16. Dimitrienko Yu.I., Modelling of Mechanical Properties of Composite Materials under High Temperatures. Part 1. Matrix and Fibres. *Applied Composite Materials*, 1997 (in print).

17. Dimitrienko Yu.I., Modelling of Mechanical Properties of Composite Materials under High Temperatures. Part 2. Unidirectional Composites. *Applied Composite Materials*, 1997 (in print).

18. 'Engineering Design for Plastics'. Ed. by E.Bacr, New York, Reinhold Publ. Corp., 1967.

19. Dimitrienko Yu.I., Modelling of Erosion Combustion of Energetic Materials in High-Enthalpy Flows, *Combustion And Flame*, 1997 (in print).

20. Laub B., Thermo-Chemical Ablation of Tantalum Carbide Loaded Carbon-Carbons. *AIAA Pap.*, 1980, N 1476.

21. Pobedrya B.E., Lectures on Tensor Analysis. Moscow State University Publ., 1987 (in Russian).